Synthesis of Zeolitic Membranes by Vapor-Phase Transport Method and Their Permeation Properties

Norikazu Nishiyama

Department of Chemical Engineering
Faculty of Engineering Science
Osaka University
1997

Synthesis of Zeolitic Membranes by Vapor-Phase Transport Method and Their Permeation Properties

Norikazu Nishiyama

Department of Chemical Engineering
Faculty of Engineering Science
Osaka University
1997

Preface

The present dissertation is a collection of author's studies which have been carried out under the direction of Professor Dr. Korekazu Ueyama and Associate Professor Dr. Masahiko Matsukata at the Department of Chemical Engineering, Faculty of Engineering Science, Osaka University from 1992 to 1997.

This thesis deals with synthesis of zeolitic membranes and their separation properties. Recent years much attention have been paid to inorganic membranes because of their high thermal resistance, chemical inertness and high mechanical strength. Typical microporous crystals, zeolites, are one of the most attractive materials as membranes owing to their molecular sieving properties. Only a few papers on zeolitic membranes had been published when author started studies on zeolitic membranes in 1992. It is noteworthy that more than a hundred papers have been published a year today.

In most studies, zeolite membranes generally have been synthesized by a conventional hydrothermal synthesis. In this thesis, zeolitic membranes are synthesized by a novel synthesis method "the vapor-phase transport (VPT) method". The interest is focused on the synthesis of defect-free zeolitic membranes and their permeation properties.

This thesis consists of seven chapters. Chapter 1 deals with the general introduction to zeolitic membranes. In chapter 2 a novel synthetic method of zeolites "VPT method" are studied. In chapter 3 the VPT method is applied to a membrane synthesis. Formation process of zeolitic membranes by the VPT method are discussed in chapter 4. Inorganic gas permeation such as H_2, He, CH_4, N_2, O_2 and CO_2 are studied in chapter 5. In chapter 6 aromatic hydrocarbons are tested for the pervaporation using the zeolitic membranes. The findings in this thesis are summarized in

chapter 7.

The author hopes that the findings obtained in this work would give some suggestions for the development of zeolitic membranes and other microporous membranes.

Norikazu Nishiyama
Department of Chemical Engineering
Faculty of Engineering Science
Osaka University
Toyonaka, Osaka 560, Japan

Contents

Chapter 1 General Introduction

Zeolites, a class of microporous crystalline aluminosilicate materials, have been extensively studied and utilized in chemical and physical processes such as gas separation and heterogeneous catalysis. Zeolites are generally used in the form of granules, and their function is based on either an adsorptive separating action or a catalytic action. The adsorptive separation processes with granular molecular sieves are a non-continuous batch process. If there were membranes composed of a sort of zeolite and the membrane separation processes superseded these processes, it would be possible to carry out separation processes continuously without changes in phase.

There is a strong interest in membranes made of inorganic materials for application in separation processes owing to their superior characteristics of thermal, mechanical and structural stability, and chemical resistance. In addition, zeolites possess the advantage of the following four characteristics.

(i) The micropore systems of zeolites are inherent for the structure. Pore diameters in zeolites are determined by the aperture resulting from 4, 6, 8, 10 or 12 membered rings of oxygen atoms and these have maximum values calculated to be 0.26, 0.34, 0.42, 0.63 and 0.74 nm, respectively. **Figure 1.1** compares the pore dimensions in zeolites with the size of several molecules. Zeolites can be classified into three main groups: first, small pore zeolites such as A (LTA), analcime (ANA) and deca-dodecasil (DDR), second, medium pore zeolites such as ZSM-5 (MFI) and ferrierite (FER), and third, large pore zeolites such as X, Y (FAU), mordenite (MOR) and beta (BEA). Suitable kinds of zeolites should be used depending on objective separation processes.

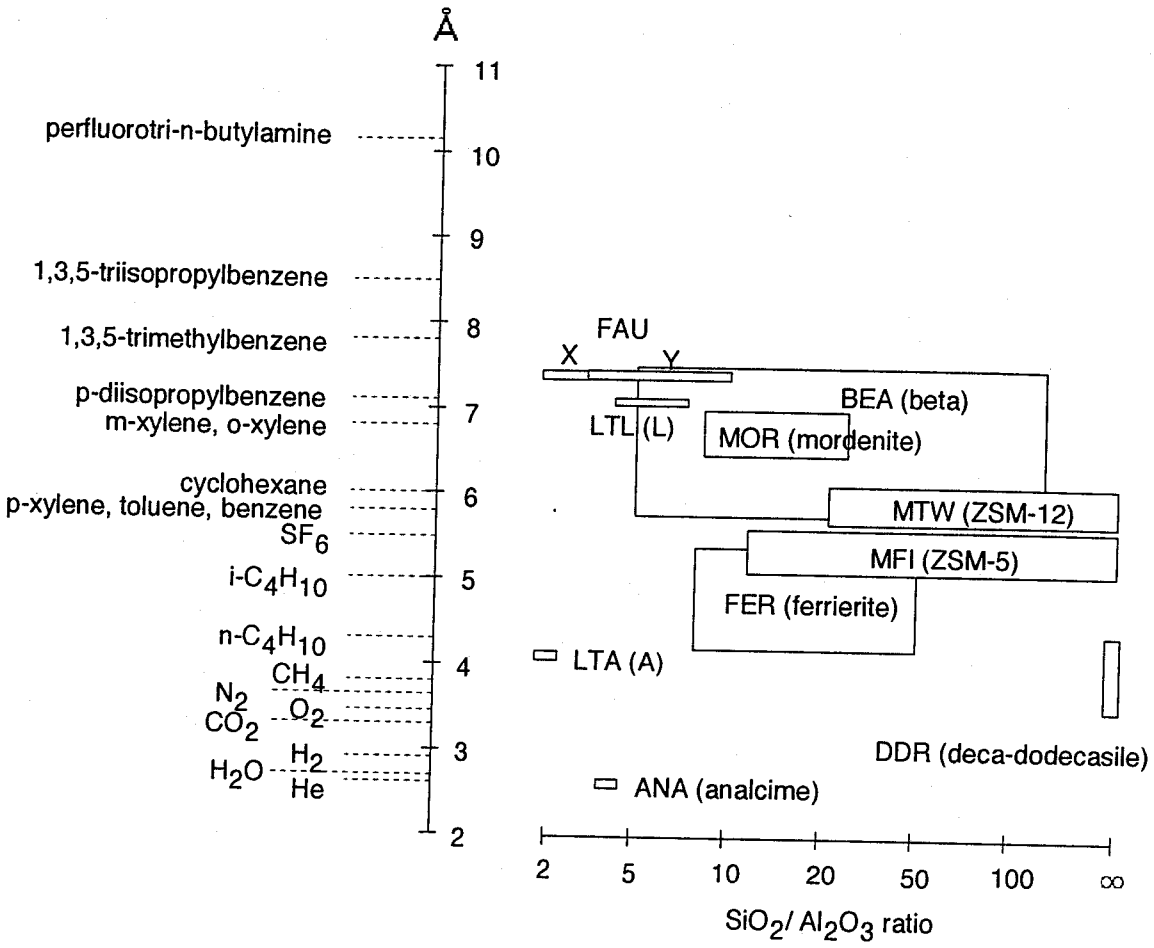

Figure 1.1 Comparison of kinetic diameters of molecules with channel diameter.

(ii) Inner surface of zeolites can be modified readily. Both actual pore size and affinity of adsorbed molecules-pore wall depend on the type of cation and are precisely controllable by ion-exchange. Outer surface can also be selectively modified by chemical vapor deposition (CVD) (Niwa et al., 1984; Sano et al., 1996a).

(iii) Hydrophilic/hydrophobic nature of zeolite surface can be tuned by changing Si/Al ratio in the framework of zeolites. The cation which balances the negative charge associated with framework aluminum ions causes an electrostatic field in zeolites. Thus, the pores of aluminum-rich zeolites are occupied by water molecules. A decrease in aluminum content in the framework leads to hydrophobic nature. The value of Si/Al ratio varies a great deal (from one to infinity) between different zeolites, as shown in **Figure 1.1**. Several reports on water-selective and organic-selective separation using low-silica hydrophilic zeolites and high-silica hydrophobic zeolites, respectively.

(iv) Since zeolites exhibit catalytic properties, they can be applied to catalytic membrane reactors. A few conceptions of membrane reactor using zeolitic membranes were proposed (Sie, 1994; Kapteijn et al., 1995a).

From the reasons described above, much attention has been paid to the preparation of zeolitic membranes.

Embedding crystals in polymer

The first attempt to make zeolites in a membrane form was carried out by embedding granular zeolites in polymer matrices, such as FAU-epoxide resin (Demertzis and Evmiridis, 1986), LTA-epoxide resin (Demertzis and Evmiridis, 1986), silicalite-1 (Al-free MFI) -silicone rubber (Hennepe et al., 1987, 1991; Jia et al., 1991) and LTA -cellulose membranes (Bellobono et al., 1991). These sorts of zeolite-filled polymeric membranes can easily

Table 1.1 Self-supporting MFI membranes

	Silica source	Alumina source	Composition (Na_2O:SiO_2:Al_2O_3:TPA:H_2O)	Substrate	Crystallization	Thickness
Sano et al. (1991)	CS	$Al(NO_3)_3$	0.05: 1:0.01:0.1:40-100	Teflon	373 -473 K 2 - 17 days	30-100 μm
Sano et al. (1992ab)	CS	$Al(NO_3)_3$	0.05: 1:0.01:0.1:80	Teflon	443 K 2 days	30-100 μm
Sano et al. (1992c)	CS	$Al(NO_3)_3$	0.05: 1:0-0.01:0.1:80	cellulose	443 K 2 days	500 μm
Tsikoyiannis and Haag (1992)	CS	-	2.2: 100:0:5.22:2832	Teflon silver stainless steel Vycor disk	453 K 0.3 - 9 days	20-250 μm
Kiyozumi et al. (1996)	CS	$Al(NO_3)_3$	0.1:0.05-0.1:1:0-0.02:20-40 0	mercury	393-453 K 2 days	

CS: colloidal silica.

be prepared in a pinhole-free form compared with self-bonded zeolitic membranes.

However, in the separation process using this type of composite membranes, one cannot make full use of the molecular sieving effect of zeolite because an undesired transport of molecules outside pores of zeolite is inevitable. In addition, the properties of zeolites, such as high thermal resistance, high mechanical strength and chemical inertness as described in the introduction cannot be taken advantage of. Thus, the next attempt was to prepare zeolitic membranes made of zeolite crystals themselves.

Hydrothermal synthesis

The configuration of zeolitic membranes has two types, one is a self-supporting membrane without support, and the other is a membrane supported by a porous material. Both types of membrane have mostly been prepared by a hydrothermal synthetic method which is a conventional preparation method of granular zeolites.

Zeolitic membranes typically prepared from hydrogel or sol composed of SiO_2, Al_2O_3, Na_2O and organic templating agent. Typical silica sources for synthesizing MFI membranes were colloidal silica and silica powder (Aerosil). Tetrapropylammonium (TPA) cation was mostly used as templating agent. Self-supporting zeolitic membranes can be hydrothermally synthesized on various substrates. **Table 1.1** summarizes the studies on the preparation of self-supporting zeolitic membranes. Sano et al. (1991) and Tsikoyiannis & Haag (1992) first reported on the synthesis of self-supporting MFI membranes.

Sano and coworkers (1991, 1992a, b) synthesized MFI membranes on a Teflon sleeve from a clear aqueous solution with a composition of 0.1 TPABr: 0.05 Na_2O: 0.01 Al_2O_3: SiO_2 : 40-100 H_2O. The synthesis

mixtures with H_2O/SiO_2 ratios higher than 70 crystallized to form MFI membranes without stirring.

Tsikoyiannis and Haag (1992) hydrothermally synthesized MFI layers with 20 - 250 μm thick on various non-porous supports including Teflon slab, silver, and stainless steel and on the external surface of a porous Vycor disk. The products were easily detached from the Teflon surface, and characterized by SEM. Although the Teflon side surface consisted of a layer of submicron-sized crystals, the solution side surface consisted of a continuous array of densely intergrown crystals in the range of 10 - 100 μm.

It is known that the mechanical strength of the self-supporting zeolitic membranes is insufficient for the application of this type of membrane to separation processes. Hence, most of the studies on the synthesis of zeolitic membranes have been performed on porous supports.

Studies on high silica MFI membranes have mainly been reported and are summarized in **Table 1.2**. Supported MFI membranes have typically been prepared from hydrogel or sol composed of SiO_2, Al_2O_3, Na_2O and TPA cation, similarly to the preparation of self-supporting membranes. A reactant mixture, in which a porous support is immersed, is placed in an autoclave. Crystallization is carried out under autogeneous pressure between 443 and 473 K.

Most of researchers have synthesized MFI membranes on macroporous supports with a pore size of 0.1-10 μm such as an α-alumina and a sintered stainless steel. A γ-alumina with an average pore size of 5 nm was also used by Jia et al. (1994).

Solid gel conversion technique

Bibby and Dale (1985) first synthesized zeolite from non-aqueous

Table 1.2 Supported - MFI membranes

	Si source	Al source	Composition (Na_2O:SiO_2:Al_2O_3:TPA:H_2O)	Suppot (pore diameter)	Crystallization	Thickness
Vroon et al. (1996)	silica	-	5.3: 100: 0: 30: 1420	α-alumina	393 K, 3 days	5 μm
Meriaudeau et al. (1995)	TEOS	-	-: 1: 0: 0.051: 22.5	porous glass (10- 20 μm)	448 K, 72 h	150 μm
Bai et al. (1995)	Aerosol	-	0.071: 1: 0: 0.071: 42	γ-alumina (5 nm)	453 K, 12 h	10 μm
Chiou et al. (1996)	TEOS	-	5: 100: 0: 10: 10000	anodic alumina (0.2 μm)	473 K, 1-4 days	130 μm
Geus et al. (1992)	Aerosil 200	-	1.6: 1: 0: 1.5: 166.66	clay, Zirconia	453 K, 1 - 5 days	100 μm
Geuset al. (1993)	Aerosil 200, CS	-	-: 100: 0: 6: 6330	sintered metal (10), stainless steel	453 K, 1-7 days	60-400 μm
Sano et al. (1994a, b)	CS	-	0.05: 1: 0: 0.1: 80	stainless steel (0.5-2 μm)	443 K, 2 days	400-500 μm
Masuda et al. (1994)	SS	$Al_2(SO_4)_3$	34: 71: 1: -	α-alumina (2 μm)	473 K, 2 days	10-25 μm
Kusakabe et al. (1996)	Aerosil 200	-	-: 1: 0: 1.0: 100	γ-alumina (5-10 nm) α-alumina (0.95, 0.15 μm)	448 K, 12-24 h	20-30 μm
Yan et al. (1995)	CS	-	2: 6: 0.005: 1: 571: 1	α-alumina (0.5 μm)	448 K, 16 h	10 μm
Yan et al. (1995)	TEOS	Al foil	0-4: 6: 0-0.06: 1: 96-700	α-alumina (0.5 μm)	448 K, 4 - 24 h	10 μm
Jia et al. (1994)	Aerosil 130	-		γ-alumina (5 nm)	453 K, 3-72 h	10 μm
Jia et al. (1993)	Aerosil 130	-	0.75: 9: 0: 1.0: 70	ceramic disk	453 K, 3-72 h	5 μm

TPA: tetrapropylammonium ion, IPA: isopropylalcohol, TEOS: tetraethylorthosilicate, CS: colloidal silica, SS: sodium silicate solution.

system, suggesting that water as solvent is not essential for the crystallization of zeolites. The pure silica zeolites with a sodalite (SOD) structure were obtained using ethylene glycol as solvent. Since that time, several types of zeolites have been synthesized using organic solvents. Huo and coworkers (1988) synthesized Al-free MFI, ZSM-39 (MTN) and ZSM-48 using glycerol, ethylene glycol or butyl alcohol as solvent. Xu et al. (1989) synthesized MFI and ZSM-35 (FER) from aluminosilicate gel in the solution of ethylenediamine (EDA) and triethylamine (Et_3N), showing that not only alcohol but also amine is effective as solvent in the non-aqueous systems.

Recently, synthetic methods of zeolites from solid gel in gas phase have been developed. **Figure 1.2** shows three types of solid gel conversion techniques reported. Water content of solid gel under crystallization is determined by reaction temperature, if liquid phase exists in the bottom of an autoclave. Xu et al. (1990) first reported that aluminosilicate dry gel was transformed to MFI in contact with vapors of water, EDA and Et_3N at 453 K, as shown in **Figure 1.2(a)**. Kim et al. (1992) and our group followed this report and confirmed that this solid gel conversion technique is useful for synthesizing various types of zeolites. Kim et al. called this method the vapor-phase transport (VPT). **Table 1.3** summarizes the synthetic conditions which lead to MFI zeolites (Xu et al. 1990; Kim et al. 1993), indicating that different organic templates gives different crystallization fields of MFI in the Na_2O-SiO_2-Al_2O_3 system. **Table 1.4** and **Table 1.5** summarize results of crystallization at 448 K in the presence and absence of water, respectively, showing that the addition of water is required for crystallization of zeolites, while crystallization occurred in steam without organic templating agent at autogeneous pressure in some cases.

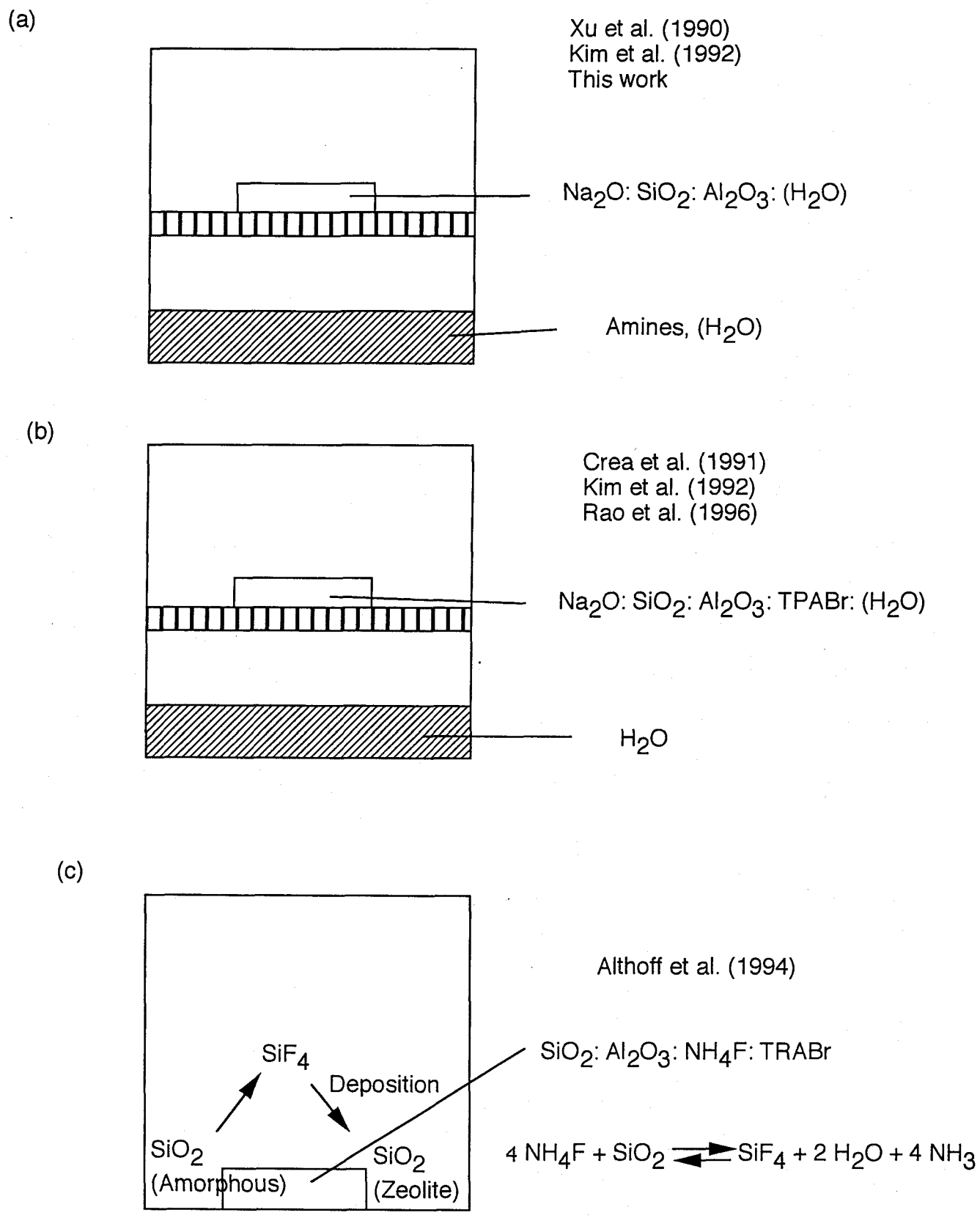

Figure 1.2 Solid gel conversion techniques.

Table 1.3 Synthetic conditions for MFI by vapor-phase transport method

	SiO_2/Al_2O_3	Na_2O/SiO_2	liquid phase
Xu. et al. (1990)	45	0.031	EDA, Et_3N, H_2O
Xu. et al. (1990)	86	0.017	EDA, Et_3N, H_2O
Kim et al. (1993)	40	0.05 - 0.2	H_2O
Kim et al. (1993)	40	0.1 - 0.2	Pr_3N, H_2O
Kim et al. (1993)	20 - 40	0.012 - 0.2	Pr_2NH, H_2O
Kim et al. (1993)	2.5 - 80	0.012 - 0.2	$PrNH_2$, H_2O
Kim et al. (1993)	2.5 - 80	0.012 - 0.2	DAP, H_2O

EDA: ethylenediamine, Et_3N: triethylamine, Pr_3N: tripropylamine, Pr_2NH: dipropylamine, $PrNH_2$: propylamine, DAP: diaminopropane.

Table 1.4 Results obtained form heating amorphous oxide powders in the presence of water vapor at 448 K for 7 days [Kim et al., 1993]

SiO_2 / Na_2O

2.5	×	ANA	ANA	ANA	ANA	ANA	CHA, GIS
5.0	quartz	quartz	MFI	MOR	×	×	×
10	quartz	quartz, NOR	MFI	MOR, MFI	×	×	×
20	quartz, mgdt	quartz, MFI	MFI	×	×	×	×
40	mgdt	×	×	×	×	×	×
80	×	×	×	×	×	×	×
	Al free	80	40	20	10	5.0	2.5

SiO_2 / Al_2O_3

×: Amorphous, mgdt: magadiite.

Table 1.5 Oxide transformations by contact with vapor at 448 K for 7 days at autogenous pressure [Kim rt al., 1993]

Dry solid phase		liquid phase	Result
SiO_2 / Al_2O_3	SiO_2 / Na_2O		
40	10	Pr_3N	×
40	10	EDA	×
40	10	methanol	×
40	10	ethanol	×
40	10	acetone	×
80	20	acetone	×
40	10	water	MFI
80	20	Et_3N, EDA	×
40	10	Et_3N, EDA	×
10	10	Et_3N, EDA	×
20	20	Et_3N, EDA	×
10	20	Et_3N, EDA	×

×: amorphous.

Dong et al. (1992) first applied the VPT method to synthesizing self-supporting MFI and FER membranes. The membranes after calcination were not compact.

Another solid gel conversion technique was studied by Crea et al. (1991), who used TPA cation as a templating agent and used a reaction system shown in **Figure 1.2(b)**. Self-bonded MFI crystals in the pelleted form were produced under steam from a dense hydrogel which contains TPA cation. Their result suggests that the solid gel conversion techniques

could be utilized for the production of a self-bonded pellet and also of a zeolitic layer.

More recently, Althoff et al. (1994) demonstrated a new reaction system for the synthesis of MFI zeolites from a fluoride-containing dry gel with a composition of 80 SiO_2: Al_2O_3: 145 NH_4F: 6 TPABr: 0-300 H_2O (**Figure 1.2(c)**). Some water was probably formed by the following reaction:

$$SiO_2 + 4\ NH_4F \rightarrow SiF_4 + 2\ H_2O + 4\ NH_3,$$

but the maximum water pressure was appreciably below the saturation pressure under their conditions. They proposed that SF_4 formed from amorphous precursor transported in a gas phase and deposited on zeolite crystals. The proposed mechanism is a different one from that in the VPT method described above, because a silicon source is the transport species in vapor phase. Their method would make it possible to develop a gas phase deposition process for zeolites and develop new ways of coating materials with a zeolitic layer.

Three types of the solid gel conversion techniques have been introduced here. Studies on these solid gel conversion techniques have just started, while development of hydrothermal synthesis has a history of 45 years. However, these solid gel conversion techniques offer a promising prospect of preparing zeolites and zeolitic membranes.

Chapter 2 Synthesis of Zeolites by Vapor-phase Transport Method

2.1. Introduction

Zeolites have been hydrothermally synthesized over the last 45 years. In the first 10 years, zeolites with low silica to alumina ratios ($SiO_2/Al_2O_3<10$) have been synthesized by crystallizing from reactive aluminosilicate gel or sol. In 1972, high silica zeolites ($SiO_2/Al_2O_3>20$) including ZSM-5 (MFI) and ZSM-11 (MEL) were first synthesized using tetrapropylammonium (TPA) cation by Mobil Oil Corporation (Argauer et al., 1972). The organic quaternary ammonium cation is said to have a structure-directing function which influences the structure of the zeolites. This structure-directing effect has been termed 'templating'. Since Mobil Oil Corporation synthesized the MFI zeolite, numerous organic templating agents including quaternary ammonium cations, amines, and alcohols have been employed for the zeolite synthesis (Lok, 1983).

Bibby and Dale (1985) first synthesized sodalite (SOD) using ethylene glycol as solvent, suggesting that water as solvent is not essential for the crystallization of zeolites. Since that time, several types of zeolites have been synthesized using organic solvents (Huo et al., 1988; Xu et al, 1989).

In recent researches, the solid phase was crystallized to zeolite in the absence of solvent. Xu and coworkers (Xu et al., 1990; Dong et al., 1992; Li et al., 1993) have developed a novel method for the preparation of MFI. MFI zeolites were synthesized from aluminosilicate dry gel under vapors of EDA and Et_3N and water.

This novel synthetic method was named "vapor-phase transport (VPT)" by Kim et al. (1992) who synthesized mordenite (MOR), ferrierite (FER), analcime (ANA) and MFI by changing compositions of gel and

vapor by the VPT method.

Xu et al. (1990) claimed that the VPT method reduces the consumption of organic materials. Addition to this, the VPT method seems attractive because of the following possibilities: (1) synthesis of zeolites with a SiO_2/Al_2O_3 ratio which is the same as that of the parent gel, (2) continuous production of zeolites because the gel is separated from the liquid, and (3) production of zeolites from amorphous gels which are arranged in the desired shape in advance.

The objective of this chapter is to investigate the potential of synthesizing zeolites by the VPT method. Further, the crystallization processes of zeolites were studied using products crystallized for different time, 0 - 8.5 days.

2.2. Experimental

2.2.1. Preparation of parent gel

Sodium silicate solution (Kanto Chemical Co., Inc.) containing 35-38 wt% SiO_2 and 17-19 wt% Na_2O was used as silica source. In some experiments, the concentration of Na ion in the resultant gel was varied by mixing colloidal silica (ST-S; Nissan Chemical Industries., Ltd.) containing 30.33 wt% SiO_2 and 0.42 wt% Na_2O with sodium silicate solution. Anhydrous aluminum sulfate, $Al_2(SO_4)_3$, (Wako Pure Chemical Industries Co., Ltd.) was used as alumina source. Parent aluminosilicate gel was prepared as follows, unless otherwise noted. Aluminum sulfate was dissolved in deionized water and mixed with the silica source. The value of pH of gel was adjusted by adding a certain amount of conc. sulfuric acid, H_2SO_4. The mixture was dried at 363 K for 4 h and then rinsed with deionized water.

2.2.2. Crystallization by vapor-phase transport method

Crystallization was carried out in a special autoclave which had a perforated partition in the middle of a Teflon vessel. The structure of the autoclave used is shown in **Figure 2.1**. The parent gel was placed on a substrate and set on the partition. Four kinds of substrate were used: 1) Polyflon filter (PF20; Advantec Toyo) made of polyethylene, 2) nonporous Teflon plate, 3) Gore-tex film (C-type; Japan Gore-tex) and 4) paper filter

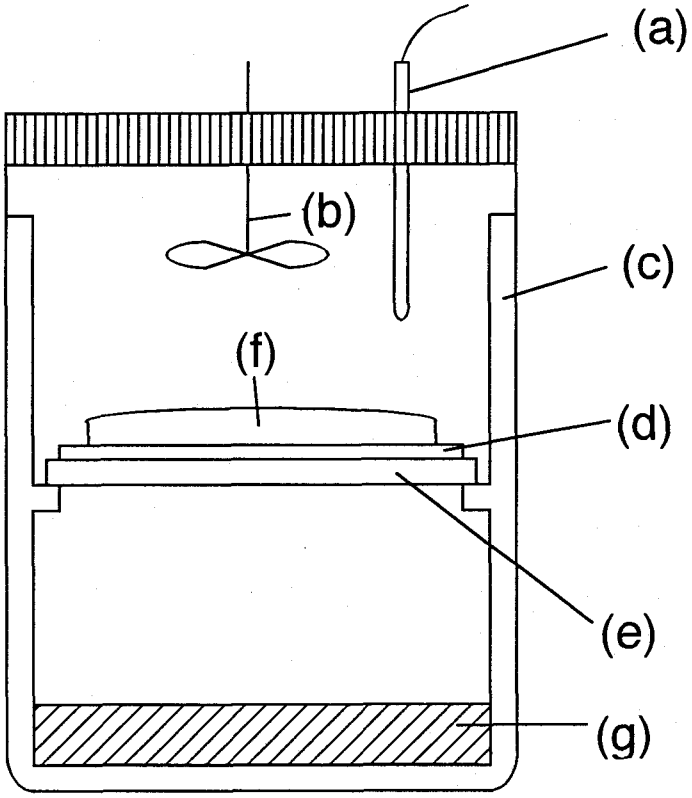

Figure 2.1 Schematic diagram of special autoclave for the vapor-phase transport synthesis: (a) thermocouple, (b) agitator, (c) Teflon vessel, (d) substrate, (e) perfolated plate, (f) amorphous gel and (g) liquid phase.

(5C; Advantec Toyo) made of cellulose. Water, Et_3N, EDA, 1-propanol (1-PrOH) and mixtures containing some of these liquids were tested as vapor source. The liquid phase was poured into the bottom of the Teflon vessel. After the autoclave was sealed, internal air containing CO_2 and O_2 which react with organic compounds was replaced by N_2. Then, the autoclave was heated to 453 K and kept at this temperature for 0-8.5 days. The parent gel in contact with vapor from the liquid phase crystallized into a zeolite. The product was rinsed with deionized water and dried at 363 K overnight. The chemical compositions of the product before and after rinse were compared by chemical analysis. The SiO_2/Al_2O_3 ratio was not changed by rinse. An as-synthesized product was calcined at 773 K for 4 h.

2.2.3. Analysis

The product was identified by X-ray diffraction (XRD) with Cu Kα radiation (Simadzu VD-1). Scanning electron microscopy (SEM) were taken on Au-coated samples using a Hitachi S-800 electron microscope. Elemental analysis of the product was carried out by a CHN corder (Model MT-3, Yanagimoto Co.).

Thermogravimetric analysis (TGA) was performed on a Simadzu DTG-50/50H thermogravimetric analyzer. A constant heating rate of 10 K min^{-1} was used.

Solid-state NMR measurements were carried out on a GSX-400 (JEOL) with a magnetic field at 11.7 T. ^{29}Si -NMR spectra were recorded at 79.30 MHz with a pulse length of 5.2 μs, a pulse interval of 10 s, a spinning rate of about 6 kHz and 1024 scans accumulated. ^{27}Al-NMR spectra were recorded at 104.05 MHz with a pulse length of 5.1 μs, a pulse interval of 5 s, a spinning rate of about 6 kHz and 512 scans accumulated.

Table 2.1 Typical results of crystallization in vapor

Run	Initial amorphous gel Composition	pH	Liquid phase composition	Product
1	$14Na_2O:Al_2O_3:29SiO_2$	12.0	H_2O	ANA
2	$14Na_2O:Al_2O_3:29SiO_2$	12.0	$EDA:5.3Et_3N:2.5H_2O$	ANA
3	$14Na_2O:Al_2O_3:29SiO_2$	11.0	H_2O	Amorphous
4	$14Na_2O:Al_2O_3:29SiO_2$	11.0	$EDA:5.3Et_3N:2.5H_2O$	FER
5[a)]	$12Na_2O:Al_2O_3:26SiO_2$	9.3	$EDA:5.3Et_3N:2.5H_2O$	FER + MFI
6	$6Na_2O:Al_2O_3:26SiO_2$	10.9	$EDA:5.3Et_3N:2.5H_2O$	MFI
7[a,b)]	$15Na_2O:Al_2O_3:31SiO_2$	9.6	$1\text{-}PrOH:2.0Et_3N$	MFI
8	$14Na_2O:Al_2O_3:29SiO_2$	9.5	$EDA:5.3Et_3N:2.5H_2O$	FER
9	$14Na_2O:Al_2O_3:29SiO_2$	9.6	$EDA:17.3Et_3N:7.4H_2O$	TON
10[a)]	$14Na_2O:Al_2O_3:29SiO_2$	9.9	$2.5EDA:H_2O$	Amorphous
11[a)]	$14Na_2O:Al_2O_3:29SiO_2$	9.9	$2.1Et_3N:H_2O$	Amorphous
12[a)]	$14Na_2O:Al_2O_3:29SiO_2$	10.0	$1.1\ 1\text{-}PrOH:H_2O$	Amorphous
13	$12Na_2O:Al_2O_3:25SiO_2$	10.9	$EDA:5.3Et_3N$	FER

Initial gel compositions and pH are the values before rinse. Compositions are shown by using molar ratio. [a)] Gel was not dried before crystallization. [b)] Crystallized at 433 K for 6 days.

The framework Si/Al molar ratio corresponds to:

$$\frac{Si}{Al} = \frac{\sum_{n=0}^{4} I_{Si\,(nAl)}}{\sum_{n=0}^{4} \frac{n}{4} I_{Si\,(nAl)}} \qquad (2.1)$$

where $I_{Si(n\,Al)}$ is the intensity of the NMR signal attributed to the Si(n Al) unit.

2.3. Results and discussion

2.3.1. Role of amines in crystallization

The concentration of Na ion, SiO_2/Al_2O_3 ratio of parent gel and the composition of the liquid phase as vapor source were varied in the crystallization experiments. The concentration of Na ion and SiO_2/Al_2O_3 ratio of parent gel determined the pH of gel. **Table 2.1** summarizes the crystallization results. Several types of zeolites were produced in the present synthetic conditions. FER was produced in vapors of Et_3N, EDA and H_2O when the pH of parent gel was in the range of 9 -11 and the molar ratio of Et_3N to EDA was 5.3 (Runs 4 and 8).

KZ-2 (TON) was obtained instead of FER when the molar ratio of Et_3N to EDA was increased from 5.3 to 17.3 (Run 9), indicating that the type of zeolite structure depended on the molar ratio of Et_3N to EDA.

eam and EDA (Run 10), and 3) steam and Et_3N (Run 11) were examined. No crystallization occurred in the water, EDA-water and Et_3N-water systems. On the contrary, Runs 4 and 8 gave fully crystallized FER, indicating that co-existence of Et_3N and EDA is required for formation of FER: that is, EDA and/or Et_3N acted as structure-directing agents.

As-synthesized FER must contain some amine molecules in the micropores. The elemental analysis for as-synthesized FER obtained from Run 4 was carried out. The results were summarized in **Table 2.2**. The molar ratio of C:H:N was 1.1:5.8:1.0. The C/N ratio of the product was the same as that of EDA, C/N= 1, and far from that of Et_3N, C/N = 6. The hydrogen content of the sample, H/C = 5.8, was slightly greater than that of EDA, H/C = 4, and far away from that of Et_3N, H/C = 2.5. It seems that only EDA was occluded in the micropores of FER. The deviation of the hydrogen content of the sample from that of EDA can be explained by the contribution of water evolved by dehydration of Si-OH groups on heating the sample in the CHN corder.

The number density of EDA molecule in the micropore of FER can be calculated as follows. From the framework density of FER (1.76 g cc^{-1}) (Szostak, 1992) and the nitrogen content (2.87 wt%), the number of nitrogen atoms per unit volume in nm^3 was determined as 2.45 nm^{-3}. The

Table 2.2 Elemental analysis for FER

Element	Weight%	x/N[a)] [mol mol^{-1}]
H	1.31	5.8
C	2.71	1.1
N	2.87	-

[a)] x = H or C.

pore structure of FER is known to be a multidimensional pore system having the intersections of 10-membered ring (0.42 x 0.54 nm) and 8-membered ring (0.35 x 0.48 nm) as schematically shown in **Figure 2.2**. Since the number of entry ports of larger pores with 10-membered ring per unit surface is 0.543 nm^{-2} (Barrer, 1990), there seemed to be 4.51 nitrogen atoms in the larger pores with 1 nm length. The distance between intersections of 10- and 8- membered rings is calculated to be 0.4875 nm (Szostak, 1992). Hence, it was finally deduced that there were 2.19 nitrogen atoms for each intersection of the 10- and 8- membered rings.

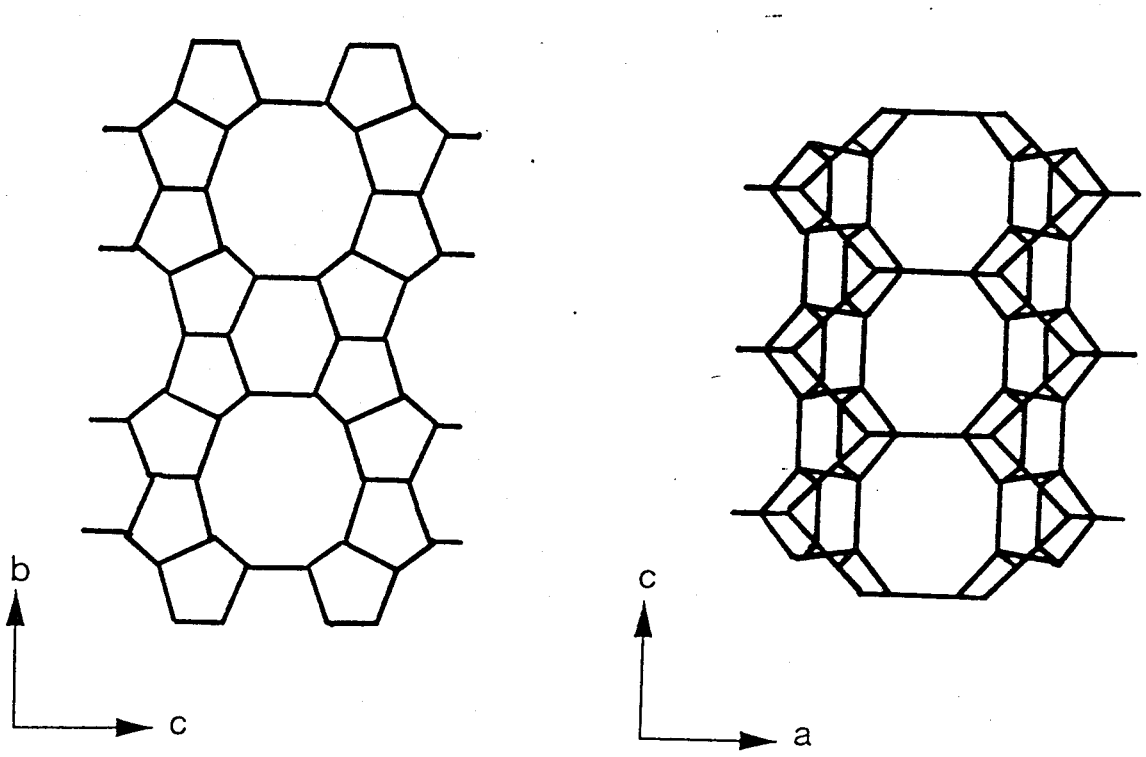

Figure 2.2 Frame work topology of FER. [Szostak, 1992]

Namely, one EDA molecule was occluded for each intersection of micropores in FER. This discussion coincides well with a hypothesis that only EDA was occluded in the micropores of FER. Therefore, EDA is believed to act as a structure-directing agent in crystallization of FER. It was reported that FER formed in a Na_2O -SiO_2 -Al_2O_3 -EDA system in hydrothermal synthesis (Gies, 1987). In this system, EDA clearly served as a structure-directing agent, being in agreement with the present result. Nevertheless, co-existence of EDA and Et_3N was required for occurrence of crystallization in the VPT method. Triethylamine may possibly act as a promoter for crystallization of FER in the VPT method.

MFI was synthesized using Et_3N and 1-PrOH at a Na_2O/Al_2O_3 ratio of 15 in parent gel, as shown in Run 7. As in the FER synthesis in vapors of Et_3N, EDA and H_2O, co-existence of Et_3N and 1-PrOH was found to be essential for synthesizing MFI, because no crystallization was observed under 1-PrOH and water vapors, as shown in Run 12.

2.3.2. Effect of gel's composition and pH on crystallization

In Et_3N, EDA and H_2O vapors, MFI and a mixture of MFI and FER were obtained when the molar ratio of Na_2O to Al_2O_3 was 6 and 12, respectively, as shown in Runs 5 and 6. Taking it into account that a pure phase of FER was obtained at 14 of the Na_2O/Al_2O_3 ratio, MFI should be produced at lower concentrations of Na in parent gel.

Figure 2.3 compares the compositions of parent gels used in Runs 4, 6 and 7 with typical ones of gels which have been used in the hydrothermal synthesis. The gel compositions used by Xu et al. (1990) is shown together. It is noteworthy that MFI with a low SiO_2/Al_2O_3 ratio of 25 was obtained in this method even at 0.48 of the Na_2O/SiO_2 ratio which was higher than those used in the conventional hydrothermal synthesis.

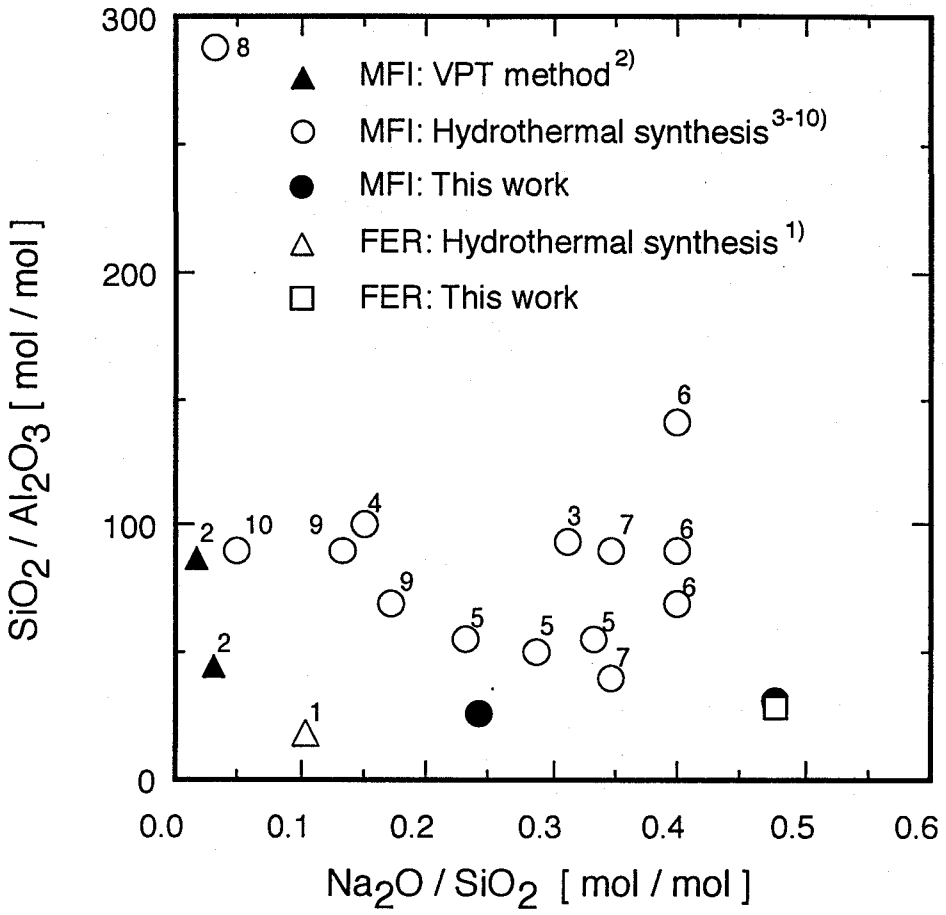

Figure 2.3 Compositions of parent gels for synthesis of MFI and FER. Figures given in the neighborhood of each plot correspond to 1) Prank et al., 1977, 2) Xu et al., 1990, 3) Mole and Whiteside,1982, 4) Narita et al., 1984, 5) Hagiwara et al., 1984, 6) Chao et al, 1981, 7) Costa et al., 1987, 8) Boxhoorn et al., 1983, 9) Inui, 1984, and 10) Nastro et al., 1985.

Although FER was formed in the pH range of 9 - 11, analcime (ANA) and ammonium analcime having a similar type of structure with ANA were produced at pH=12 in steam and in vapors of EDA, Et_3N and H_2O, respectively. At similar SiO_2/Na_2O and SiO_2/Al_2O_3 ratios, Kim et al. (1993) also obtained ANA at 448 K using water, propylamine-water, dipropylamine-water or diaminopropane-water as vapor source. The pH of parent gel is another factor to govern the structure of resultant zeolite.

2.3.3. Effect of water on crystallization

Recent studies on zeolite crystallization under water-lean conditions raised a question on the role of water during zeolite crystallization. Crystallization of zeolite occurs in organic solvents without additional water as described in the introduction. Clearly, excess water is not always essential for zeolite crystallization. Althoff et al. (1994) also reported that crystallization of a dry gel can take place under water-free conditions.

Figure 2.4 presents the effect of water on crystallization. A parent gel was dried at 473 K for 4 h prior to crystallization. Crystallization of FER occurred without the addition of water in liquid phase, but a longer crystallization time, 7 days, was necessary, comparing with that in the presence of water (Run 13). On the basis of this result, water certainly encourages the crystallization of FER similarly to Et_3N.

The thermogravimetric analysis for the parent gel showed that the water content was 3.0 wt% after drying at 473 K. While water necessarily forms by condensation of Si-OH groups during crystallization, the maximum pressure of steam in the autoclave was less than 0.8 atm during Run 13; much less than 9.9 atm of the steam pressure under the experimental temperature. From the Kelvin equation, it is estimated that the autogeneous pressure inside the autoclave at 453 K cannot cause

capillary condensation in an amorphous phase with pore diameter of more than 0.3 nm. Pure water was assumed for the values of surface tension, density and vapor pressure. Capillary condensation, however, did not practically occur to form liquid water in the dry gel, because the Kelvin equation generally cannot hold when the pore diameter is less than about 3 nm. Therefore, the liquid phase of water is not required for crystallization of FER in the VPT method using a mixture of EDA and Et_3N.

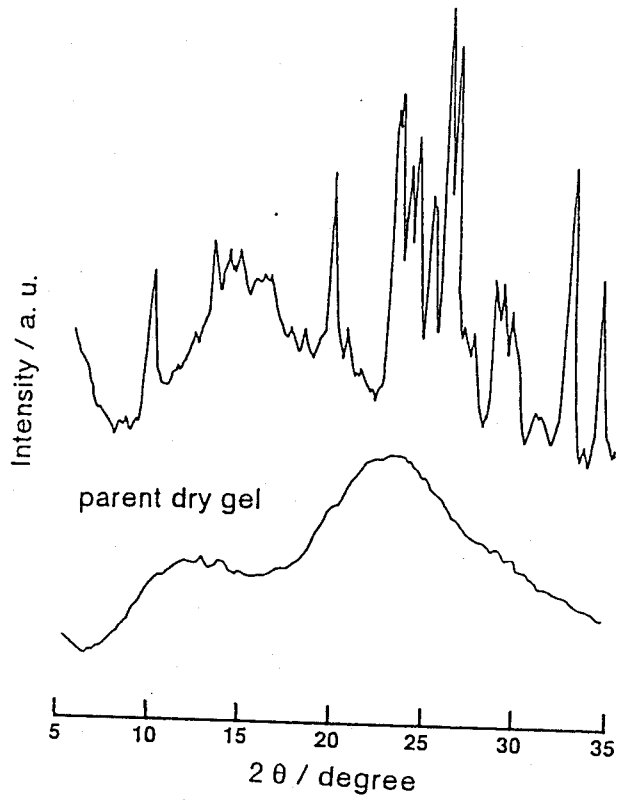

Figure 2.4 XRD pattern for solid crystallized in the absence of water. The XRD pattern for the parent dry gel was compared.

This is not in agreement with the conclusion by Kim et al. (1993) who claimed that the addition of water is required for MFI crystallization in the VPT method. The present results do not prove that zeolite crystallization took place without water, but it can be concluded that zeolite has formed under water-lean conditions. The roles of Et_3N and water in crystallization and the mechanisms of the encouragement of crystallization are still open questions.

2.3.4. Variation in structure and crystallinity

Figure 2.5 shows the time-course of XRD patterns for solids crystallized using a mixture of EDA, Et_3N and water as liquid phase (Run 4). The intensities of reflection peaks for FER increased during the first 3 days while a trace amount of MFI was formed, as indicated in the XRD pattern. After 8.5 days the peaks for FER significantly decreased and those of MFI appeared.

Figure 2.6 presents the variation in the morphology with crystallization time. Flake-like crystals disappeared after 8.5 days and needle-like crystals formed instead. Development of flake-like morphology and its disappearance corresponded to increasing intensities of reflection peaks for FER and their decrease, respectively.

The ^{27}Al- and ^{29}Si-NMR measurements were carried out using the same solids as those used for the XRD measurements. **Figure 2.7** shows the ^{27}Al-NMR results. Even in the spectrum for the solids crystallized for 1 day, the signal solely appeared at 55 ppm and octahedrally coordinated-Al was hard to observe at around 0 ppm. Thus, all atoms were incorporated in the zeolite framework in the very early stage of crystallization. The values of the peak width at half height were 10.4, 6.8, 6.8 and 7.0 ppm for the products after 1, 2, 3 and 8.5 days, respectively: the peak at 55 ppm

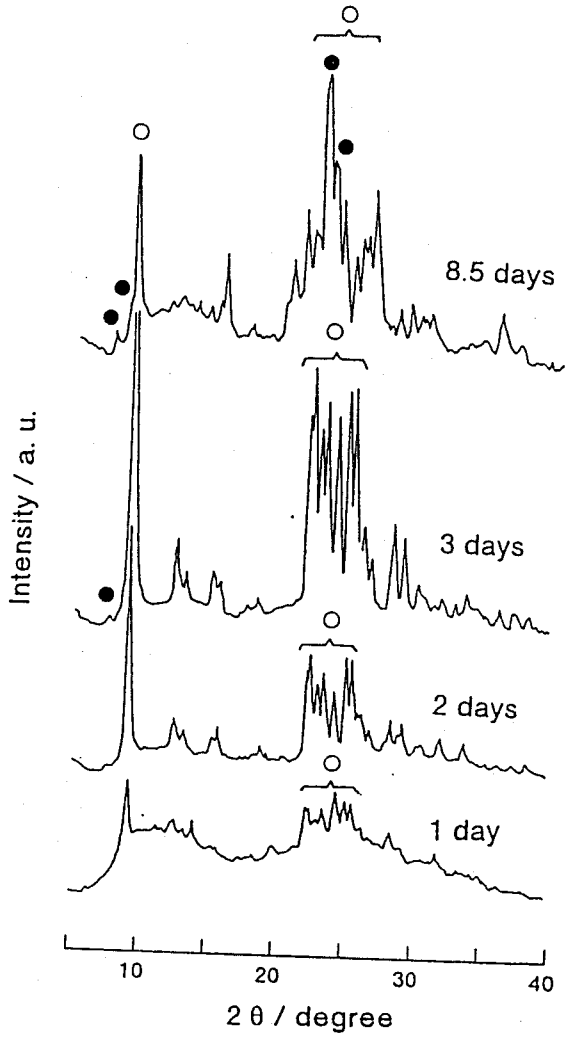

Figure 2.5 Effect of crystallization time on structure and crystallinity. Open symbol; FER, solid symbol; MFI.

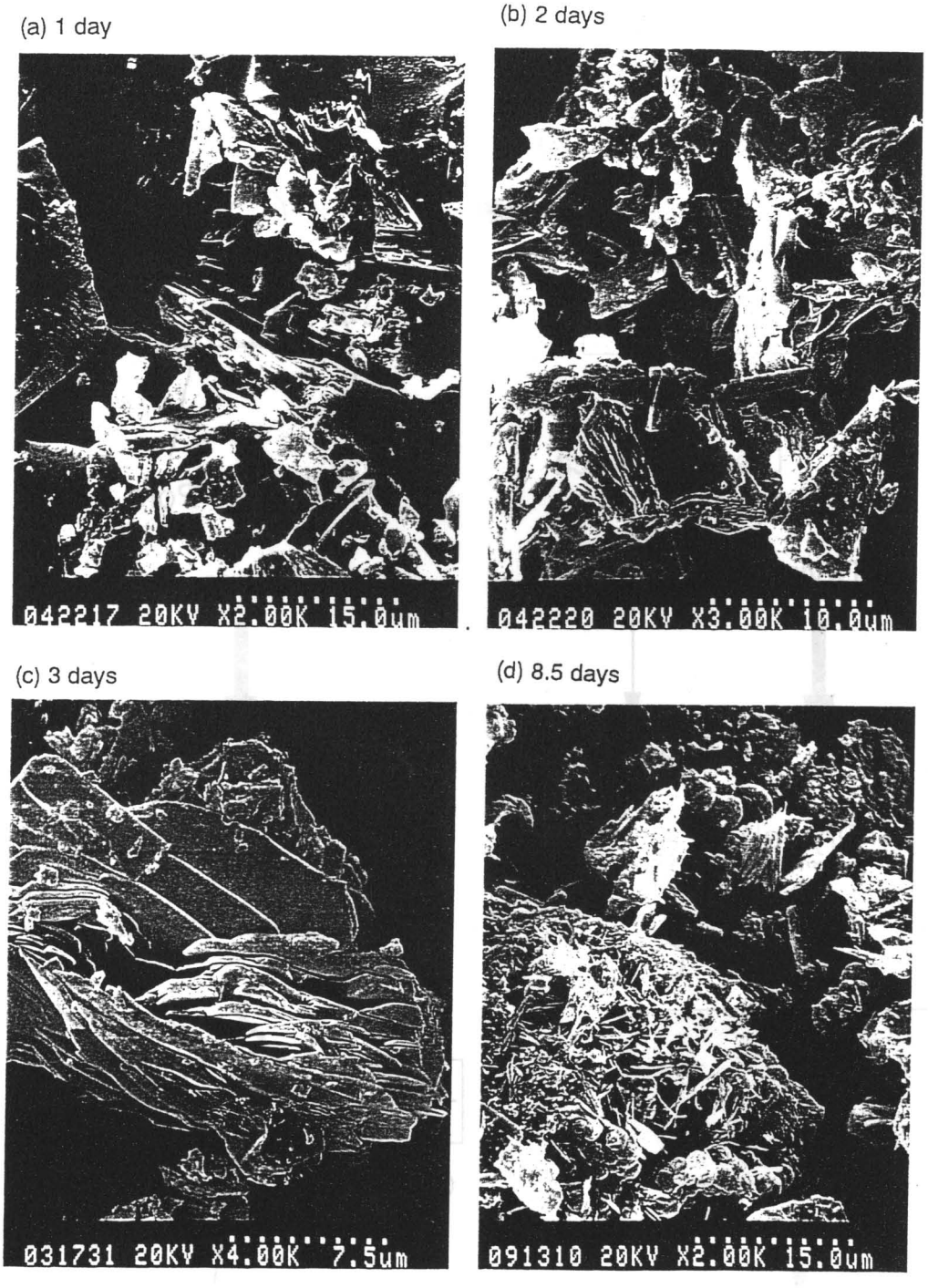

Figure 2.6 SEM images for solids with different crystallization time.

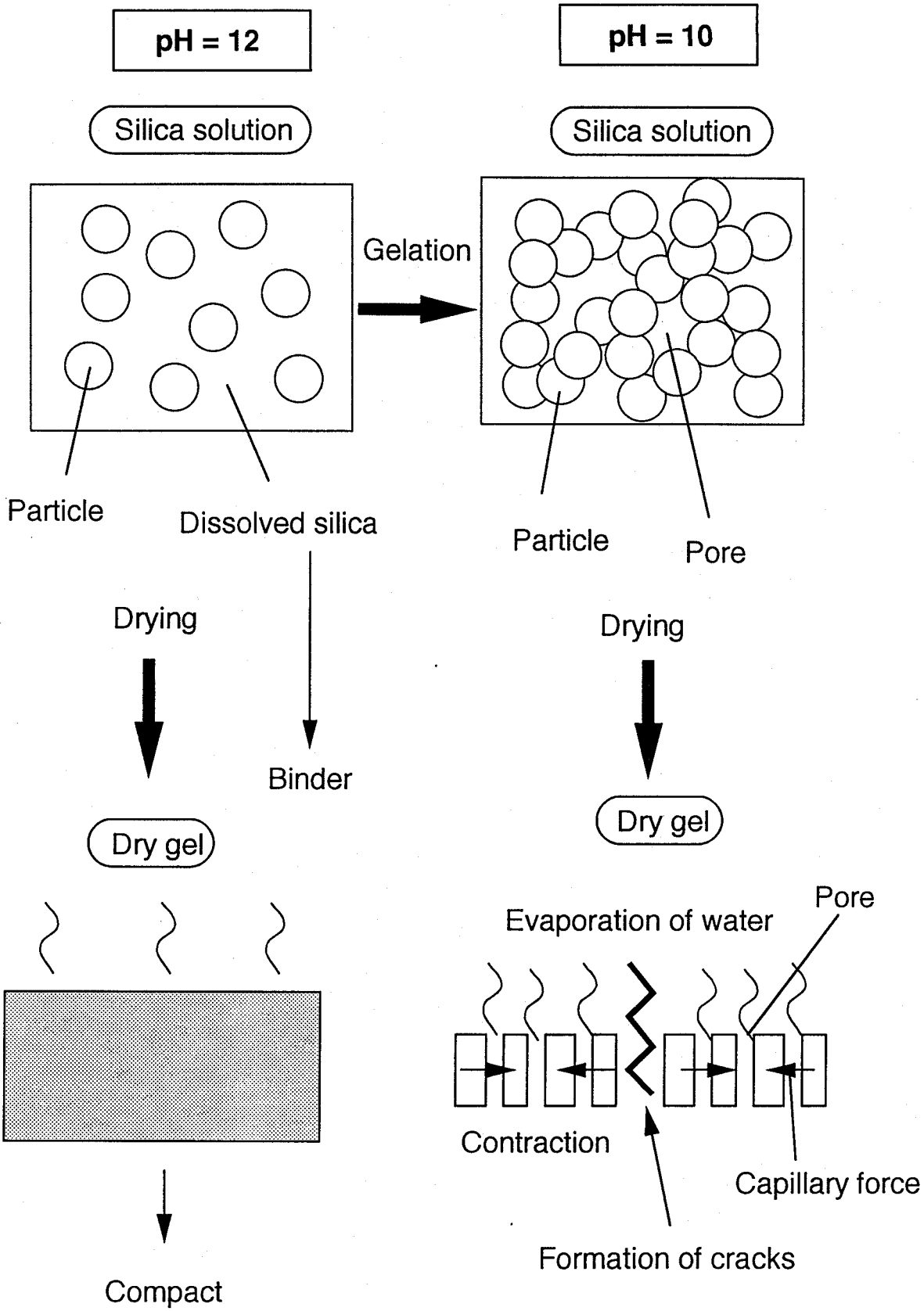

Figure 3.7 Formation mechanism of cracks.

became narrower up to 2 days. In addition, the peak became less asymmetric up to 2 days. Alteration in the shape of peak was difficult to observe with prolonged crystallization. Accordingly, the local order around Al atoms increased up to 2 days. In other words, local crystallization around Al atoms was completed up to 2 days. These results of the ^{27}Al-NMR were in good agreement with those reported by Kim et al. (1993) who prepared MFI under vapors of water alone or a mixture of vapors of dipropylamine and water.

Figure 2.8 presents the variation in the ^{29}Si-NMR spectra with prolonged crystallization. Although a mixed phase of FER and MFI formed after 8.5 days as described above, the shift of peaks was hardly observed. As a result, FER and MFI probably gave the peaks at the same values of chemical shift. This consideration is reasonable because the frameworks of FER and MFI are made of the same subunits. The values of SiO_2/Al_2O_3 ratio were determined by Eq. 2.1 using these spectra as given in **Figure 2.8**. The SiO_2/Al_2O_3 ratio monotonously increased with prolonged crystallization and after 8.5 days reached almost the same value as that of parent gels, 29. From the results of the ^{27}Al-NMR and ^{29}Si-NMR, crystallization starts around Al and then crystallization of a Si-rich phase follows.

Another noteworthy issue was raised by the XRD patterns shown in **Figure 2.5**. The reflection intensities from FER had a maximum and MFI appeared with decreasing FER intensities, i.e., with increasing crystallization time, as has been mentioned before. Taking into account the monotonous increase in the SiO_2/Al_2O_3 ratio with time, it can be deduced that FER partly transformed to MFI.

Table 2.3 listed the values of SiO_2/Al_2O_3 calculated from NMR spectra for the products, ANA in Run 2 and MFI in Runs 6 and 7. At each

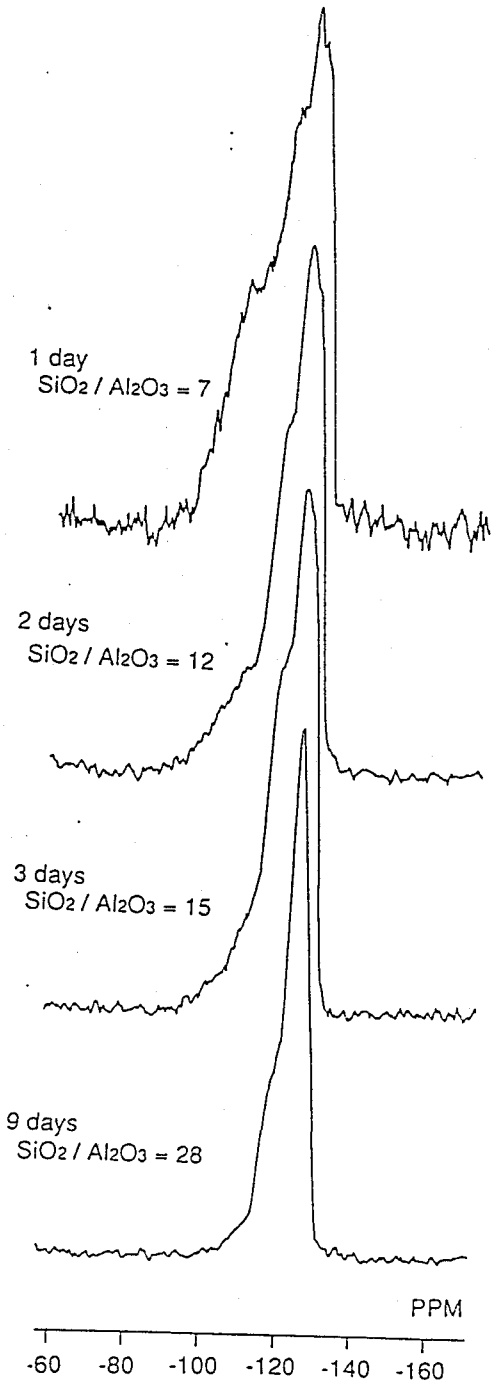

Figure 2.8 Variation in the ^{29}Si-NMR spectrum for solids with different crystallization time. The SiO_2/Al_2O_3 ratio was calculated using the spectra.

Table 2.3 Crystallization results

Run	Product	SiO_2/Al_2O_3	
		Parent gel	NMR[a)]
2	ANA	29	4
6	MFI	26	25
7	MFI	31	30

Compositions were expressed in molar ratio. [a)]The SiO_2/Al_2O_3 was calculated by the ^{29}Si-NMR spectrum.

run, it was confirmed that all of Al atoms were incorporated in the zeolite framework by ^{27}Al-NMR measurements. The SiO_2/Al_2O_3 ratio of the product indicated that dry gel was fully crystallized to MFI. On the other hand, the SiO_2/Al_2O_3 ratio of ANA was inherently 4 and cannot be varied (Szostak, 1992). The result of Run 2 indicated that further crystallization of the rest hardly occurred after formation of ANA.

In hydrothermal synthesis, it is very difficult to fully crystallize Si and Al atoms in the solution (Lechert et al. 1995). On the country, it was confirmed that crystallization of raw materials is completely accomplished in the VPT method. This conclusion gives a promising prospect to improve the productivity in zeolite system.

2.3.5. Effect of substrates on crystallization

Figure 2.9 showed the crystallization results using different supports on which the dry gel was placed in the autoclave. The signal intensity of the (200) reflection from FER and the (501) reflection from MFI were plotted. Both on a Gore-tex film and a Teflon plate, FER was crystallized

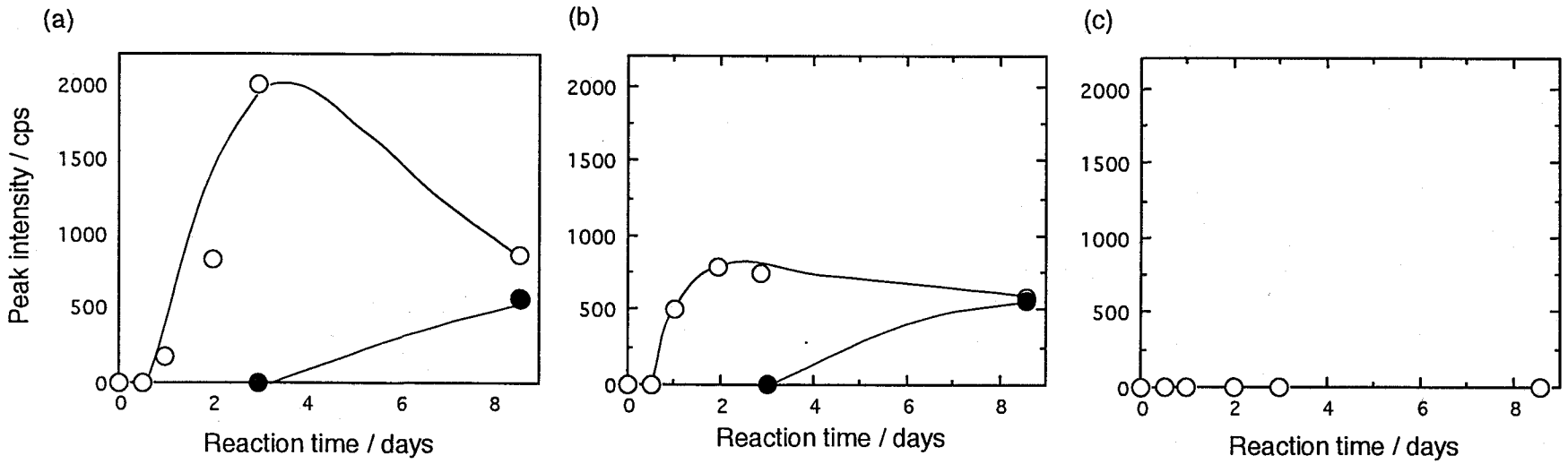

Figure 2.9 Effect of the kind of substrate on crystallization of a dry gel.
Substrate: a) Gore-tex, b) Teflon plate c) paper filter.
Open symbol; FER, solid symbol; MFI.

first after an induction period of about 0.5 day. The intensities of reflection peaks from FER to MFI were observed, as well as crystallization on the polyflon filter. Crystallization was difficult to occur on a filter paper as shown in **Figure 2.9(c)**. On the other hand, OH groups contained in a cellulose substrate were reported to provide the unique sites for the crystallization of zeolites by Sano et al. (1992c) who hydrothermally synthesized MFI on the cellulose substrate. The roles of OH groups are still open question. However, the present results may suggest that the interface between dry gel and support played a key role of initiating crystallization.

2.4. Conclusions

The results in this chapter are summarized as follows:

(1) Various types of zeolite, FER, MFI and ANA and so on, can be produced by the VPT method.

(2) In crystallization of FER by the VPT method, EDA acted as a structure-directing agent and both Et_3N and water encouraged crystallization.

(3) All Al were incorporated in zeolitic framework in the early stage of crystallization and crystallization of a Si-rich phase followed.

(4) Transformation of FER to MFI occurred with prolonged crystallization.

(5) Dry gel can be fully converted to zeolite by selecting appropriate synthetic conditions.

(6) The interface between dry gel and support may play a key role in initiating crystallization.

The present study confirmed the usefulness of the VPT method for production of various zeolites. This synthetic method offers promising

prospects for the synthesis of zeolites possessing the same SiO_2/Al_2O_3 ratio with that of parent gel, and the production of zeolites shaped in advance, as mentioned in the introduction. The VPT method is prospective for the continuous production of zeolites by crystallizing parent gel arranged on a belt conveyer, for instance.

Chapter 3 Synthesis of Zeolitic Membranes by Vapor-phase Transport Method

3.1. Introduction

Zeolites are recognized as attractive materials to prepare inorganic membranes for realizing separation processes at molecular levels because of their molecular sieving properties, thermal resistance, chemical inertness and mechanical strength. Taking into account that zeolites have inherent pore diameter and their physicochemical properties can be modified by ion exchange, fine control of permeability could be expected.

Most of attempts have been made to prepare a zeolitic thin layer by conventional hydrothermal synthetic methods. Another preparation method, vapor-phase transport (VPT) method, originated by Xu et al. (1990) is useful for synthesizing various zeolites as shown in the preceding chapter. One of the main advantages of the VPT method is that it is feasible to prepare membranes even on supports having complicated shapes like honeycombs. In addition, the prepared aluminosilicate gel can be fully crystallized to zeolite by the VPT method. Namely, zeolites with a SiO_2/Al_2O_3 ratio which is the same as that of the parent gel can be synthesized although it is difficult for Si and Al atoms in the solution to crystallize fully (Lechert et al., 1995).

In this chapter, the VPT method is applied to prepare zeolitic membranes on a porous alumina support. A defect-free zeolitic membrane is expected to be formed if a thin layer of dry aluminosilicate gel is formed in a compact form on a porous ceramic support prior to crystallization.

The objective in this chapter is first to explore the synthetic conditions to prepare a compact gel layer on a porous alumina support. The second

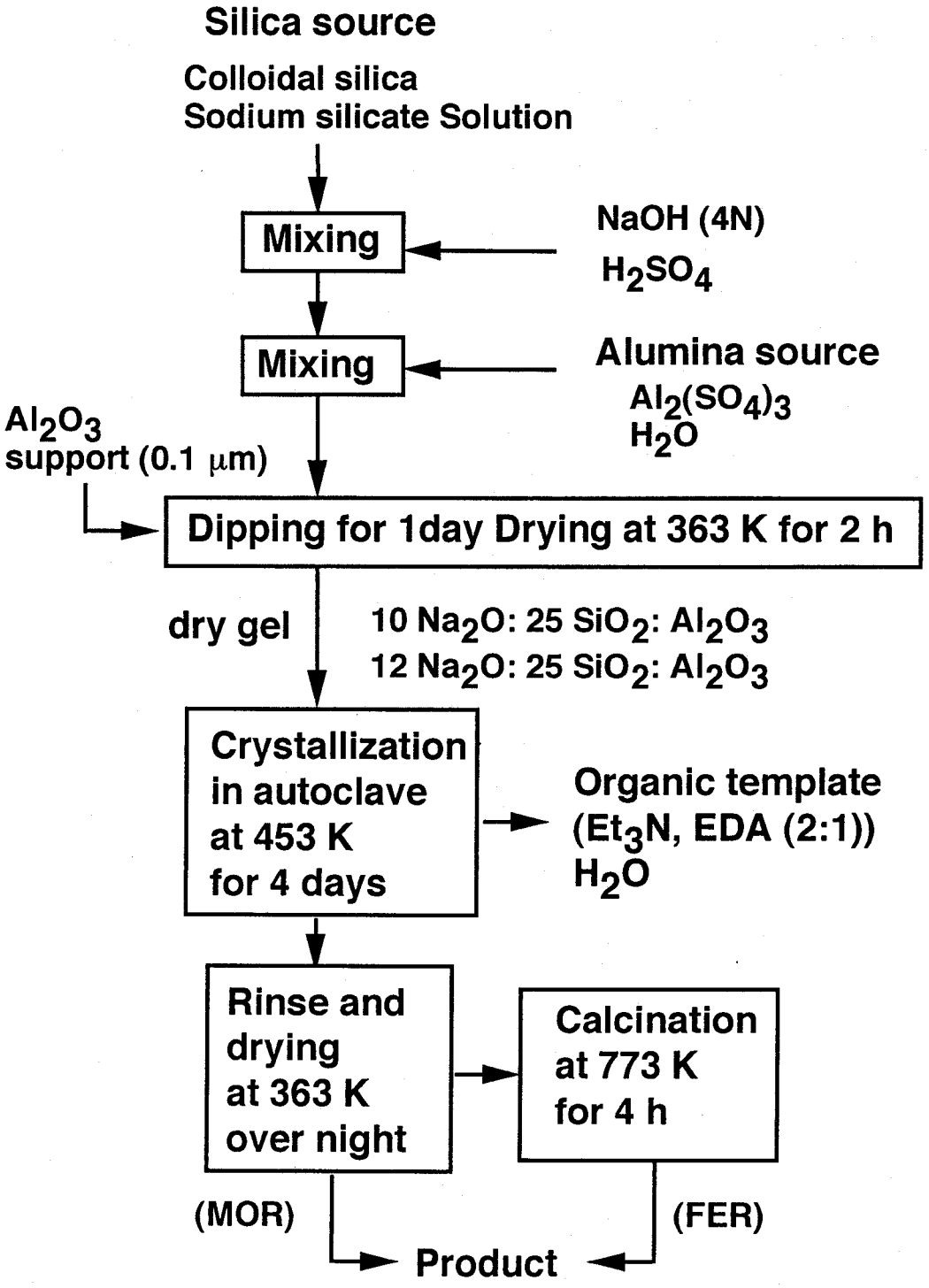

Figure 3.1 Typical preparation method of zeolitic membrane.

objective is to elucidate the factors which govern the structural types of zeolites formed on the porous alumina support by the VPT method. The compactness of the resultant zeolitic membranes was finally examined.

3.2. Experimental

3.2.1. Preparation of parent gel

Figure 3.1 shows typical preparation procedure for zeolitic membranes. Two types of parent aluminosilicate gels were prepared using different silica sources: colloidal silica containing 30.3 wt% of SiO_2 and 0.42 wt% of Na_2O (ST-S; Nissan Chem. Ind., Ltd.) and sodium silicate solution containing 35-38 wt% of SiO_2 and 17-19 wt% of Na_2O (Kanto Chem. Co., Inc.). Aluminum sulfate anhydride, $Al_2(SO_4)_3$, (Wako Pure Chem. Ind. Co., Ltd.) was used as alumina source. Aqueous solutions of NaOH and H_2SO_4 were added to colloidal silica and sodium silicate solution, respectively. The quantity of NaOH or H_2SO_4 added to the silica source determined the pH of a resultant gel. The silicate gel was mixed with an $Al_2(SO_4)_3$ aqueous solution. The composition of the mixture was x Na_2O: Al_2O_3: 25 SiO_2 (x= 10 for the gel using colloidal silica and x= 12 for the gel using sodium silicate solution).

A porous α-alumina support with an average pore diameter of 0.1 μm (Nihon gaishi Co., Ltd.) was used. In some case, the surface of the alumina supports was treated with colloidal silica with pH of about 10. Two types of dipping method were examined for the preparation of FER membranes. First, the porous alumina support was dipped in a gel for 1 day, as shown in **Figure 3.2(a)**. In the second method, after dipping the support in the gel for 1 day, the gel was forced to penetrate into the pores of the alumina support by evacuating the support from one side, as shown in **Figure 3.2(b)**. Hereafter the FER membranes synthesized by the

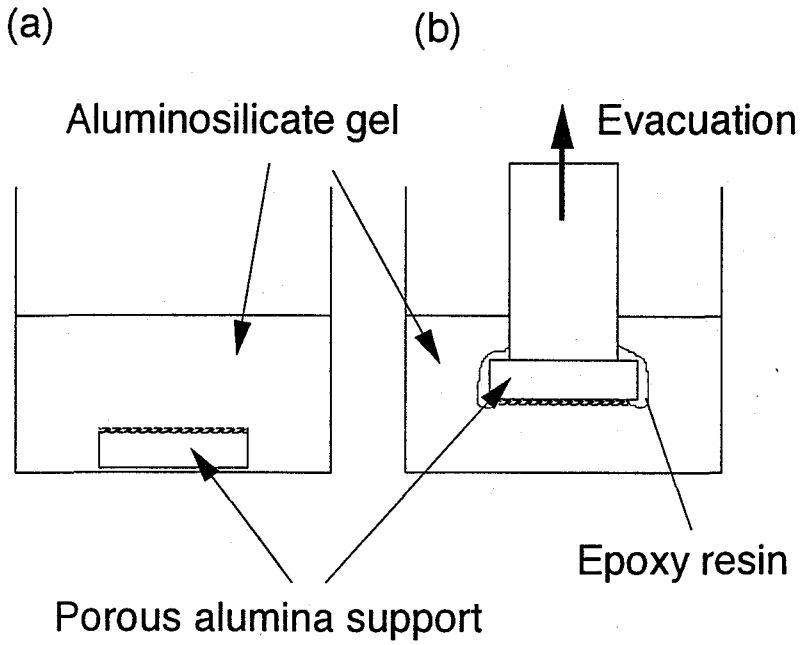

Figure 3.2 Dipping method.

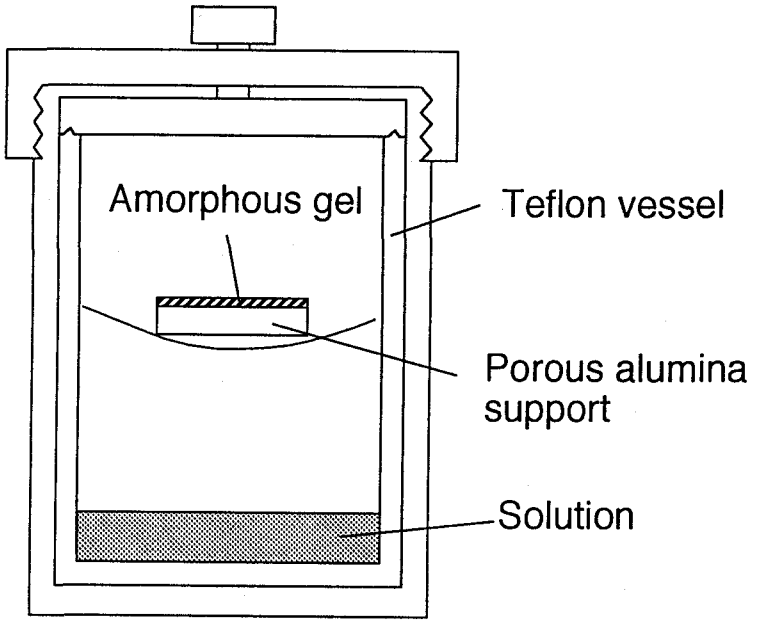

Figure 3.3 Schematic diagram of special autoclave for the vapor-phase transport synthesis.

dipping methods (a) and (b) is called FER membranes (a) and (b), respectively. For the synthesis of zeolitic membranes except FER membranes, only the method (a) was used for dipping of the support.

The specific surface area of dry gel was measured by the BET method using N_2 adsorption at 77 K (Simadzu, Flowsorb II2300).

3.2.2. Crystallization by vapor-phase transport method

After Et_3N, EDA and water as vapor source were poured into the bottom of an autoclave, the alumina support coated with the aluminosilicate dry gel was set horizontally in the autoclave, as shown in **Figure 3.3**. The gel was crystallized in the mixed vapors of Et_3N, EDA and water under autogeneous pressure at 453 K for 4 days.

An as-synthesized FER membrane was calcined in air at 773 K for 4 h using a temperature-programmed pattern shown in **Figure 3.4**. Heating

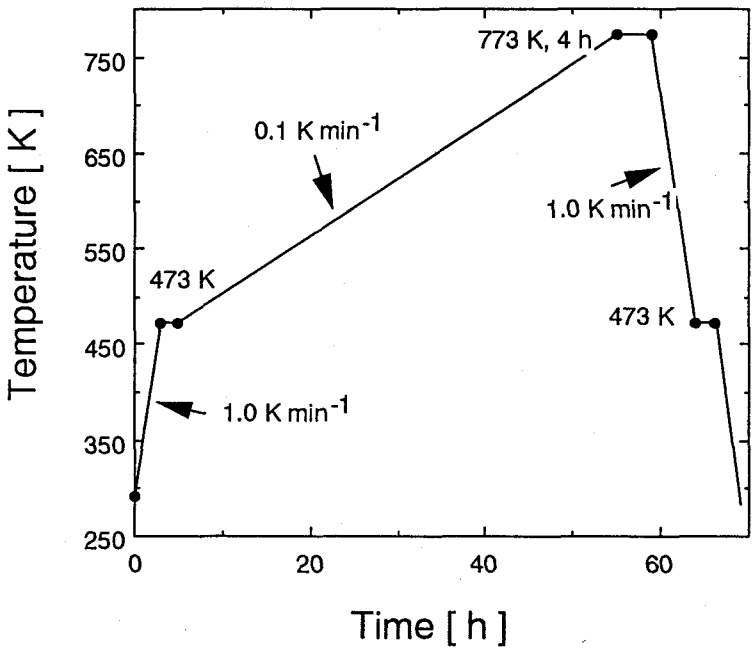

Figure 3.4 Temperature-programmed pattern for calcination.

rate should be as small as possible because high heating rate possibly causes the formation of cracks in the FER membrane during calcination due to the difference in the thermal expansivity between FER and α-alumina support. The heating rate of 0.1 K min^{-1} was adopted in the temperature range of 473 -773 K.

The product was identified by X-ray diffraction (XRD) with Cu Kα radiation on a Simadzu VD-1. The surface and cross-section of the membrane were characterized by scanning electron microscopy (SEM, Hitachi, S-800) using Au-coated samples.

3.2.3. Evaluation of the compactness of zeolitic membranes

The compactness of zeolitic membranes was checked by the pervaporation of 1,3,5-triisopropylbenzene (TIPB) at room temperature. **Figure 3.5** shows a schematic diagram of the experimental apparatus for

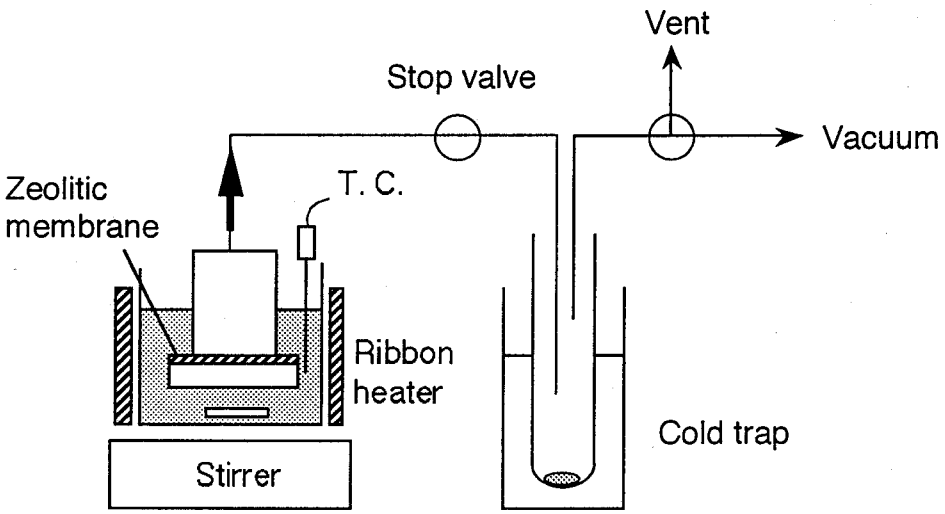

Figure 3.5 Schematic diagram of the experimental apparatus for pervaporation tests.

pervaporation tests using zeolitic membranes. The zeolitic membrane, attached on an end of a stainless tube with a cross sectional area of 2.2 cm^2, was placed in liquid TIPB. The permeation side was kept under vacuum. The permeant was collected for 10 h in a cold trap using liquid nitrogen and analyzed by a gas chromatograph with a flame ionization detector.

3.3. Results and discussion

3.3.1. Preparation of compact gel

A compact dry amorphous gel is required to be formed on the support prior to crystallization for the preparation of zeolitic membranes in a compact form.

Formation of cracks was observed visually in the course of a drying process even at room temperature when the gel with a pH of 11 had been

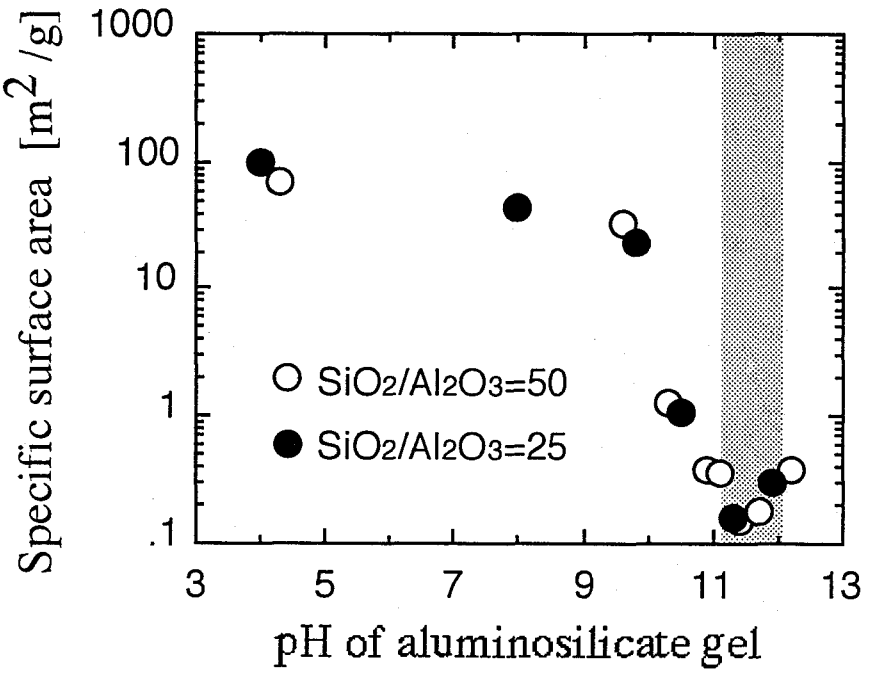

Figure 3.6 Effect of pH of at which gel was prepared on its specific area.

applied on the alumina support. Moreover, the gel which had been prepared at pH of 10 easily scaled off the alumina support during a drying process. The pH of gel seemed to influence its compactness. **Figure 3.6** shows the specific surface area of aluminosilicate gel dried at 363 K overnight as a function of pH at which the gel was prepared. The compactness of gel can be evaluated by its specific surface area. When the gel becomes more compact, the specific surface area should become smaller because compact gel possesses few microvoids. The specific surface areas of the both dry gels with SiO_2/Al_2O_3 of 25 and 50 exhibited the same pH dependence. The specific surface area largely decreased with increasing

Table 3.1 Effect of pH at which gel was prepared on the surface area and the compactness of the dry gel film on a glass plate

Silica source	SiO_2 / Al_2O_3	pH	Specific surface area [m^2 g^{-1}]	Compactness
Sodium Silicate Solution	50	11.66	0.21	good
		11.45	0.27	poor
	25	11.82	0.20	good
		11.58	0.43	poor
		11.28	5.22	poor
Colloidal Silica	25	12.13	0.11	good
		11.81	0.16	poor
		11.54	0.20	poor

SiO_2 / Na_2O = 2.1.

pH in the range of 9.5-11.5, indicating that the dry gel became compact when the gel had been prepared at pH greater than 11.5. Further details of the pH dependence were studied using gels prepared at pH of 11.0-12.0. A glass plate was dipped in a gel prepared at a given pH and room temperature. The resultant gel film on the glass plate was dried at 363 K for 1 h. Compactness of the film was visually evaluated as listed in **Table 3.1**. When sodium silicate solution was used, a compact continuous film with SiO_2/Al_2O_3 ratio = 50 was obtained on the glass plate at pH =11.66, while numerous cracks were visually observed on the gel film prepared at pH =11.45. A continuous compact film with SiO_2/Al_2O_3 ratio = 25 was similarly obtained using the sodium silicate solution at pH =11.82. A value of pH, 12.13, was required for the formation of a continuous compact film when colloidal silica was used.

Table 3.1 lists the specific surface area of dry gels which were prepared at different pH values. As discussed above, the specific surface area of each dry gel decreased with increasing pH, indicating that a dry gel became denser at higher pH. Judging from the results of visual observations, compact films were prepared under the conditions where gels became as dense as possible. Thus it is essential to control the value of pH precisely for obtaining a compact continuous layer of dry amorphous gel on a support.

In general, both dissolved silica and silica particles coexist in a silica solution. Alexander (1967) reported that with decreasing pH from 12 to 10, the content of dissolved silica in a silica solution dramatically decreased and particles formed instead. He measured the specific surface area and pore volume of silica after drying, and found that both their specific surface area and pore volume increased with decreasing pH of gel from 12 to 10. A larger amount of dissolved silica was transformed into particles during

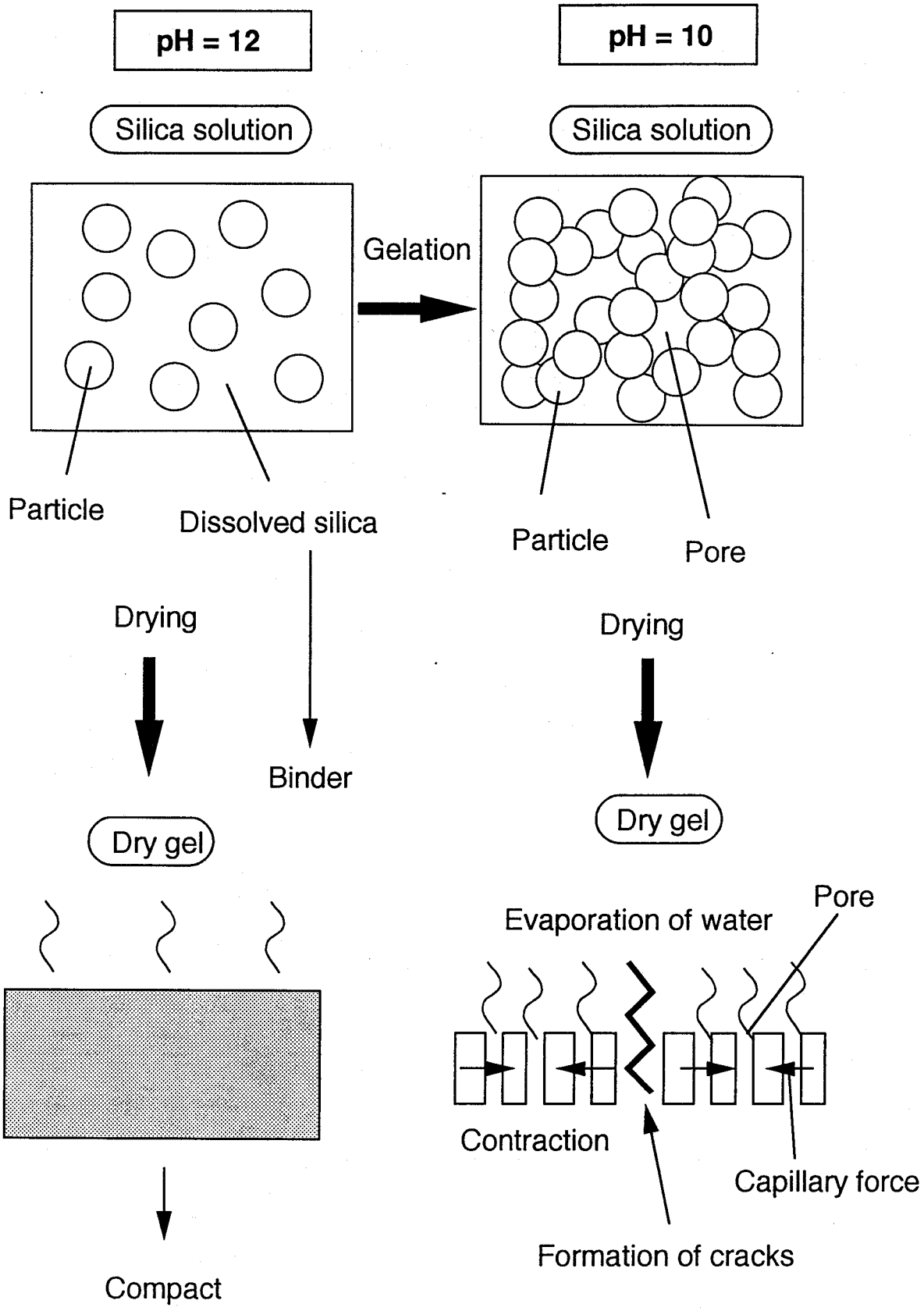

Figure 3.7 Formation mechanism of cracks.

gelation of a silica solution at lower pH. The gel prepared at higher pH becomes compact, because the dissolved silica acts as a binder of the particles during drying. The specific surface area of aluminosilicate gels, similarly to silica gel reported by Alexander, dramatically decreased with increasing pH when pH > 10 as seen in **Figure 3.6**. **Figure 3.7** schematically summarizes a formation mechanism of cracks deduced from Alexander's and the present results. When water evaporates from the pores within an aluminosilicate gel, the gel greatly contracts due to the capillary force. As a result, cracks were formed in the gel during a drying process. In conclusion, a compact gel can be prepared using a silica solution containing a sufficient amount of dissolved silica.

3.3.2. Synthesis of zeolitic membranes

Aluminosilicate gels were prepared at pH =11.7 and 12.0 using sodium silicate solution and colloidal silica, respectively. Under these conditions, a continuous gel layer was formed on a porous alumina support after drying. **Table 3.2** summarizes the typical results of crystallization of the

Table 3.2 Synthesis of zeolitic membranes on porous alumina support with and without surface treatment

	Silica source	pH	Products
No treatment	Sodium silicate solution	11.7	ANA
	Colloidal silica	12.0	MOR
Surface treatment	Sodium silicate solution	11.7	FER
	Colloidal silica	12.0	MFI
On Teflon plate	Sodium silicate solution	11.7	FER
	Colloidal silica	12.0	MFI

aluminosilicate gels on the alumina support. The results on a Teflon plate are tabulated together. It should be noted that products obtained on the alumina support were different from those on the Teflon plate. When one uses sodium silicate, analcime (ANA) was obtained on the alumina support while FER was formed on the Teflon plate. For colloidal silica, mordenite (MOR) was obtained on the alumina support, while MFI was formed on the Teflon plate, respectively. The SiO_2/Al_2O_3 ratios of ANA and MOR are generally lower than those of FER and ZSM-5 (MFI): The SiO_2/Al_2O_3 ratios of ANA and FER are about 4 and 15-20, respectively. Those of MOR and MFI are 8-20 and more than 20, respectively. The result that SiO_2/Al_2O_3 ratio of zeolites formed on a Teflon plate is much higher than that on an alumina support is attributed to the dissolution of alumina support and its incorporation into the framework of zeolite. Geus et al. (1992) similarly observed partial dissolution of an alumina support during hydrothermal synthesis of zeolitic membrane. They claimed that the Si/Al ratio of the product after hydrothermal treatment decreased from 100000 (parent gel) to 5 (ANA) owing to the Al leaching from the alumina support.

The surface treatment of the support was carried out using colloidal

Table 3.3 Flux of 1,3,5-triisopropylbenzene through zeolitic membranes synthesized by a vapor-phase transport method

	Temperature [K]	Flux [mol m^{-2} s^{-1}]
MOR	300	$< 1.0 \times 10^{-9}$
FER(a) *1	291	1.0×10^{-7}
FER(b) *2	303	$< 1.0 \times 10^{-9}$

*1) before calcination *2) after calcination at 773 K.

silica with a pH of about 10 to depress the dissolution of alumina. The alumina support was dipped in colloidal silica for 1 day and then dried to form a thin silica layer on the alumina support. The aluminosilicate gels on the support coated with silica were crystallized to FER and MFI using the sodium silicate solution and colloidal silica, respectively. As seen in **Table 3.2**, these results were the same as those for the Teflon plate.

3.3.3. Evaluation of compactness of zeolitic membranes

The pervaporation of TIPB, which has a kinetic diameter (0.85 nm) greater than the pore dimensions of FER (0.42 x 0.54 nm) and MOR (0.65 x 0.70 nm), was carried out for 10 h at room temperature using the MOR membrane, FER membranes (a) before calcination and (b) after calcination. The FER membranes (a) and (b) correspond to the membranes synthesized by the dipping methods (a) and (b), respectively, as described before. **Table 3.3** compares the fluxes of TIPB through the MOR and FER membranes.

No permeation of TIPB through the MOR membrane was detected by a gas chromatograph, which means that the flux of TIPB was less than 1.0×10^{-9} mol m^{-2} s^{-1}, the minimum flux which can be determined in the experimental procedure used in this study. Therefore, it is concluded that in the MOR membrane there practically existed no pinhole greater than the molecular dimension of TIPB.

The permeation of TIPB was detected for the FER membrane (a) before calcination. The flux of TIPB was 1.0×10^{-7} mol m^{-2} s^{-1}, indicating that the membrane (a) possessed cracks. While, permeation of TIPB through the FER membrane (b) was not detected by a gas chromatograph even after calcination, which means that the flux of TIPB was less than

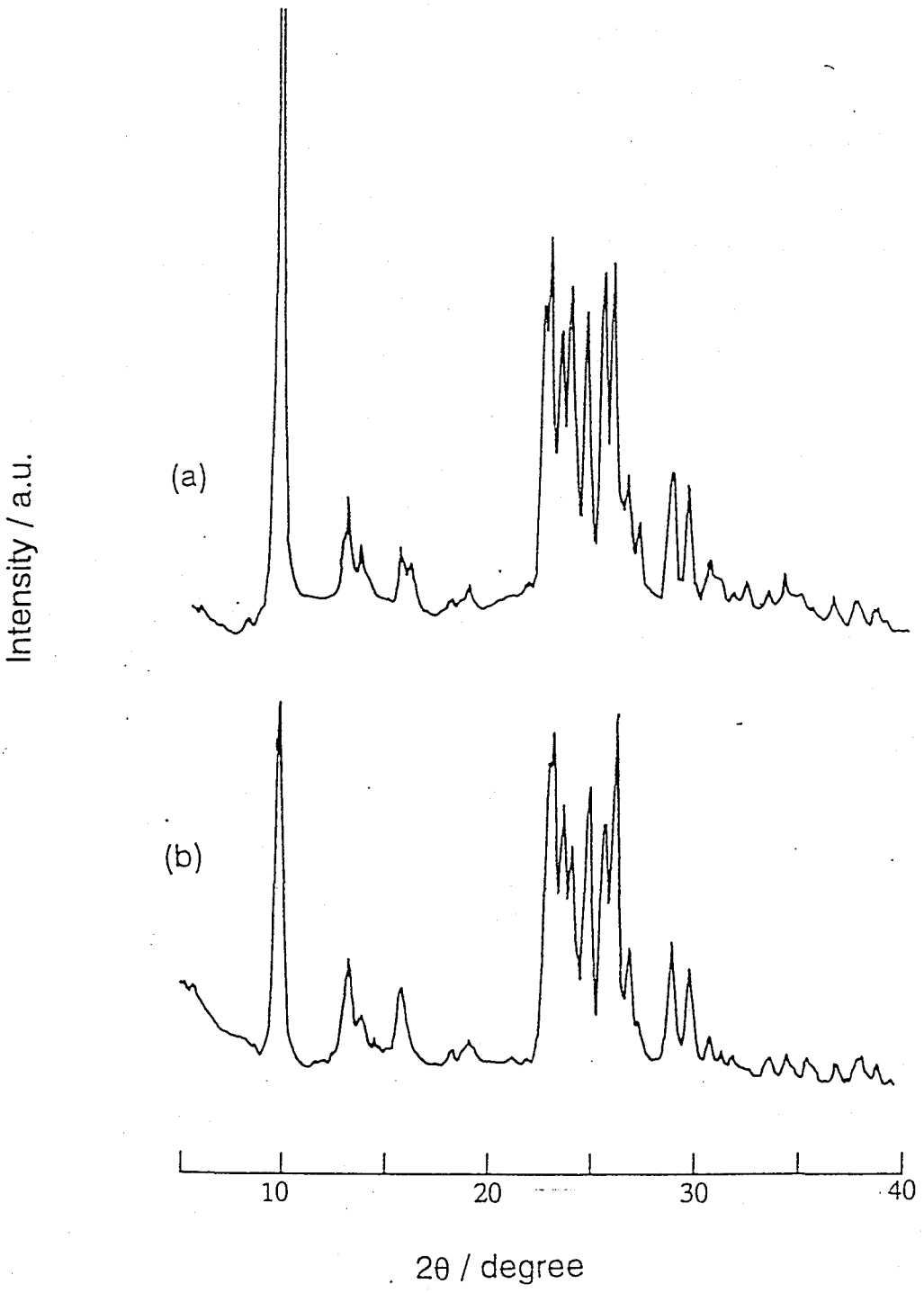

Figure 3.8 XRD patterns of (a) FER membrane on a porous alumina support and (b) FER in a powdery form.

$1.0x10^{-9}$ mol m^{-2} s^{-1}. Therefore, it is also believed that in FER membrane (b) there practically existed no pinhole greater than the molecular dimension of TIPB. In conclusion, a forced penetration of a gel into an alumina support was necessary to obtain a defect-free FER membrane.

3.3.4. Morphology of zeolitic membranes

Figure 3.8(a) shows the XRD pattern for the FER membrane (a) before calcination. No amorphous phase was observed in the XRD pattern for the FER membrane (a). The XRD pattern for FER powder synthesized by the VPT method is shown in **Figure 3.8(b)**. Comparison of these two XRD patterns confirmed that randomly-oriented polycrystalline FER was formed on the alumina support. Since the XRD pattern for the FER membrane (b) was similar to that for the FER membrane (a), the macroscopic structure of these two FER membranes seem to be similar to each other.

The XRD pattern for MOR membrane was also similar to that from common powder MOR (Szostak, 1992), indicating that randomly-oriented polycrystalline MOR was formed on the alumina support.

Figure 3.9 shows the SEM images of the top views of the ANA, MOR, FER and MFI membranes before calcination. Each image shows a typical morphology of each zeolite crystal. The top layer of zeolitic membranes consisted of randomly-oriented polycrystals. The plate-like FER crystals on the alumina support were similar in shape to that of the FER powder as shown in **Figure 2.6**. Although the FER and MOR membranes were defect-free as described in the previous section, numerous voids were observed among zeolite particles on the alumina support. The top views of zeolitic layers which formed on the surface of the alumina support were clearly incompact.

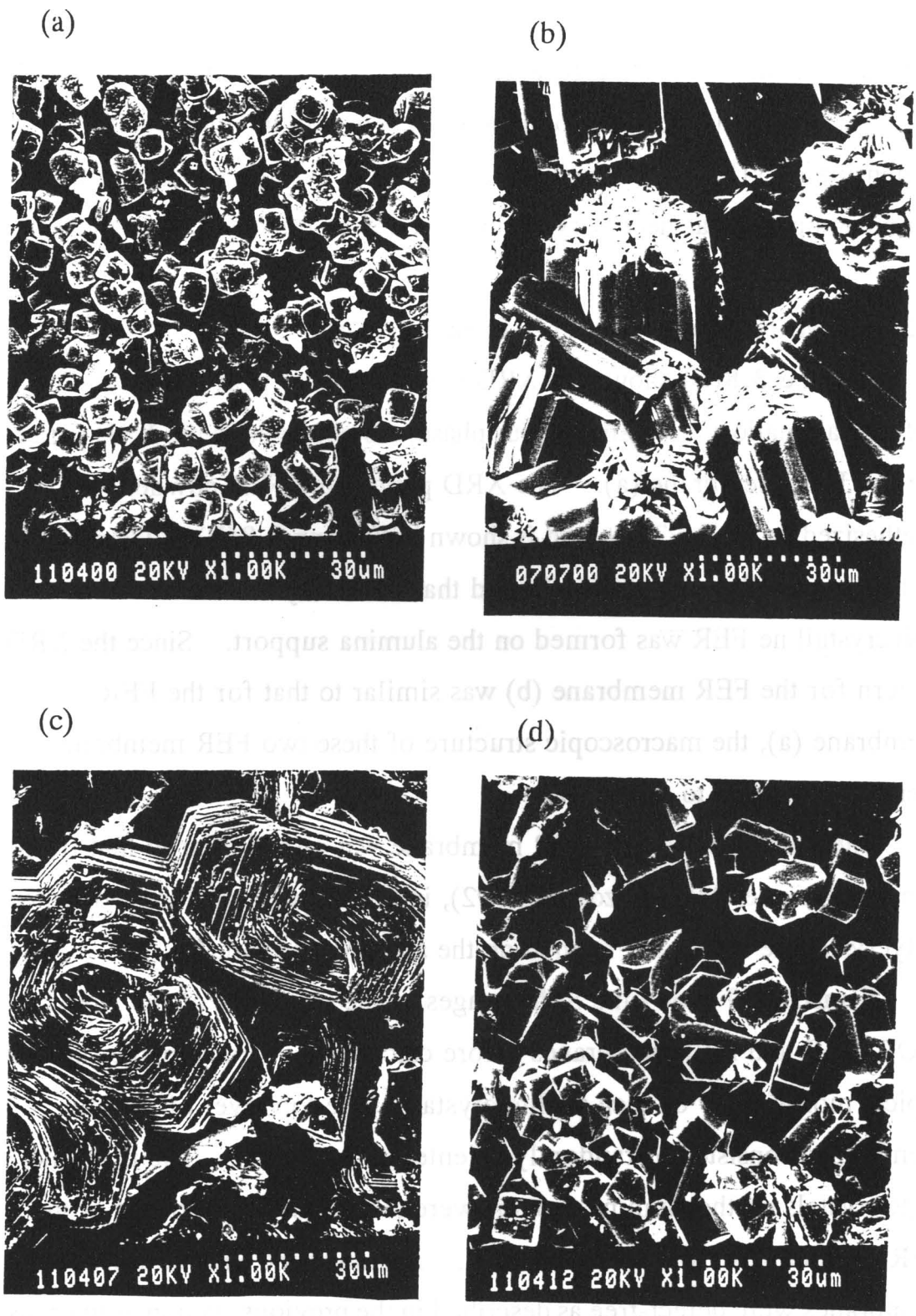

Figure 3.9 SEM images of the top views of zeolitic membranes. (a) ANA, (b) MOR, (c) FER and (d) MFI membranes.

Figure 3.10 gives the SEM images of the cross-sectional views for the MOR and FER membranes. By comparing the cross-sectional view of the fresh support (**Figure 3.10(a)**) with the zeolitic membranes (**Figures 3.10(b)** and **(c)**), a continuous layer showing dark contrast in the alumina support was observed in **Figures 3.10(b)** and **(c)**: that was hard to be observed in **Figure 3.10(a)**. It is supposed that a composite layer consisting of porous alumina and zeolites was formed, taking into account that no amorphous phase was observed in the XRD pattern of the zeolitic membrane. Thus, the zeolite-alumina composite layer is believed to be compact. The thickness of the continuous layer showing dark contrast was about 20 μm for the MOR membrane and 40 μm for the FER membrane. The SEM image of the MOR membrane indicates that gel was penetrated into the alumina pores even using the dipping method (a) without suction.

However, these XRD patterns and SEM images do not give conclusive evidence that the zeolite crystals formed in the pore of alumina. Details will be discussed in the next chapter.

Jansen et al. (1994) and other researchers (Geus, 1992,1993; Tsikoyiannis and Haag, 1992; Yan, 1995) pointed out that the intergrowth of crystals formed on the surface of support is essential to obtain a defect-free zeolitic membrane in the hydrothermal synthesis. The morphological feature of the zeolitic membranes prepared by the VPT method was different from their membranes prepared in the conventional hydrothermal synthetic method. The formation process of the zeolite-alumina composite layer will be discussed in the next chapter.

3. 4. Conclusions

(1) A high pH around 12 of the gel was required for the preparation of the continuous dry gel in a compact form.

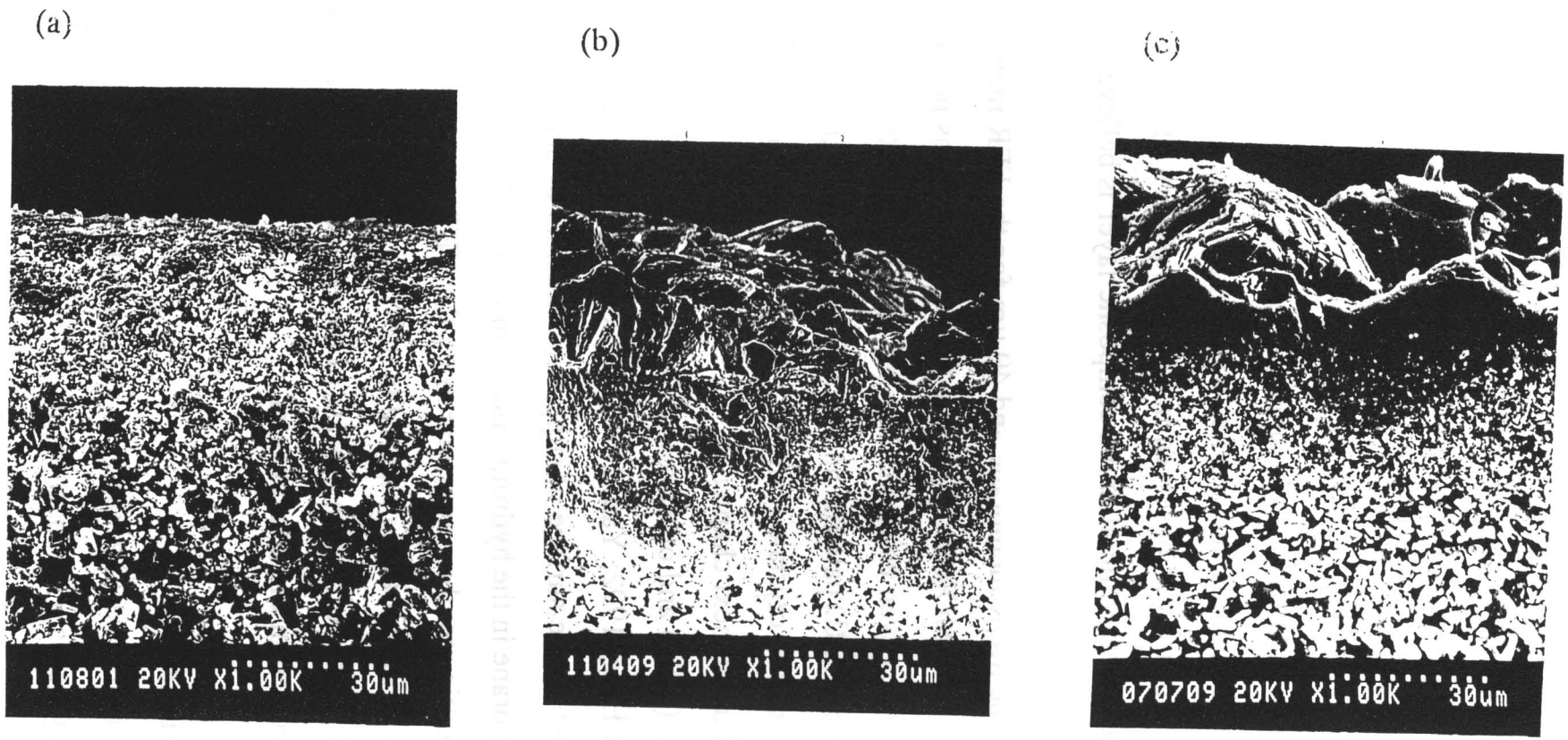

Figure 3.10 SEM images of the cross-sectional views of (a) alumina support, (b) FER membrane and (c) MOR membrane.

(2) Membranes of low silica zeolites, analcime (ANA) and mordenite (MOR), were formed because alumina was partly dissolved and incorporated into the framework of zeolite. Coating of the alumina support with colloidal silica depressed the dissolution of alumina.

(3) The compactness of the MOR and FER membranes was confirmed by the pervaporation test of TIPB. Since no permeation of TIPB was detected, it was concluded that there existed no pinholes and cracks in the zeolitic membranes. The gel in the alumina pore seemed likely to be crystallized to zeolite in a compact form.

(4) A forced penetration of a gel into an alumina support was necessary to obtain a defect-free FER membrane.

Chapter 4 Formation Process of Zeolitic Membrane

4.1. Introduction

Many formation processes of zeolitic membranes have been proposed. **Figure 4.1** shows the formation process of an ZSM-5 (MFI) membrane proposed by Sano et al. (1992b). The MFI zeolite membrane was formed through a successive accumulation of large zeolite crystals of 5 to 10 μm size and followed by a filling pores of voids among the large crystals with microcrystals.

Myatt et al. (1992) proposed four types of formation mechanisms of zeolitic membranes as dipicted in **Figure 4.2**.

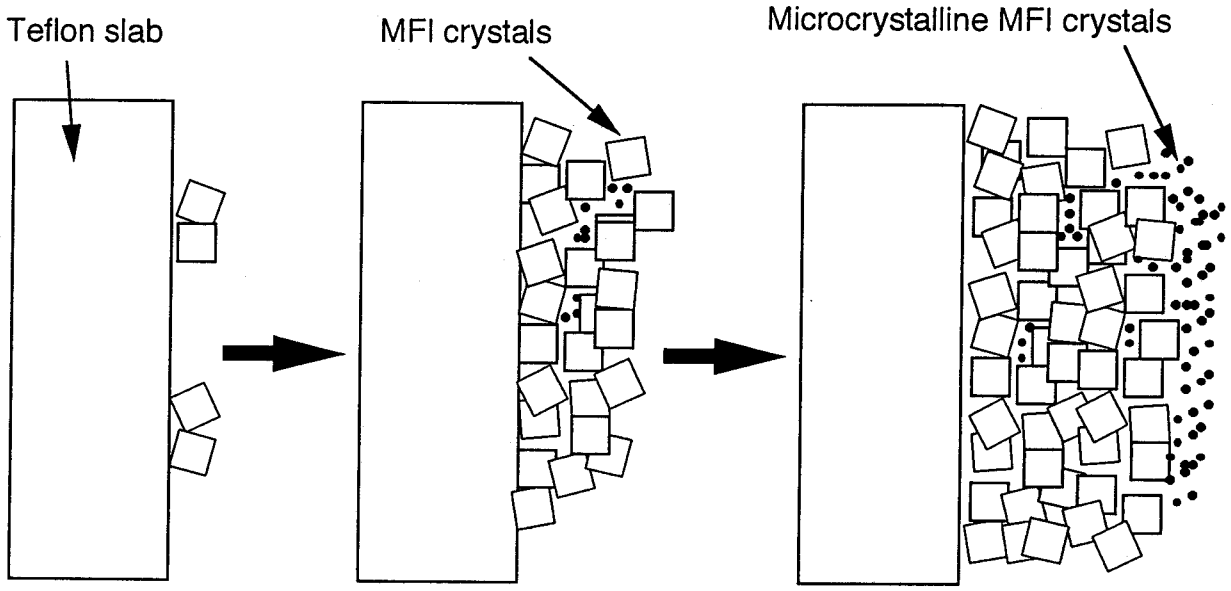

Figure 4.1 Schematic growth process of MFI membrane. [Sano et al., 1992b]

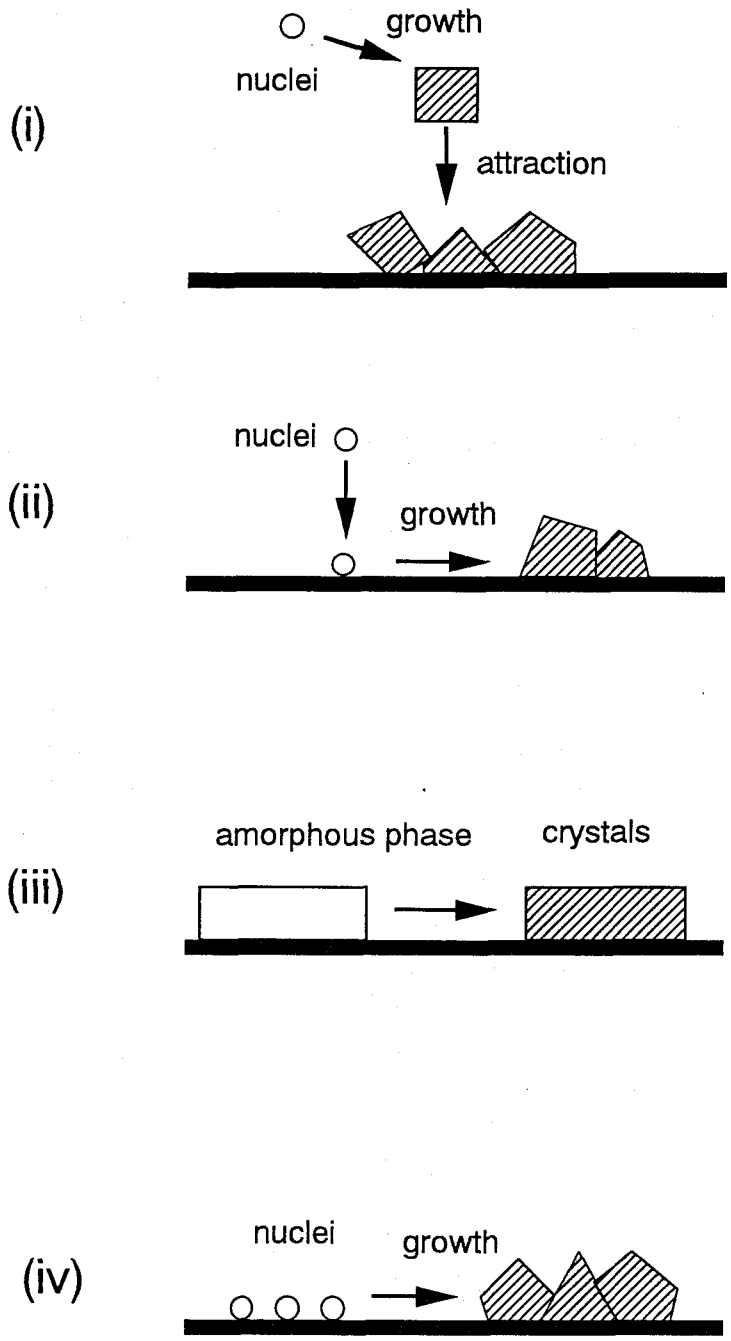

Figure 4.2 Formation mechanism of zeolitic membrane. [Myatt et al., 1992]

(i) Production of nuclei and growth of crystals in the bulk solution followed by their attraction to, or collision and association with the substrate.

(ii) Production of nuclei in the bulk solution, but diffusion to, and accumulation at the support before significant growth has occurred.

(iii) Diffusion of colloidal amorphous aluminosilicate to, and concentration at the substrate, providing more favorable conditions of nucleation and growth in the vicinity of the substrate.

(iv) Production of nuclei on the substrate surface, followed by growth.

They synthesized self-supporting LTA membranes on a polyethylene substrate from a clear solution with a composition of 50 Na_2O: 5 SiO_2: Al_2O_3: 1000 H_2O. In their system *in situ* observation is possible under crystallization, because a pressurized apparatus is not required for the preparation of LTA type zeolite. A clear solution which contained no precipitate became slightly cloudy after crystallization for 18 h. After crystallization for 24 h, a deposit was observed on the polyethylene substrate. The clouding was always observed prior to a deposition of LTA. Thus they concluded that the LTA membrane was formed by the mechanism (i).

Valtchev et al. (1995) reported on the growth of MFI and FAU (Y type) zeolites on a copper substrate. There are three stages of film growth: initial nucleation on the substrate, a linear increase in crystal size, and saturation of film growth, which are similar to the formation mechanism (iv) described above.

The formation process proposed by Kita (1995) is that a gel layer is formed on the surface of the support at first and then the gel layer is crystallized, which corresponds to the mechanism (iii).

The MFI crystals prepared by Jansen et al. (1994) were oriented

parallel to the b-direction, and the straight channels of the pore system were perpendicular to the support surface. They studied the crystallization process of MFI particles and membranes in detail and proposed a novel formation mechanism of the oriented MFI membranes. According to an *in situ* observation of a synthesis, without supports, large gel spheres are formed during crystallization. Infrared and elemental analysis indicated that no TPA ions were present in the gel phase. Therefore the crystallization started at the interface of gel spheres and liquid phase, as shown in **Figure 4.3**. Crystals with smooth rounded top faces, caused by kinetic roughening under the high supersaturation prevailing, were formed.

As the MFI-crystals on support show smooth rounded top faces and a gel layer was observed on support prior to the crystallization, they concluded that a similar growth process occurred. Thus the MFI crystals nucleated at the interface of gel phase formed on the support and the liquid. This is similar to the mechanism (iii).

As soon as the crystal touched the support surface, the support surface was attracted with the ac-plane, the largest plane of the crystal. The crystals then became laterally oriented to the support surface.
Many researchers (Tsikoyiannis and Haag (1992); Jia et al. (1993); Yan et al. (1995a)) observed intergrowth of zeolite crystals by scanning electron micrograph, and Yan et al. proposed that the intergrowth of zeolite crystals is required for the synthesis of a compact zeolitic membranes under hydrothermal conditions.

Amorphous dry gels on a porous alumina support were crystallized by a vapor-phase transport (VPT) method in the previous chapter. The ferrierite (FER) and mordenite (MOR) membranes were confirmed to be defect-free because no permeation of 1,3,5-triisopropylbenzene (TIPB) was detected. Although the top layer of the zeolitic membranes on the alumina

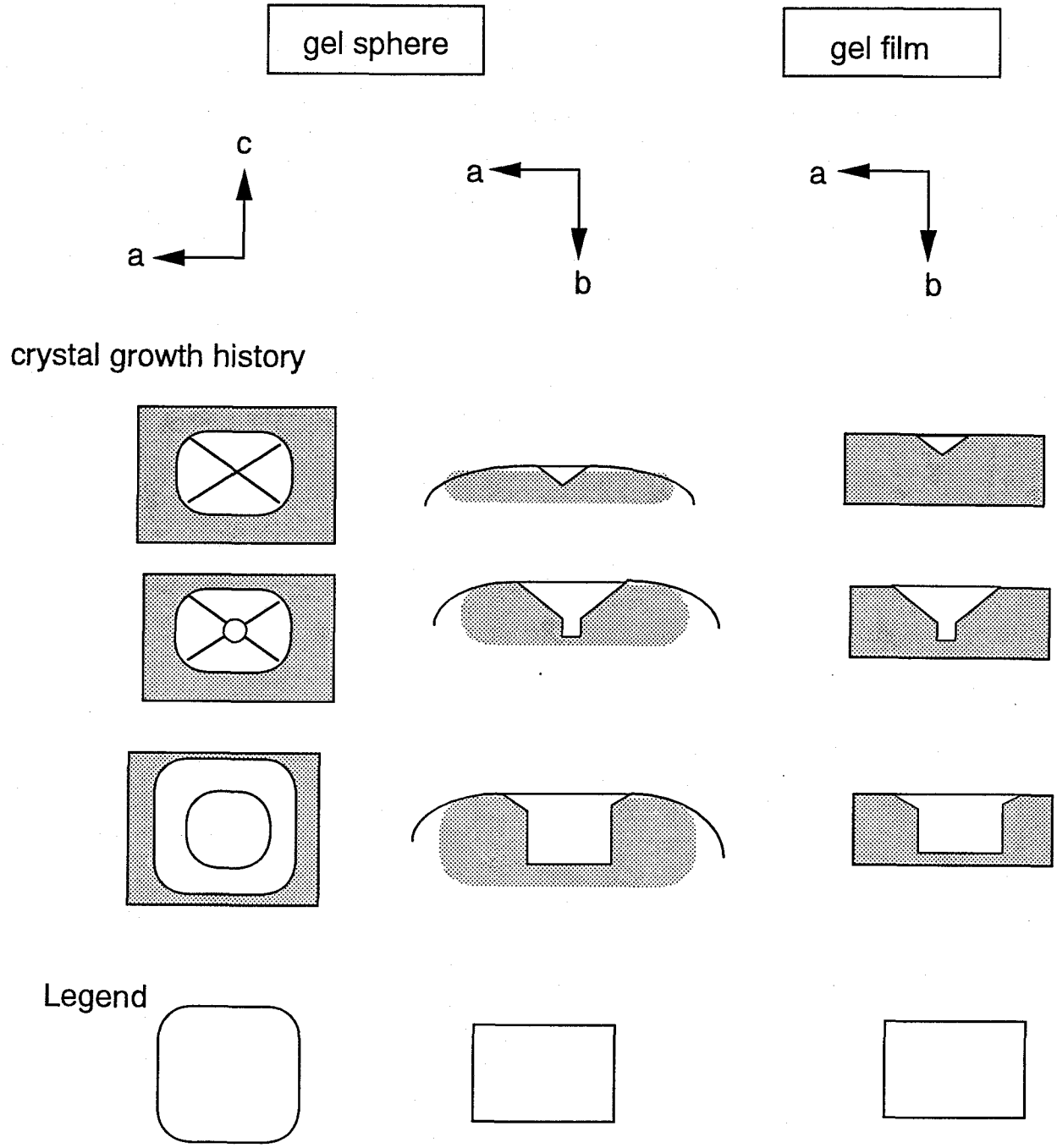

Figure 4.3 Comparable events of MFI crystallization in free gel spheres and supported gel film. [Jansen et al., 1994]

support had numerous voids, continuous layers showing dark contrast were observed in the SEM images of the cross-sectional views for the zeolitic membranes. These continuous layers were thus believed to be compact. However, these SEM images does not give conclusive evidence that zeolite crystals formed in the pores of alumina support. In addition, the formation process of zeolite-alumina composite layer is still open questions. The objective in this chapter is to observe the morphology of zeolitic membranes in detail and their formation process.

4.2. Experimental

The FER and MOR membranes were prepared on a porous alumina support by the VPT method in the same manner as shown in section 3.2.

The structure and crystallinity of the products were determined by X-ray diffraction (XRD) with Cu Kα radiation (Simadzu VD-1 and Philips X's Pert-MRD).

The morphology of the products was examined by scanning electron microscopy (SEM) (Hitachi S-800 and S-2250). Field Emission SEM (FE-SEM) (Hitachi S-5000L) was also used for characterization.

Concentration profiles for Si and Al were measured by energy-dispersive X-ray analysis (EDX, Philips, EDAX DX-4) attached to the SEM (Hitachi, S-2250N).

4.3. Results and discussion

4.3.1. Morphology of zeolite-alumina composite layer

1. FER membrane

For the purpose of clarifying the growth of FER in the pores of the alumina support after crystallization, FER particles formed on the surface of the alumina support were removed by polishing with sand paper.

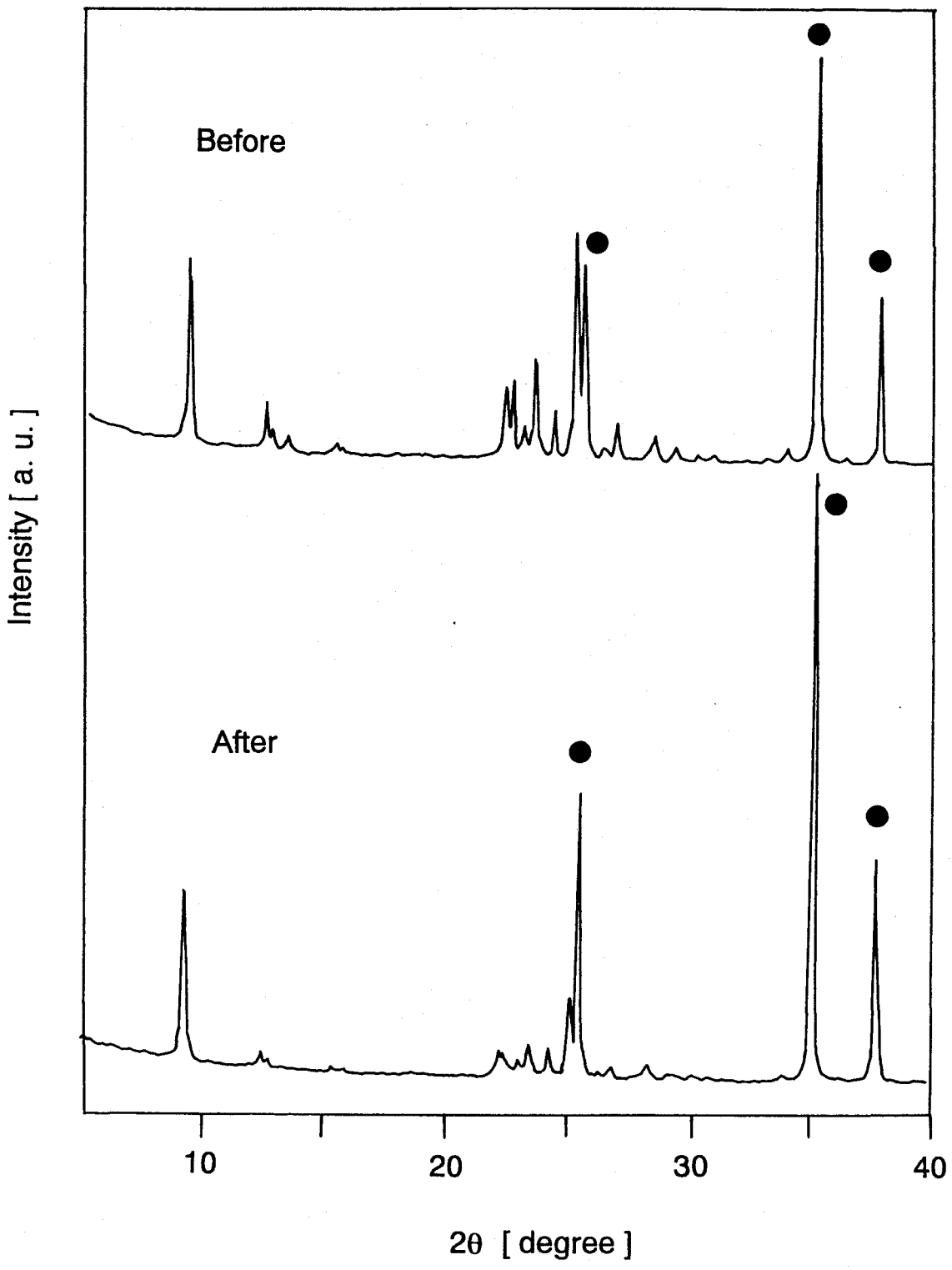

Figure 4.4 XRD patterns for FER membranes (a) before and (b) after removal of FER particles on alumina support. Solid symbol, alumina.

Figures 4.4 (**a**) and (**b**) show the XRD patterns for the FER membranes before and after the removal of the FER particles on the surface of the support, respectively. **Figures 4.5** (**a**) and (**b**) show the top views of the FER membrane before and after the removal of FER particles on the alumina support, respectively. No FER particles were observed over the whole alumina support after the removal of FER particles. The reflection peaks for FER were observed in **Figure 4.4(b)** although no FER crystals existed on the surface of the alumina support. These XRD measurements indicated that FER was formed even in the pores of alumina support, namely, a FER-alumina composite layer was formed.

Figures 4.6 (**a**) and (**b**) show the FE-SEM images for the cross-section of the porous alumina support and the FER-alumina composite layer in the FER membrane, respectively. In **Figure 4.6** (**b**), nano-particles with diameters of about 50 nm are observed in the pores of the alumina support and voids were hardly observed. **Figure 4.7** shows the FE-SEM images of FER powder produced by the VPT method. A large plate-like FER particle is composed of assembled needle-like FER nano-crystals with a diameter of about 30 nm. By comparing **Figure 4.6** (**b**) with **Figure 4.7**, it is believed that the nano-particles observed in the alumina pores are certainly FER nano-crystals.

In conclusion, FER nano-crystals grew in the pores of alumina support and filled there up to form a compact composite layer of FER and alumina.

2. MOR membrane

The FE-SEM image for the cross-section of the MOR membrane is shown in **Figure 4.8**. Nano-particles are observed in the alumina pores. Similarly to the FER membrane, they seem to be assembled MOR nano-crystals.

(a)

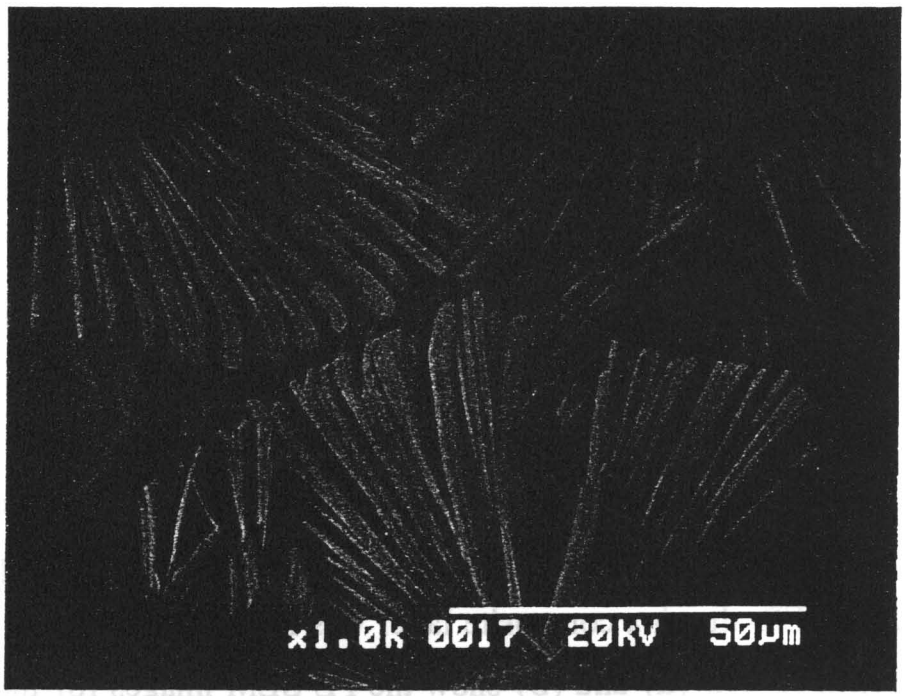

(b)

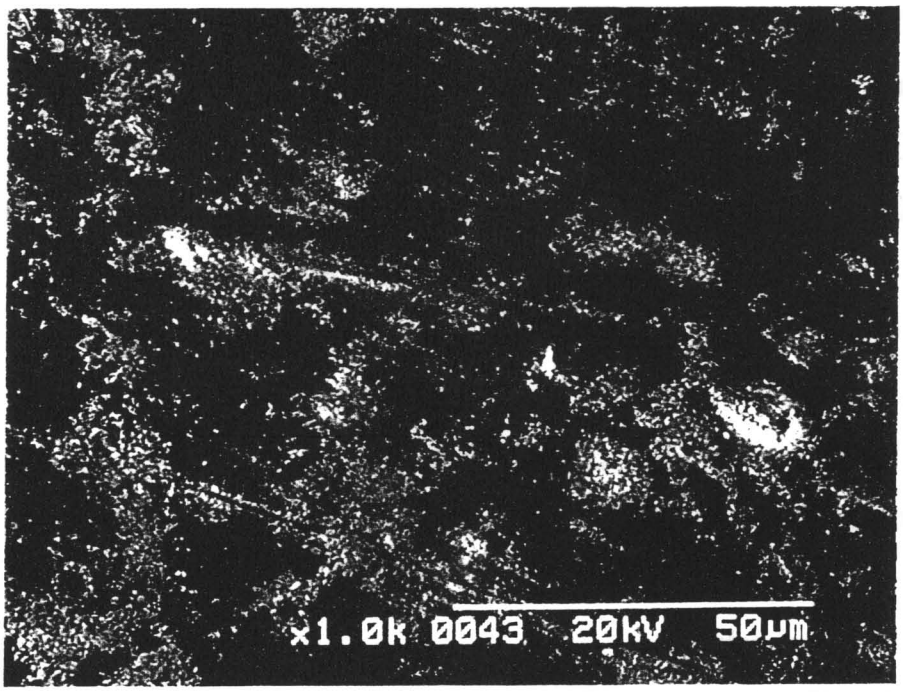

Figure 4.5 SEM images for the top views of FER membranes (a) before and (b) after removal of FER particles on alumina support.

(a)

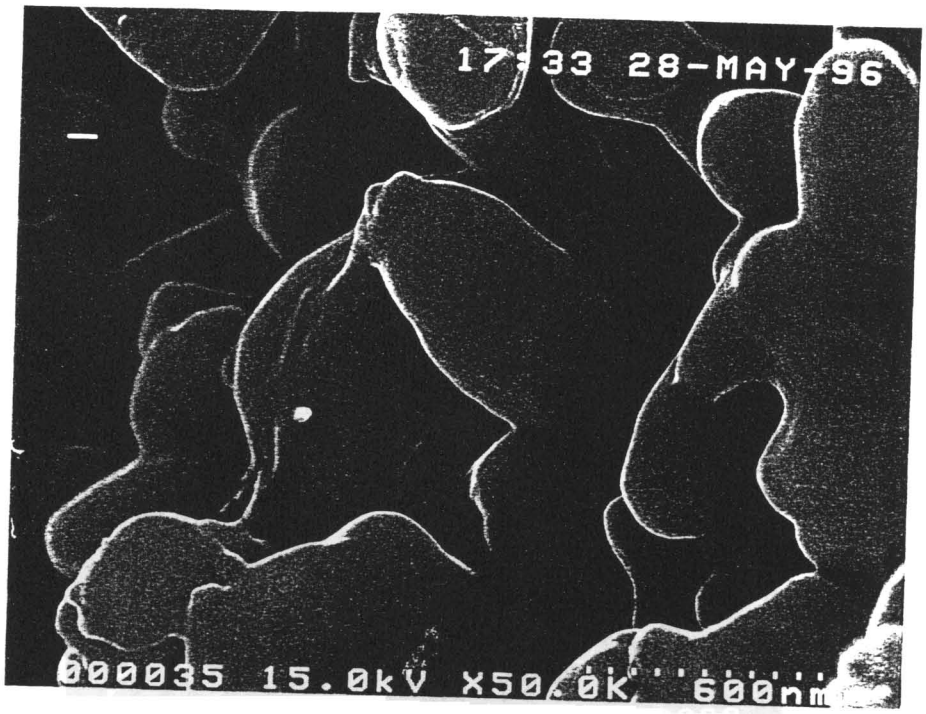

(b)

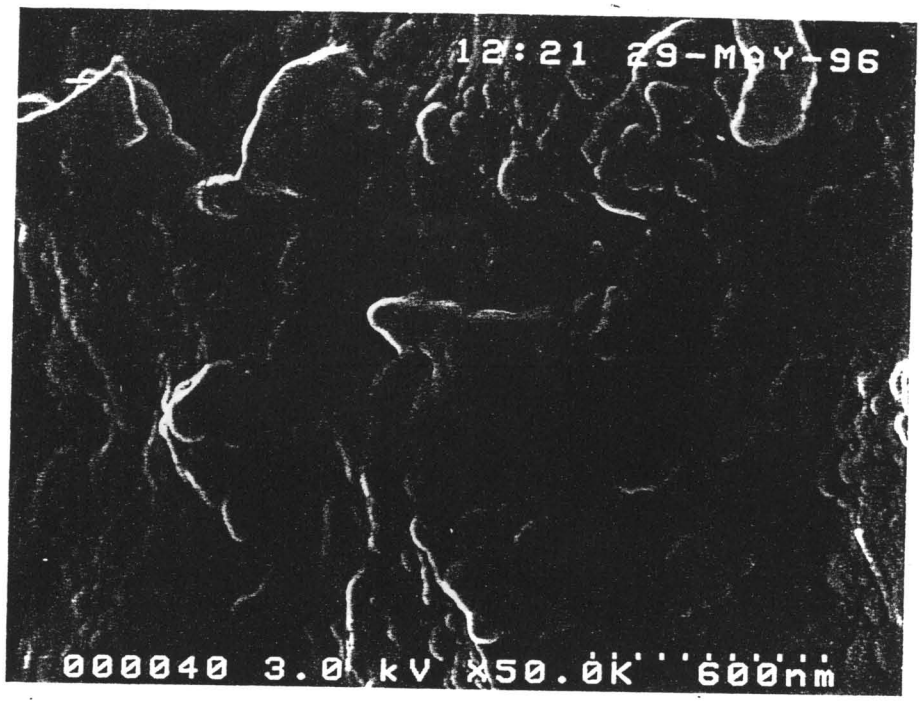

Figure 4.6 FE-SEM images for the cross-section of (a) porous alumina support and (b) FER membrane.

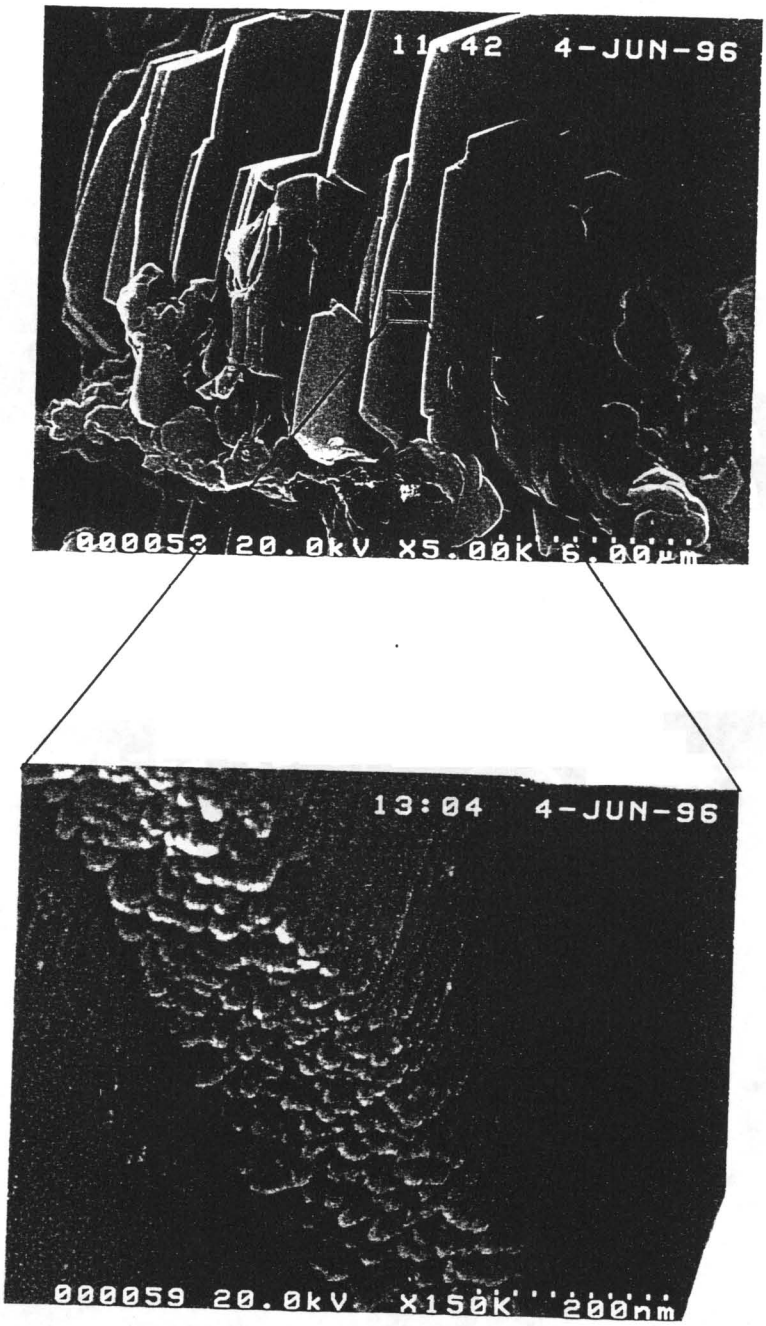

Figure 4.7 FE-SEM images of FER powder produced by VPT method.

4.3.2. Formation process of zeolite-alumina composite layer

1. MOR membrane

Figure 4.9 shows the XRD patterns of the MOR membranes crystallized for 1, 2 and 4 days. **Figure 4.10** shows the SEM images of the top views of the corresponding MOR membranes. It was difficult to observe a broad reflection peak corresponding to the amorphous phase in the XRD pattern from a MOR membrane crystallized for 2 days (**Figure 4.9(b)**). **Figure 4.9(c)** shows that the reflection peak of MOR became

Figure 4.8 FE-SEM images for the cross-section of MOR membrane.

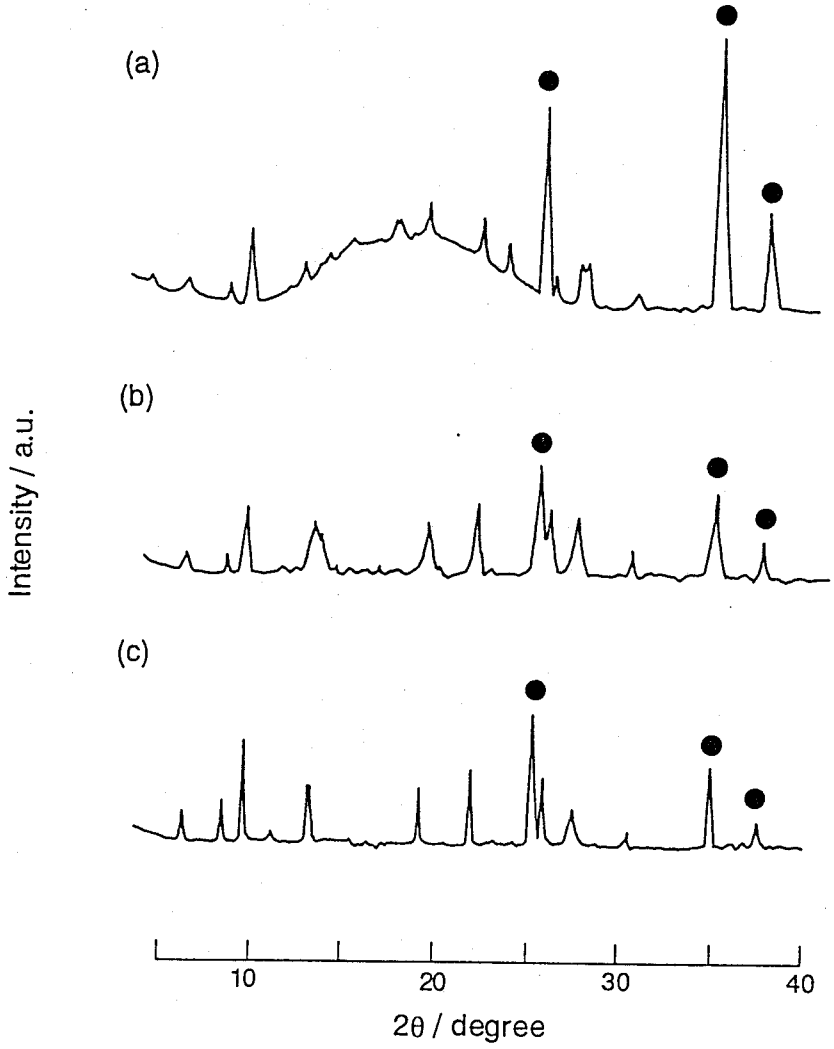

Figure 4.9 XRD patterns of MOR membranes for (a)1, (b) 2 and (c) 4 days. Solid symbol, alumina.

narrower with prolonged crystallization, indicating that the crystallinity of MOR was improved from 2 to 4 days. **Figure 4.10 (a)** shows that MOR crystals began to form on the alumina support after 1 day. Growth of MOR crystals were observed after 2 days, as shown in **Figure 4.10(b)**. In **Figure 4.10(c)**, the morphology of the MOR crystals was further changed after 4 days. Though the MOR membrane was defect-free as previously described, voids were observed among the MOR crystals on the surface of the alumina support. The top views of the MOR layers which formed on the surface of the alumina support were clearly not compact.

Figure 4.11 shows the SEM images of the cross sectional views of the MOR membranes crystallized for different times. It is noteworthy that the part showing dark contrast in the alumina support was bound with MOR crystals formed on the surface of alumina support as shown in **Figure 4.11(a)**. These parts showing dark contrast in the alumina support spread with crystallization time and finally linked together after 4 days. These parts with dark contrast are therefore believed to be MOR-alumina composite layer.

Figure 4.11(a) shows, thus, that the gel in the pore of the alumina support partly crystallized to MOR after 1 day. **Figures 4.11(b)** and **(c)** imply that crystallization from the gel to MOR in the pore of the alumina support proceeded and a continuous composite layer of MOR crystals and the porous alumina, 10 - 20 mm thick, was formed after 4 days. It is believed that the MOR-alumina composite layer was defect-free because no TIPB permeated through the MOR membrane and there are numerous voids among the MOR crystals on the support as shown above. Judging from the SEM images, growth of MOR crystals in the pores of the alumina support would be slower than that of the gel on its surface.

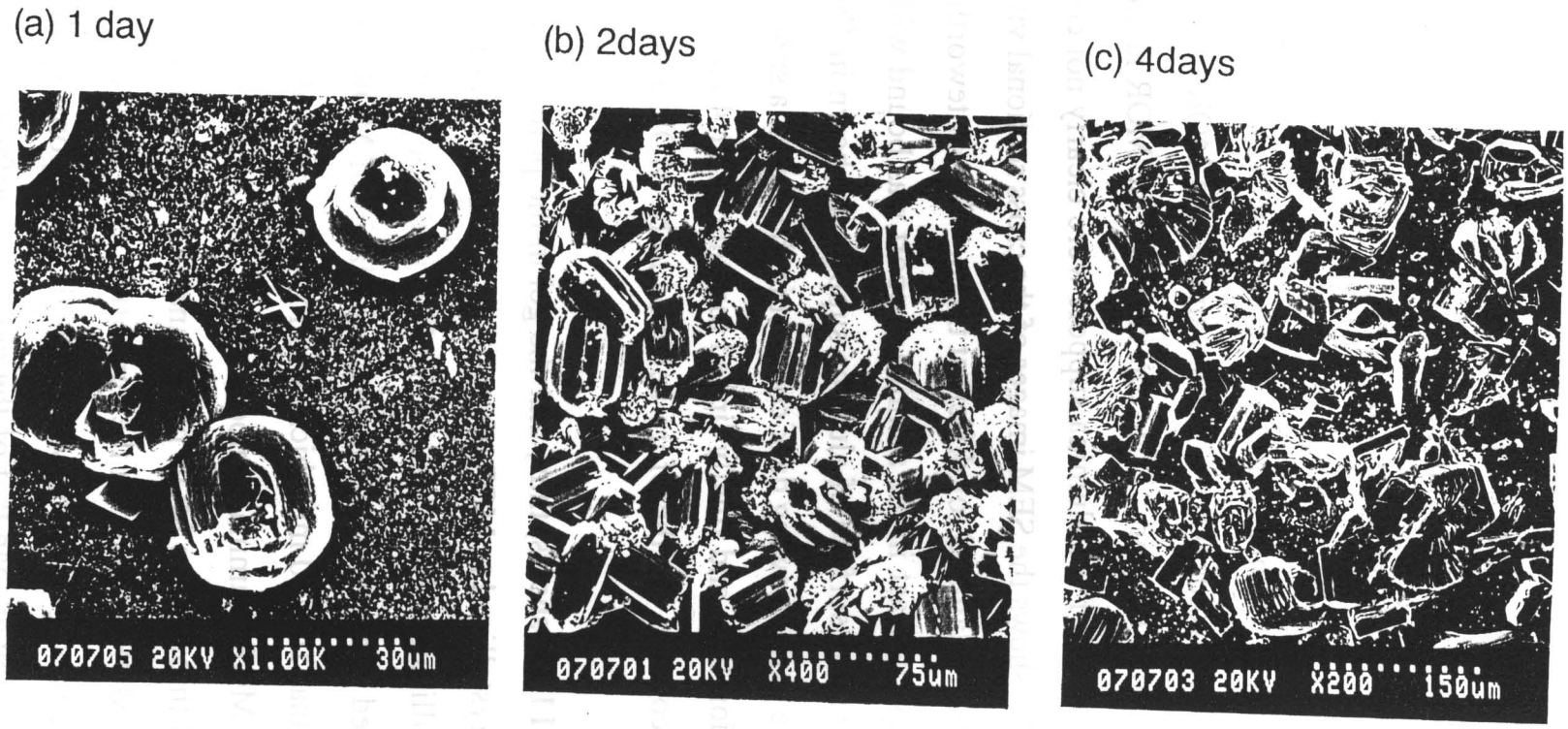

Figure 4.10 SEM images for the top views of MOR membranes for (a)1, (b) 2 and (c) 4 days.

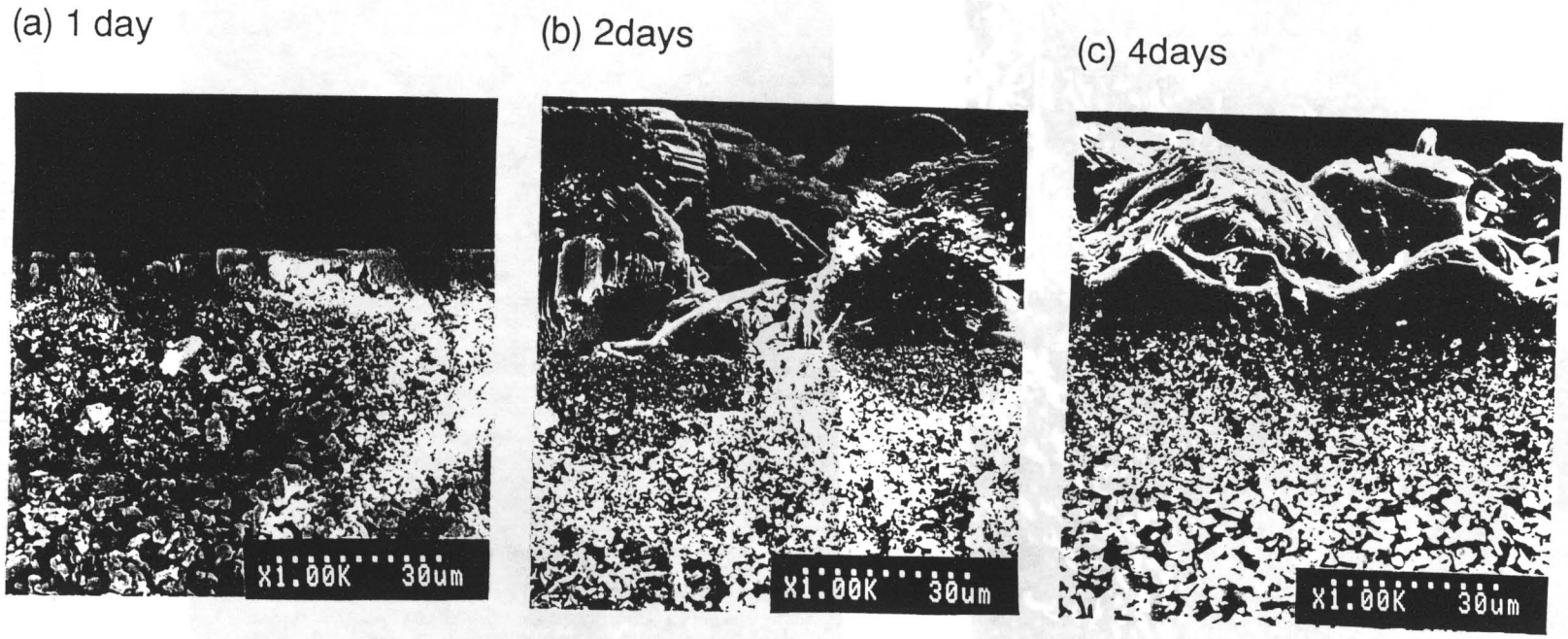

Figure 4.11 SEM images for the cross-section of MOR membranes (a)1, (b) 2 and (c) 4 days.

(a)

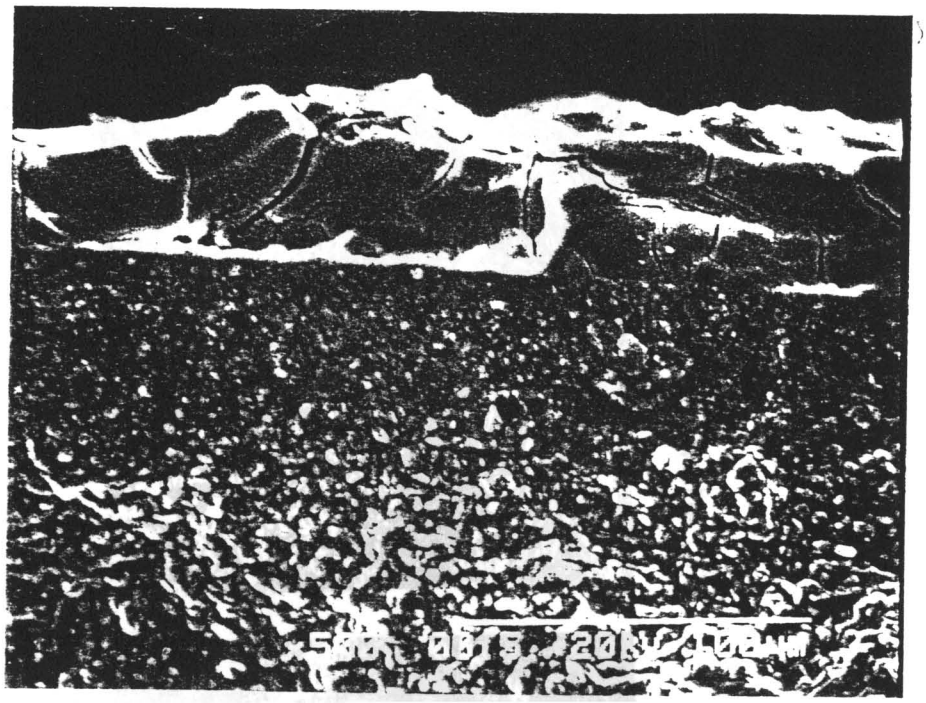

(b)

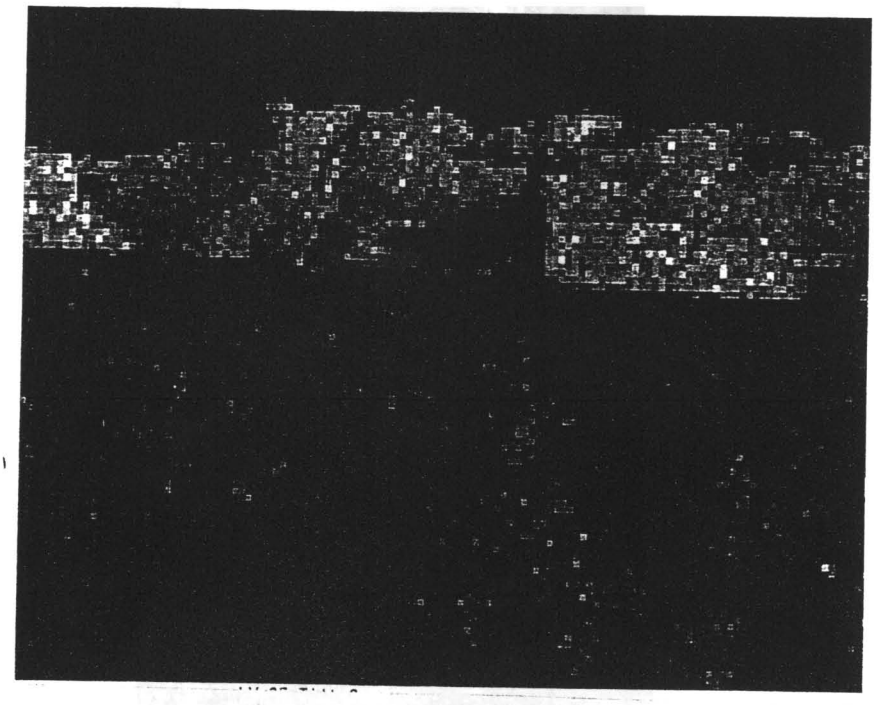

Figure 4.12 (a) SEM and (b) EDX elemental images for the cross-section of alumina support coated with aluminosilicate gel. White dots: Si.

Figures 4.12 (a) and (b) show the SEM and EDX elemental images for the cross-section of the alumina support coated with an aluminosilicate gel, respectively. White dots in **Figure 4.12(b)** corresponds to silicon. In **Figure 4.12(b)**, silicon can be observed in the alumina support, indicating that the aluminosilicate gel partly penetrated into the pores of alumina before crystallization.

Figure 4.13 (a) and (b) present SEM and EDX elemental images, respectively, of the cross-sectional view for the MOR membrane crystallized for 1 day. It is noteworthy that the Si signal in the part of crystal is stronger than that in the amorphous phase around the MOR crystals, indicating that amount of gel which had penetrated into the pore of alumina before crystallization was insufficient for full crystallization in the alumina pores. The SiO_2/Al_2O_3 ratio of aluminosilicate gel on the support was determined by EDX. The SiO_2/Al_2O_3 ratio of aluminosilicate gel was about 25 and comparable to that of the parent gel. An MFI membrane was obtained on the alumina support when the surface treatment of the support with colloidal silica was carried out although a MOR membrane was formed on the untreated support as described before. The SiO_2/Al_2O_3 ratio of MOR is generally 8-15, which is lower than that of MFI, 15 -∞. The result that SiO_2/Al_2O_3 ratio of zeolites formed on the untreated support was much lower than that on the treated support should be attributed to the dissolution of alumina support and its incorporation into the framework of zeolite. However, the SiO_2/Al_2O_3 ratio of aluminosilicate gel on the support was similar to that of the parent gel as described above. In other words, aluminum dissolved from the alumina support existed not in the whole gel but around interface between the gel and the support before crystallization. However, the surface treatment led to different types of zeolites. Therefore, the crystallization seems to occur from the gel layer

(a)

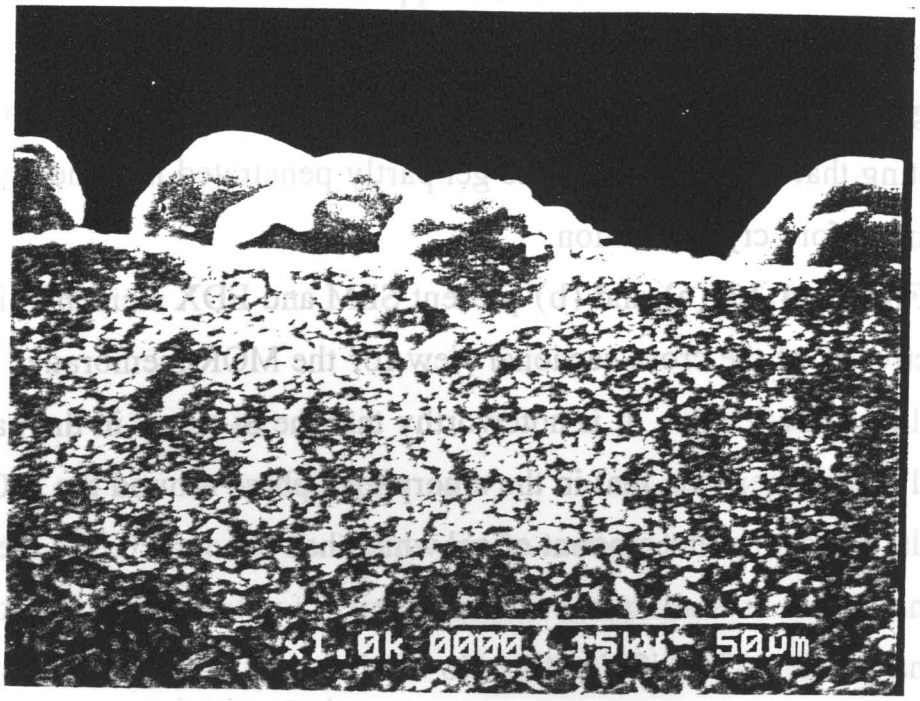

(b)

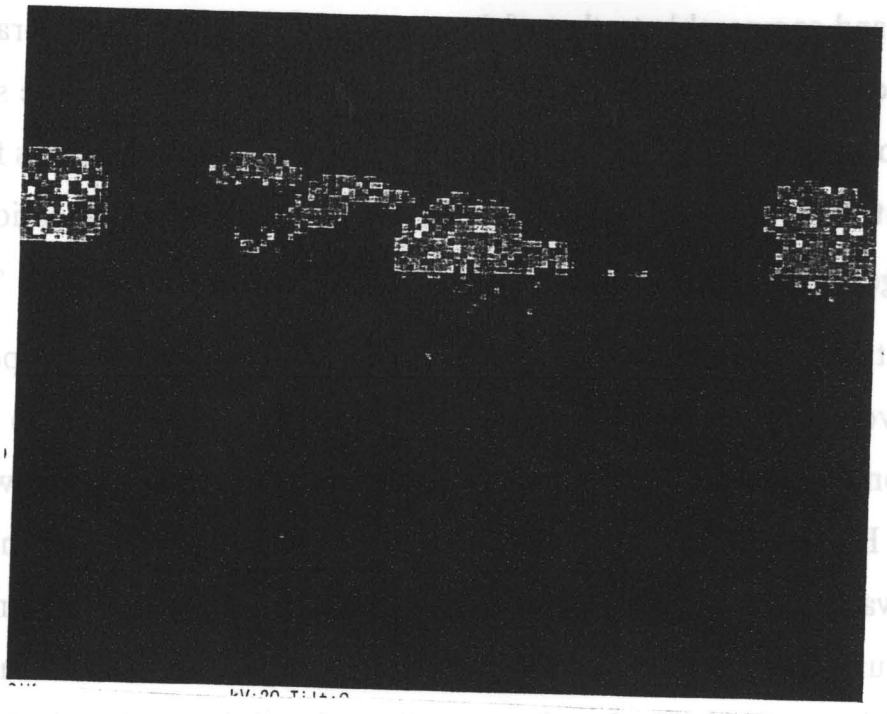

Figure 4.13 (a) SEM and (b) EDX elemental images for the cross-section of MOR membrane crystallized for 1 day.

which is in contact with the surface of the alumina support. It ssems that aluminum species diffused from the surface of the alumina support by the movement of aluminosilicate gel particles to the whole gel layer during crystallization.

2. FER membrane

The EDX elemental images for the FER membranes crystallized for 1 and 4 days are shown in **Figures 4.14 (a)** and **(b)**, respectively, suggesting that silicon content in the alumina support increased with prolonged crystallization. This result suggests that gel was successively supplied from the gel layer on the support and then continuous FER-alumina composite layer formed.

A droplet of dilute aluminosilicate gel was placed on the alumina support and dried at 363 K for 4 h. Crystallization was then carried out at 453 K for 4 days by the VPT method. **Figures 4.15 (a)** and **(b)** show the SEM images for the same position of the membrane before and after crystallization, respectively. It is observed in the SEM image for the part surrounding the rectangle in **Figure 4.15(b)** that the gel moved a few tens μm in the horizontal direction after crystallization. Further, gel seems to have penetrated into the vertically direction from the SEM image for the part surrounding the rectangle in **Figure 4.15(b)**.

The gel particles were placed on the alumina support and then treated under vapors of EDA, Et_3N, and water at 453 K for 4 days. After crystallization, an XRD pattern and SEM images were taken for the sample. We found that the XRD pattern of the product contained reflection peaks for FER even after washing the membrane surface with deionized water. Thus, FER crystals presumably ipenetrated into the alumina support. **Figure 4.16** shows the SEM image for the cross-section of the FER

(a)

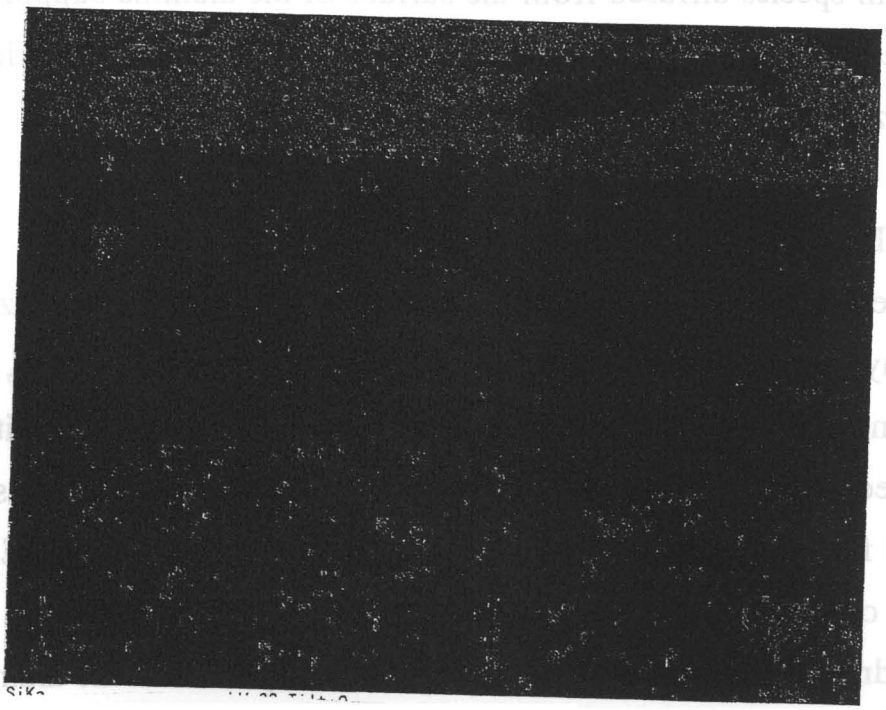

(b)

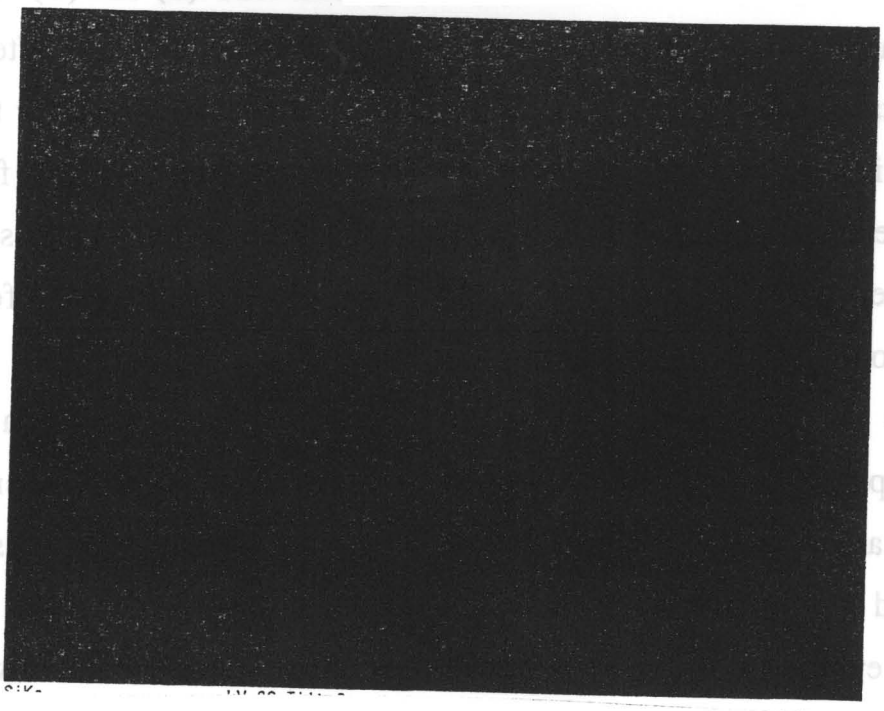

Figure 4.14 EDX elemental images for FER membrane crystallized for (a) 1 and (b) 4 days. White dots: Si.

(a)

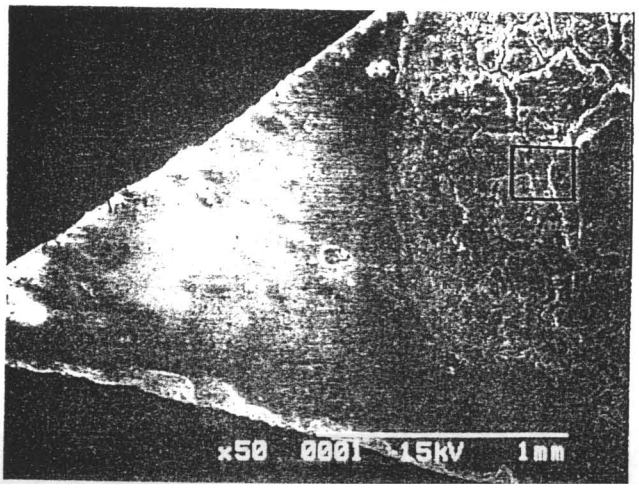

(b)

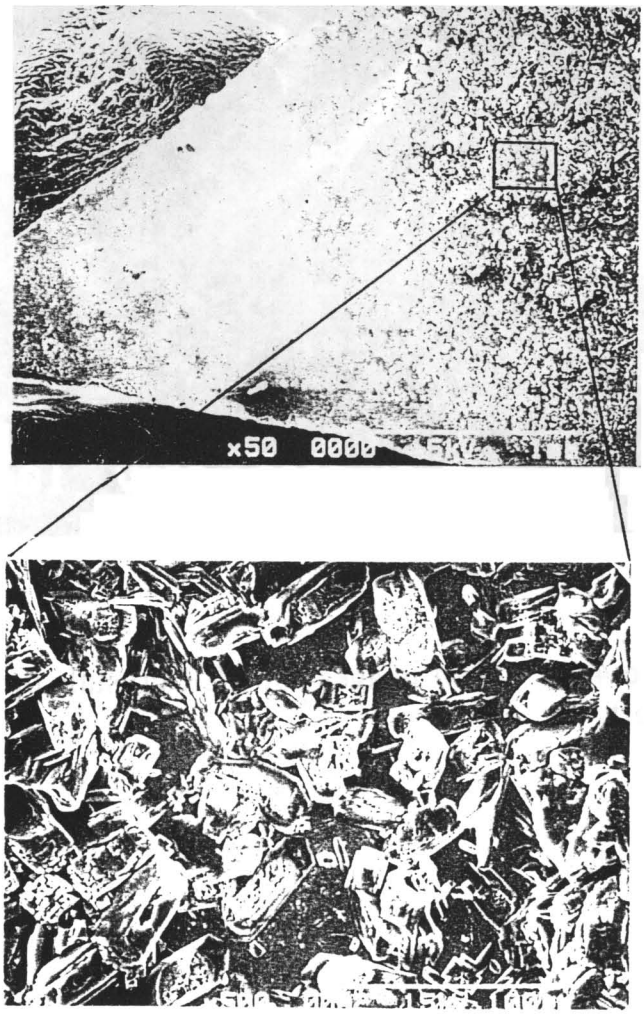

Figure 4.15 SEM images for the top views of membranes (a) before and (b) after crystallization.

membrane. The FER crystals were observed on and even in the alumina support, supporting that dry gel penetrated into the alumina support during crystallization.

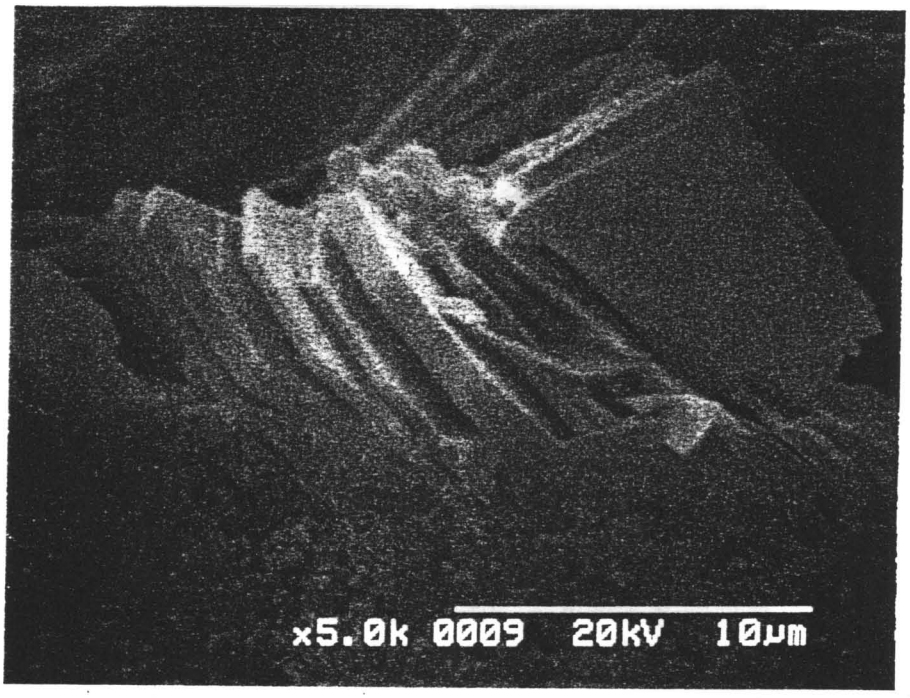

Figure 4.16 SEM images for FER crystals on alumina support.

4.3.3. Summary of formation process of zeolitic membranes

Figure 4.17(a) schematically illustrates the plausible formation process of the zeolitic membrane by the VPT method. An aluminosilicate gel partly penetrates into the pores of alumina support before crystallization. The crystallization starts to occur on the surface of the alumina support. Then, crystallization proceeds both on the alumina support and in the pores of alumina. The gel is successively supplied into the pores of alumina support from the gel layer on the support. Zeolite crystals formed in the pores of alumina support are composed of nano-particles. Finally a zeolite-alumina composite layer is formed in a compact form, while voids are formed among the crystals on the alumina support.

The formation mechanism of the defect-free zeolitic membrane hydrothermally obtained has been proposed as shown in **Figure 4.17(b)**. Sano et al. (1992) synthesized an MFI membrane on a Teflon slab hydrothermally and suggested that the MFI membrane is formed mainly through a successive accumulation of zeolite crystals which are formed via homogeneous nucleation in the liquid phase, as shown in **Figure 4.1**. On the other hand, Geus et al.(1992, 1993) and other researchers (Tsikoyiannis and Haag, 1992; Jansen et al., 1994; Yan, 1995) suggested that crystallization starts by heterogeneous nucleation on the surface of a support. Irrespective of the formation mechanisms of membrane, once a zeolite layer is formed on the surface of a support, an aluminosilicate solution finds it difficult to penetrate into the support to fill up the pores. The intergrowth of crystals formed on the surface of support is probably essential to obtain a defect-free zeolitic membrane in either crystallization process under hydrothermal conditions.

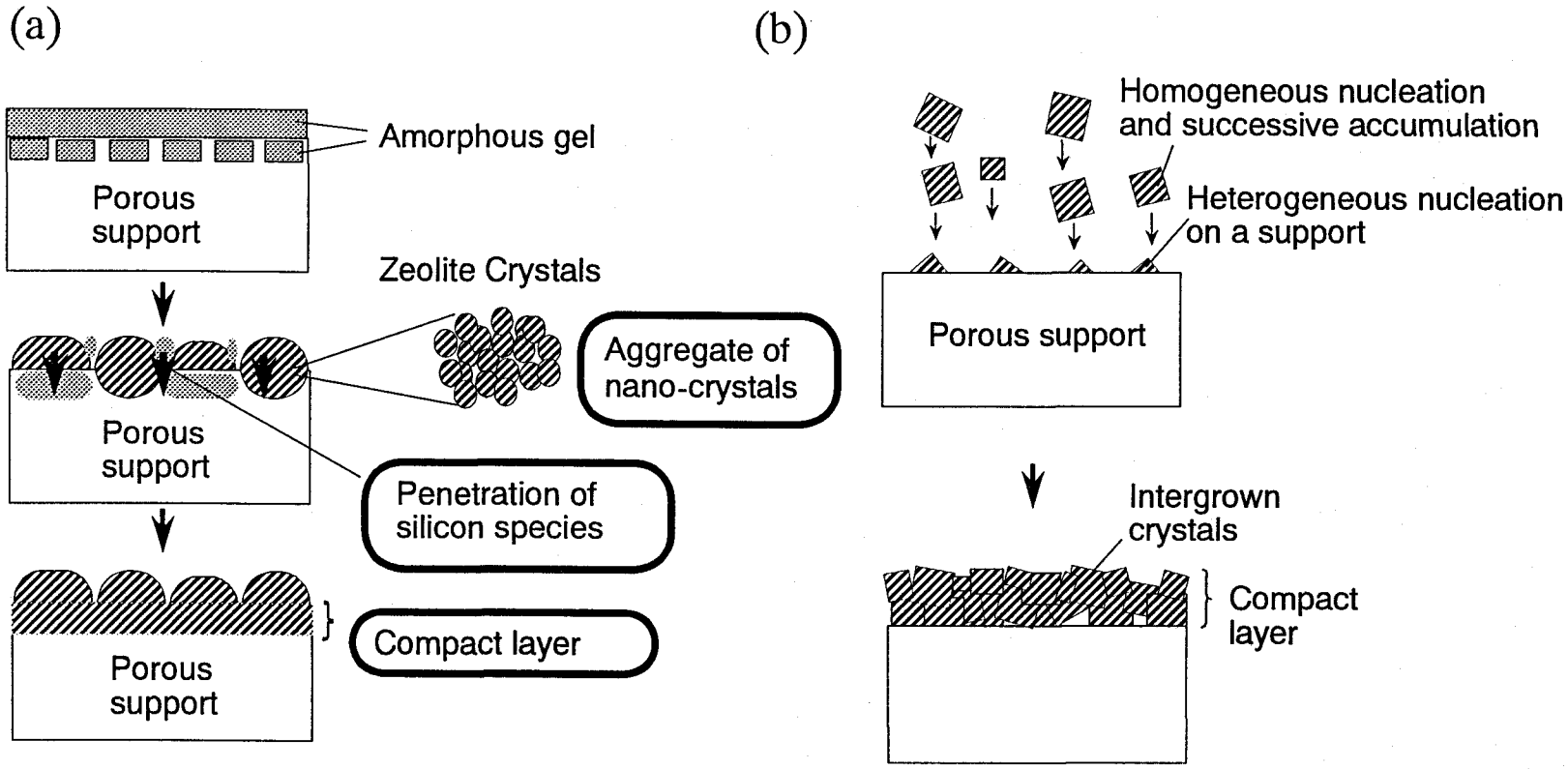

Figure 4.17 Formation mechanism of zeolitic membrane (a) by vapor-phase transport method and (b) by hydrothermal synthesis.

4.4. Conclusions

The gel in the pores of alumina support crystallized to zeolite and then zeolite-alumina composite layer formed by the VPT method. The formation mechanism of zeolite-alumina composite layer by the VPT method was proposed as follows.

(1) Crystallization occurs from the gel layer which is in contact with the surface of the alumina support.

(2) Gel is successively supplied from the gel layer on the support during crystallization.

(3) Zeolite crystals are composed of assembled zeolite nano-crystals.

(4) Finally a zeolite-alumina composite layer is formed in a compact form.

Chapter 5 Gas Permeation through Zeolitic Membranes

5.1. Introduction

Permeation measurements of single-component gas including inorganic gases and light hydrocarbons such as n-butane and i-butane through MFI membranes have been carried out and are summarized in **Table 5.1**. The permeation tests have been performed by either the PG or CG method. Most measurements have been carried out below 450 K, except for several reports of groups at Delft Tech. Univ. (Bakker et al., 1993; Kapteijn et al., 1995) and Colorado Univ. (Noble et al., 1995; Bai et al., 1995), because it is hard to seal an apparatus at a high temperature where polymeric sealing materials cannot be used.

$$P'\ (Permeability) = \frac{Flux\ [\mathrm{mol\ s^{-1}\ m^{-2}}] \cdot d\ [\mathrm{m}]}{\Delta \mathrm{p}} \tag{5.1}$$

$$P\ (Permeance) = \frac{Flux\ [\mathrm{mol\ s^{-1}\ m^{-2}}]}{\Delta \mathrm{p}} \tag{5.2}$$

The permeability defined as Eq. 5.1 is generally used for polymeric membranes. On the other hand, in most case for discussing an inorganic membrane performance, "permeance" defined as Eq. 5.2 is used, because the effective thickness of inorganic membranes cannot be easily determined.

The permeances of butane isomers have been discussed to evaluate how compact the obtained MFI membranes are. Jia et al. (1993) reported that the permeance ratio as high as 6.2 for n-butane over i-butane through an MFI membrane was obtained. The results from several other groups also show higher permeances of n-butane than that of i-butane.

For example, Yan et al. (1995a, b) synthesized defect-free MFI

Table 5.1 Single-gas permeation measurements through MFI membranes

	method	Sweep gas	T [K]	gas
Geus et al. (1992)	P		294 -418	H_2, N_2, CH_4, CO_2, O_2, CF_2Cl_2
Geus et al. (1993)	C	He	298	CH_4, Ne, n-C_4, i-C_4
Vroon et al. (1996)	C	He	273 - 473	CH_4, C_2H_6, C_3H_8, n-C_4, i-C_4
Bakker et al. (1996)	C	He	193 - 673	CH_4, C_2H_6, C_2H_4, C_3H_8, C_3H_6, nC_4, i-C_4, CO_2, H_2, i-C_8
Kapteijn et al. (1994)	C	He	300 - 630	i-C_4
Meriaudeau et al. (1995)	P		298 - 419	H_2, He, N_2, i-C_4
Kusakabe et al. (1996)	C	He	303 - 373	He, CO_2, N_2, CH_4, n-C_4, i-C_4
Bakker et al. (1993)	C	He	300 - 623	Kr, C_2H_6, Ar, n-C_4, Ne, CF_2Cl_2, i-C_4
Yan et al. (1995a)	P		303 - 458	H_2, He, N_2, O_2, CH_4, n-C_4, i-C_4
Jia et al. (1993)	P		293	N_2, He, CO_2, CH_4, C_2H_6, C_3H_8, n-C_4, i-C_4, c-C_6
Jia et al. (1994)	P		298 - 373	N_2, H_2, He, n-C_4, i-C_4
Yan et al. (1995b)	P		303 - 453	H_2, N_2, O_2, CO_2, n-C_4, i-C_4, neo-C_5H_{12}
Bai et al. (1995) Noble et al. (1995)	C, P	Ar, SF_6	300 - 737	H_2, Ar, n-C_4, i-C_4, SF_6
Exter et al. (1996)	C	He	200 - 623	CH_4, C_2H_4, C_2H_6, n-C_4, i-C_4
Kusakabe et al. (1996)	C	Ar	303 - 423	CO_2, N_2, CH_4, C_2H_6, n-C_4, i-C_4

Table 5.2 Mixed gas permeation measurements

	Sweep gas	Temp.	Gas
Tsikoyiannis and Haag (1992)	He	296, 322	N_2/O_2, H_2/CO, n-C_6/2,2DMB
Geus et al. (1993)	He	298 - 623	CH_4/n-C_4, CH_4/n-C_4/i-C_4
Bai et al. (1995) Noble et al. (1995)	Ar,SF_6	300 - 737	H_2/SF_6, Ar/SF_6, H_2/i-C_4
Kapteijn et al. (1995a)	He	300 - 673	H_2/n-C_4, CO_2/H_2
Kapteijn et al. (1995b)	He	292	C_2H_6/C_2H_4, C_3H_8/C_3H_6
Exter et al. (1996)	He	300, 200-650	CH_4/C_2H_6, C_2H_6/C2H_4
Kusakabe et al. (inpress)	Ar	373	n-C_4/iC_4
Vroon et al. (1996)	He	298 - 473	CH_4/n-C_4, n-C_4/i-C_4, n-C_6/2,2DMB
Bakker et al. (1996)	He	295 - 623	n-C_4/H_2, H_2/CO_2, n-C_4/i-C_4, CH_4/i-C_8
Bakker et al. (1993)	He	293 - 623	CH_4/n-C_4, CH_4/i-C_4, CH_4/Ne, i-C_8/CH_4

DMB: dimethylbutane

membranes on a porous α-alumina support and observed good permeation selectivities for butane isomers: the permeability ratio of n-butane to i-butane was 18 at 303 K.

Transient gas permeation measurements were performed by Geus et al. (1993) who measured permeances of CH_4, n-butane, neon, i-butane at room temperature. Those values were in this order: CH_4> n-butane> neon> i-butane. In particular, they found that the permeance ratio of n-butane to i-butane was as high as 64 at 298 K. These results that MFI membranes are permeable to n-butane compared with i-butane seem reasonable in view of the larger kinetic diameter of i-butane than that of n-butane.

The permeation of two-component mixtures shows interesting feature. The permeation tests for a mixed gas through zeolitic membranes have been performed using a Wicke-Kallenbach cell. Either Ar or He in most cases has been used as a sweep gas. **Table 5.2** listed mixed-gases permeation measurements reported so far.

Tsikoyaiannis and Haag (1992) studied the permeances for three binary mixtures (O_2/N_2, H_2/CO_2, and n-hexane/2,2-dimethylbutane) through self-supporting MFI membranes at 296 and 322 K. The observed selectivity for a n-hexane/2,2-dimethylbutane mixture was 17.2, much higher than that in the Knudsen region, 1. This is the first case that the separation of mixed gases at the molecular level using zeolitic membranes was shown to be possible.

Bai et al. (1995) reported that the separation selectivities for H_2/SF_6 and H_2/i-butane were 12.8 and 11.9, respectively, at 583 K and were significantly above Knudsen diffusion selectivities.

Geus et al. (1993) observed the transient permeation behavior for a 50/50 methane/n-butane mixture. The permeance of n-butane was similar to that in the pure gas permeation experiment for n-butane, indicating that

the presence of methane hardly affected the permeation behavior of n-butane. In this case, separation was apparently governed by the reduced mobility of methane within the zeolite micropores in the presence of strongly adsorbing molecules. Owing to the strong adsorption of n-butane, any methane might hardly enter the zeolite micropores, and the driving force for methane permeation was substantially reduced.

Geus et al. (1993) studied the permeation behavior of the 50/50 methane/n-butane mixture. A monotonous increase in the n-butane flux was observed up to 430 K. The methane permeation rate remained low up to 410 K, and selectivity was in favor of n-butane. At higher temperatures, the methane flow became substantial and even exceeded the n-butane flow up to 500 K. At higher temperatures, methane permeation leveled off. From these results at low temperatures, the methane permeation rate is governed by the n-butane adsorbate concentration. At higher temperatures, the n-butane which was preferentially adsorbed at lower temperature molecules, desorbed, and both the driving force for methane permeation and methane mobility are increased. All observed features may be related to the effect that both diffusion and adsorption are temperature dependent.

Similar trends have been found for H_2/n-butane mixture (Kapteijn et al., 1995). In the single-component measurement, the steady state H_2 permeation flux was about 20 times larger than that of n-butane. The results for the permeation test of a 95:5 mixture of these components showed that H_2 permeated first, but then dropped quickly and reached a low value, as n-butane appeared. The H_2 permeation flux at steady state was reduced by a factor of more than 100 compared with that for a single component measurement, while the n-butane flux remained unaltered, indicating that the permeation behavior of n-butane was hardly affected by

the permeation of H_2.

A numerous single gas and mixed gas permeation measurements have been presented here. However, the number of types of zeolitic membranes that have been used for gas permeation tests is still limited. Among those studies, ZSM-5 (MFI) membranes, especially silicalite (Al-free MFI) membranes, were used most frequently. In this study, two different types of zeolitic membranes, ferrierite (FER) and mordenite (MOR), have been synthesized on a porous alumina support. The dimension of the main channel of MOR (0.65 x 0.70 nm) is larger than that of FER (0.42 x 0.54 nm). In this chapter, permeation tests for inorganic gases, H_2, He, CH_4, N_2, O_2 and CO_2, were carried out using these zeolitic membranes. A parallel diffusion model will be proposed and the temperature dependence of permeances for the inorganic gases are analyzed. The effect of pore size on the permeation properties will be discussed according to the present diffusion model.

5.2. Experimental

The FER and MOR membranes were prepared by the VPT method in the same manner as described in section 3.2.

The zeolitic membranes were stuck on a glass or a stainless steel tube with epoxy resin. The effective membrane area was 2.2 cm^2. The permeation tests of H_2, He, CH_4, N_2, O_2 and CO_2 through the zeolitic membranes were performed. Before the gas permeation test for each gas, water and gas adsorbed in the zeolitic membranes were removed by evacuating at 373 K for 1 h. **Figure 5.1** shows the schematic diagram of the experimental apparatus for determining the permeances of gases. The pressure difference between the feed and permeate sides was kept at 0.2 MPa. The permeation side was set at atmospheric pressure. The flow

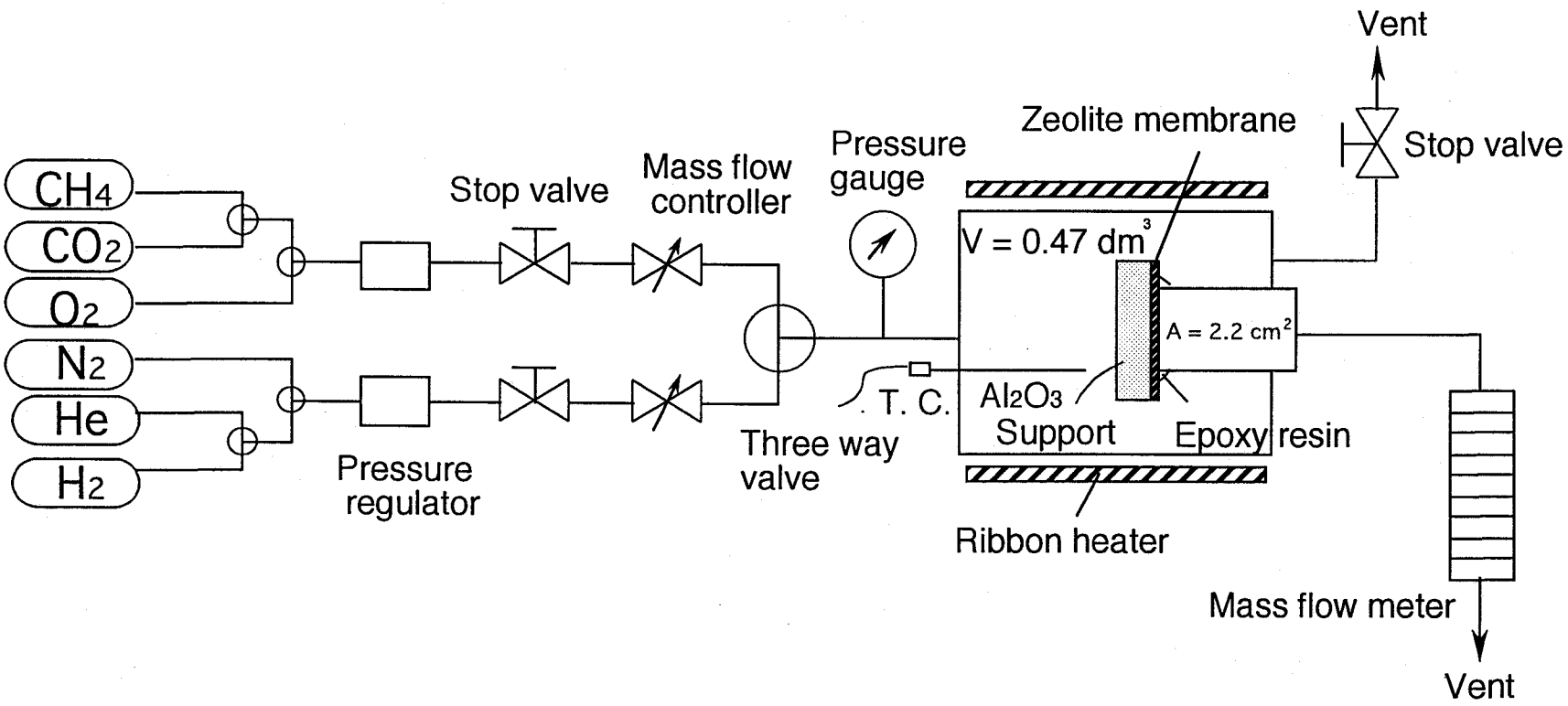

Figure 5.1 Schematic diagram of the experimental apparatus for gas permeation measurements.

rates of gases through the zeolitic membranes were measured at 290 - 400 K. The permeances of gases were calculated by Eq. 1.2.

5.3. Results and discussion

5.3.1. Hydrogen permeation through FER membranes before calcination

The permeation of H_2 was carried out using both the FER membranes (a) and (b) before calcination. These membranes were prepared by different dipping methods (a) and (b) as described in chapter 2. The compactness of FER membranes was checked by the pervaporation of 1,3,5-triisopropylbenzene (TIPB) as described in chapter 2. It was confirmed that the FER membrane (a) is not compact although the FER membrane (b) is practically defect-free. **Figure 5.2** shows the permeances of H_2 through these membranes in the temperature range from 290 to 400 K. The membrane (b) was gas-tight before calcination, indicating that the micropores of FER were blocked by amines before calcination. Hydrogen permeated through the membrane (a) even before calcination. The permeance of H_2 through the membrane (a) monotonously decreased with increasing temperature. Therefore, the controlling mechanism of H_2 permeation can be explained by Knudsen diffusion. It is considered that all H_2 molecules passed through pinholes and cracks among FER crystals, since the micropores of FER were blocked by amines before calcination as suggested from the fact that no H_2 permeated through the membrane (b).

5.3.2. Effect of compactness of FER membranes on H_2 and CH_4 permeation

The permeation tests of H_2 and CH_4 were carried out at room

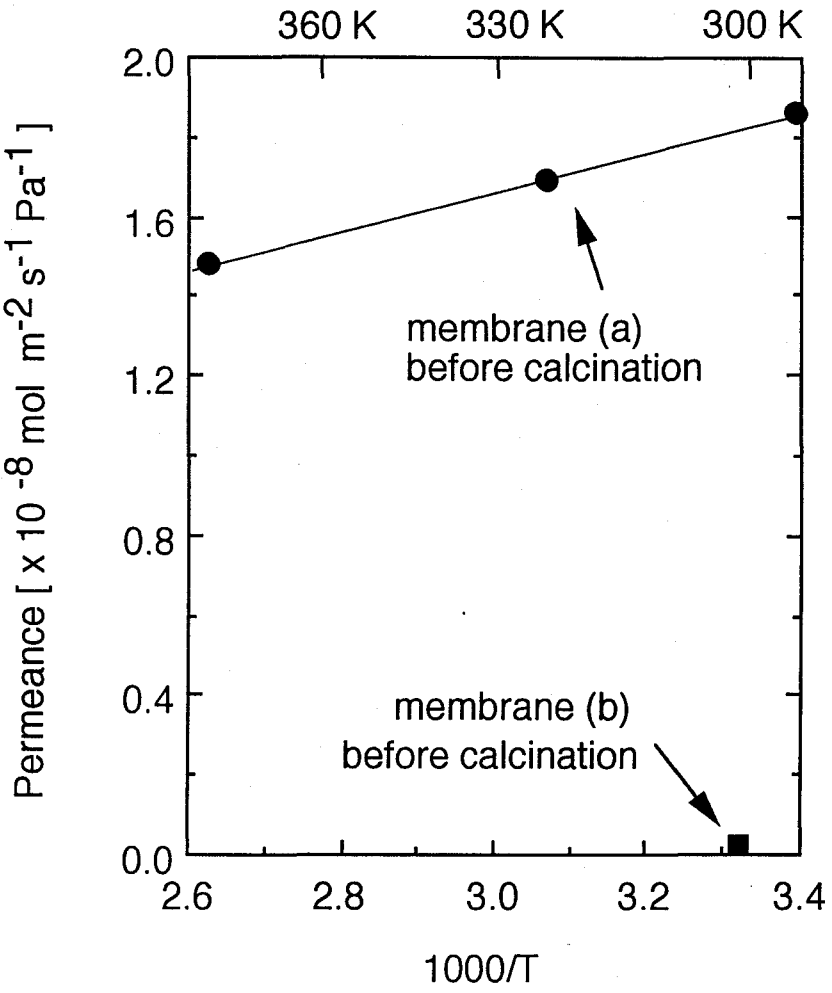

Figure 5.2 Permeances of H_2 through FER membranes before calcination.

temperature using five FER membranes including the defect-free FER membrane (b) and four incompact FER membranes after calcination. The permeance ratios of H_2/CH_4 were plotted as a function of the H_2 permeance through the FER membranes in **Figure 5.3**. The H_2/CH_4 permeance ratio through an alumina support was 2.24 and was also plotted in **Figure 5.3**. The theoretical value for viscous flow and Knudsen diffusion are 1.25 and

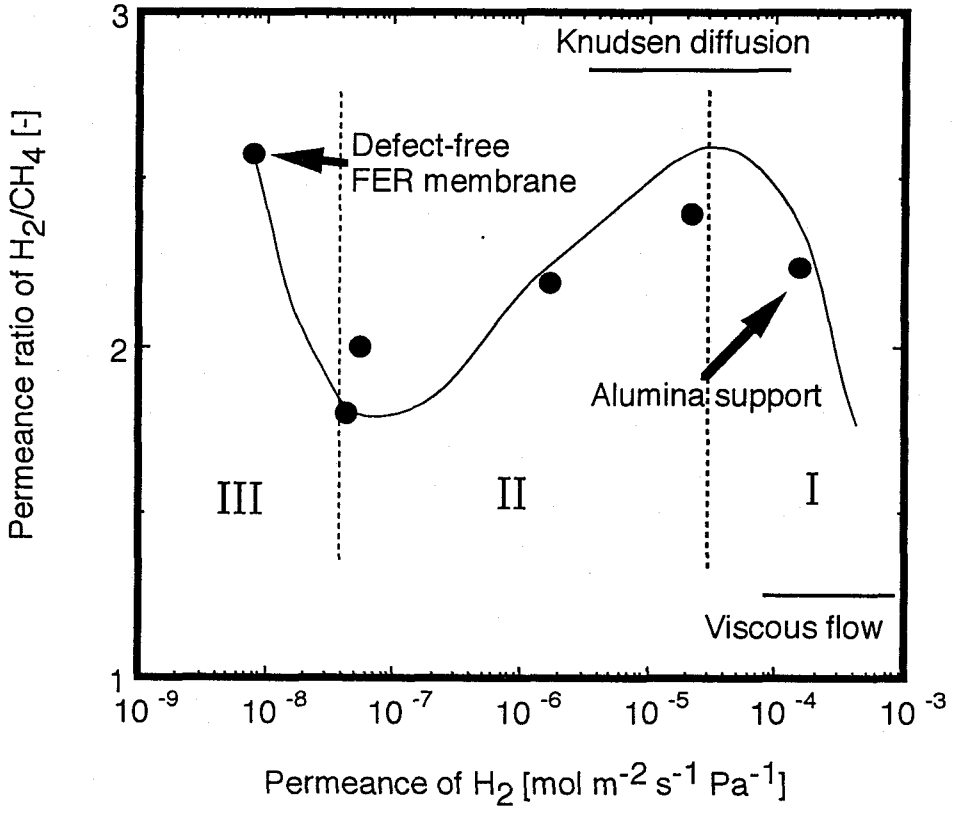

Figure 5.3 Permeance ratios of H_2/CH_4 as a function of H_2 permeation through FER membranes. Temperature: 303 K.

2.82 , respectively, and given in the **Figure 5.3**. The H_2/CH_4 permeance ratio through the alumina support, is between the two theoretical values for viscous flow and Knudsen diffusion, indicating that the transport of H_2 and CH_4 was governed by the flow in the transition region between viscous flow and Knudsen diffusion. Mean free path of H_2 and CH_4 at 298 K and 0.2 MPa are 0.05 and 0.03 μm, respectively. These values are smaller than the average pores diameter of alumina support, 0.1 μm. Thus, the assumption described above would be reasonable.

The behavior of H_2/CH_4 permeation ratio could be classified into three regions as shown in **Figure 5.3**. The H_2/CH_4 permeance ratio approached to the theoretical value for the Knudsen diffusion with decreasing H_2 permeance in region I. In region II, the H_2/CH_4 permeance ratio decreased with decreasing H_2 permeance. In this region, surface diffusion of CH_4, which is more adsorbable than H_2, appeared in addition to Knudsen diffusion. Therefore, the H_2/CH_4 permeance ratio was less than the theoretical value for Knudsen diffusion. In region III, the H_2/CH_4 permeance ratio increased again with decreasing H_2 permeance. The

Table 5.3 Effect of pore blocking by benzene molecules on hydrogen permeation through MOR membrane

	Permeability of H_2 [mol m^{-2} s^{-1} Pa^{-1}]
Before permeation of benzene	1.12×10^{-7} (310 K)
After permeation of benzene	
accompanied by evacuation (383 K, 1 h)	2.47×10^{-10} (310 K)
accompanied by evacuation (400 K, 10 h)	3.48×10^{-8} (310 K)

Permeability of C_6H_6 = 1.14×10^{-9} (323 K) , Δ p (C_6H_6) = 0.036 MPa.

extreme left plot in **Figure 5.3** corresponds to the FER membrane which was confirmed to be defect-free in chapter 3. This behavior may be due to the larger molecular size of CH_4 than that of H_2 (configurational diffusion).

5.3.3. Effect of pore blocking by benzene on H_2 permeation through MOR membrane

Table 5.3 shows the effect of pore blocking by benzene molecules on H_2 permeation through the MOR membrane. No TIPB permeated through the MOR membranes as described in chapter 3. The permeances of H_2 through the MOR membrane was 1.12×10^{-7} mol m^2 s^{-1} Pa^{-1} at room temperature. After vapor permeation of benzene through the MOR membrane and evacuation at 383 K for 1 h, the H_2 permeance through MOR membrane was reduced to 1/460 of its original value. Even after additional evacuation at 400 K for 10 h, the H_2 permeance was not recovered to its original value, clearly showing that benzene molecules blocked the micropores of MOR and reduced the H_2 permeation.

Pore blocking effect of benzene on the H_2 permeation shows that the high temperature is necessary to remove benzene molecule adsorbed in the micropore of MOR. This results strongly support the conclusion that the MOR membrane was defect-free as shown in the previous chapter, because benzene molecules physisorbed in the defects are thought to be easily removed at 400 K for 10 h.

In addition, even CO_2 molecules were not perfectly removed from the pores of zeolites even after evacuation at room temperature for 2 h. The evacuation at 373 K for 2 h was necessary for removing adsorbed CO_2 from the zeolitic membranes, suggesting that pretreatment of membranes is important for permeation measurements using zeolitic membranes.

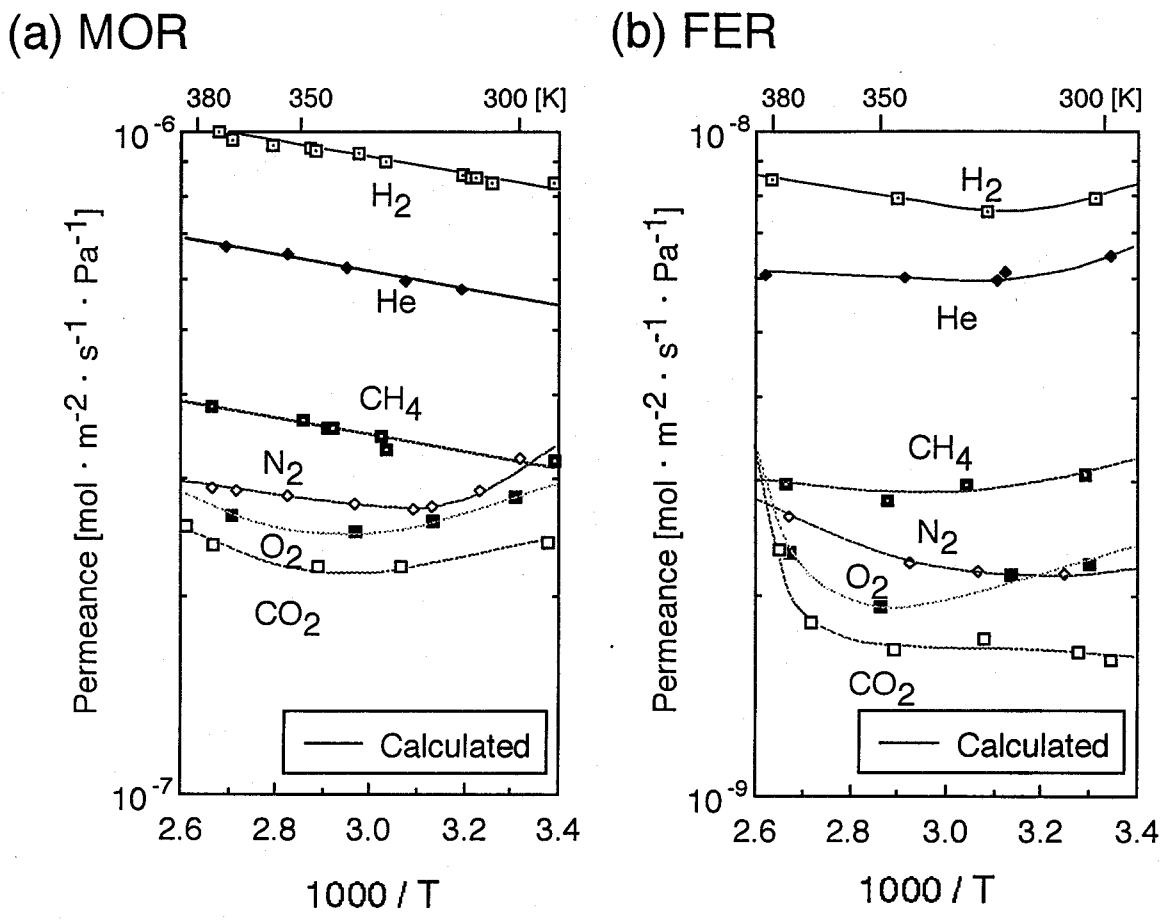

Figure 5.4 Permeances of single gases through (a) MOR and (b) FER membranes.

5.3.4. Temperature dependence of permeance through MOR and FER membranes

Figure 5.4 shows the permeances of H_2, He, CH_4, N_2, O_2 and CO_2 through the MOR and FER membranes in the temperature range from 290 to 400 K. Judging from the results of the permeation tests of TIPB, these inorganic gases permeated almost through the micropores of zeolite. The permeance of each gas through the MOR membrane was about 100 times greater than those through the FER one. This is due presumably to the pore diameter of MOR larger than that of FER, since the thickness of the compact layer in the MOR membrane was almost comparable to that of the FER one as described in chapter 3.

The permeances of H_2, He and CH_4 through the MOR membrane monotonously increased with increasing temperature, indicating that the controlling mechanism of permeation did not change in this temperature region. This temperature dependence of the permeances is evidently caused by the activated diffusion. The permeances of gases through the MOR and FER membranes, except for H_2, He and CH_4 through the MOR membrane, had minimums with increasing temperature, which suggests that a controlling mechanism has changed.

Provided that the permeation of gases through the membranes is governed by Knudsen diffusion, the permeance must have decrease with increasing temperature. However, permeation of H_2 through the FER membrane at room temperature was not governed by Knudsen diffusion, as described in the previous section. As for the MOR membrane, the permeance ratios at room temperature can be checked using data plotted in **Figure 5.4**. The permeance must be proportional to the square root of the reciprocal of molecular weight, provided that the permeation of gases occurs by Knudsen diffusion mechanism. It was observed in **Figure 5.5**

that the permeation of gases did not follow Knudsen diffusion mechanism. Thus, Knudsen diffusion mechanism does not account for the permeation through the zeolitic membranes at room temperature.

5.3.5. Analysis of permeance through zeolitic membranes by "parallel diffusion model"

Barrer(1990, 1991) first discussed the permeation through a zeolitic membrane. His theory was based on the assumption that the entry of

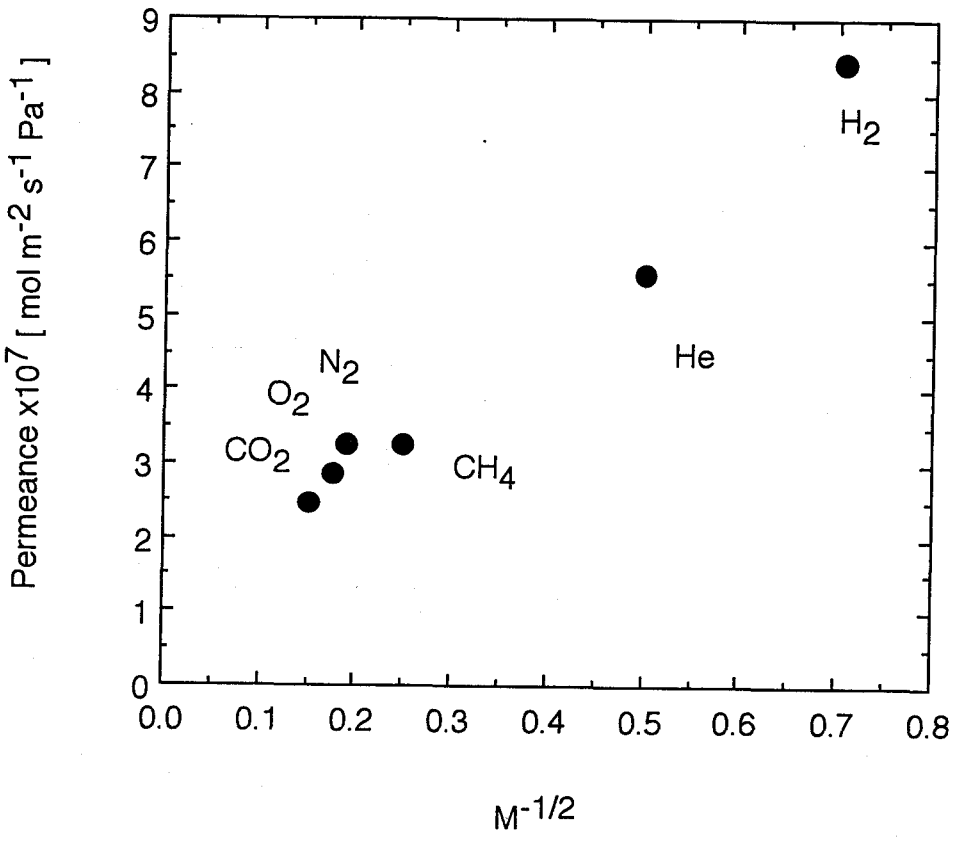

Figure 5.5 Permeance of gases as a function of the square root of the reciprocal of molecular weight. Temperature: 300 K.

molecules into the membrane and their escape from there proceed via an externally adsorbed layer, which has been called the interface process. He concluded that the contribution of the interface processes to the steady flow through zeolitic membrane would become less significant with increasing temperature and membrane thickness. On the basis of his theory, the value of a flux through a pore at room temperature can be estimated by assuming equilibrium concentrations at the both ends of the pore, if the pore length is larger than 100 μm.

Shelekhin et al.(1995) modeled single gas permeation through the molecular-sieve glass membranes. In their model, the total concentration of gas molecules inside the membrane is the sum of the gas-phase and adsorbed-phase concentrations. They concluded that the effect of the adsorbed diffusant on the total flow is significant for highly adsorbable gas.

The Shelekhin's approach and the simple Fick formulation considering the concentration dependence of diffusivity cannot account for the appearance of the minimum permeances through the MOR and FER membranes. To explain the temperature dependence, the micropores of zeolite should be considered as the energetically heterogeneous surface. Seidel and Carl (1989) and Kapoor and Yang (1989) assumed that surface consists of parallel paths such that each path has uniform but different energy, and surface diffusion occurs along these parallel paths. Their parallel-paths assumption contains a continuous energy distribution. Their parallel paths conception is, however, rather complicated. Actually, molecules in the micropore collide with each other and with the wall of the micropore as depicted in **Figure 5.6(a)**. Now, two parallel paths in the micropores are considered in the simplified parallel diffusion model as depicted in **Figure 5.6(b)**. The molecules adsorbed in the micropore diffuse in parallel through the central region of a pore and along the wall

region of a pore. The ratio of the numbers of molecules diffusing through each path expresses the probability of the existence of molecules in each path.

Based on Barrer(1990)'s discussion, the rate limiting process of permeation through a zeolitic membrane is assumed for intracrystalline

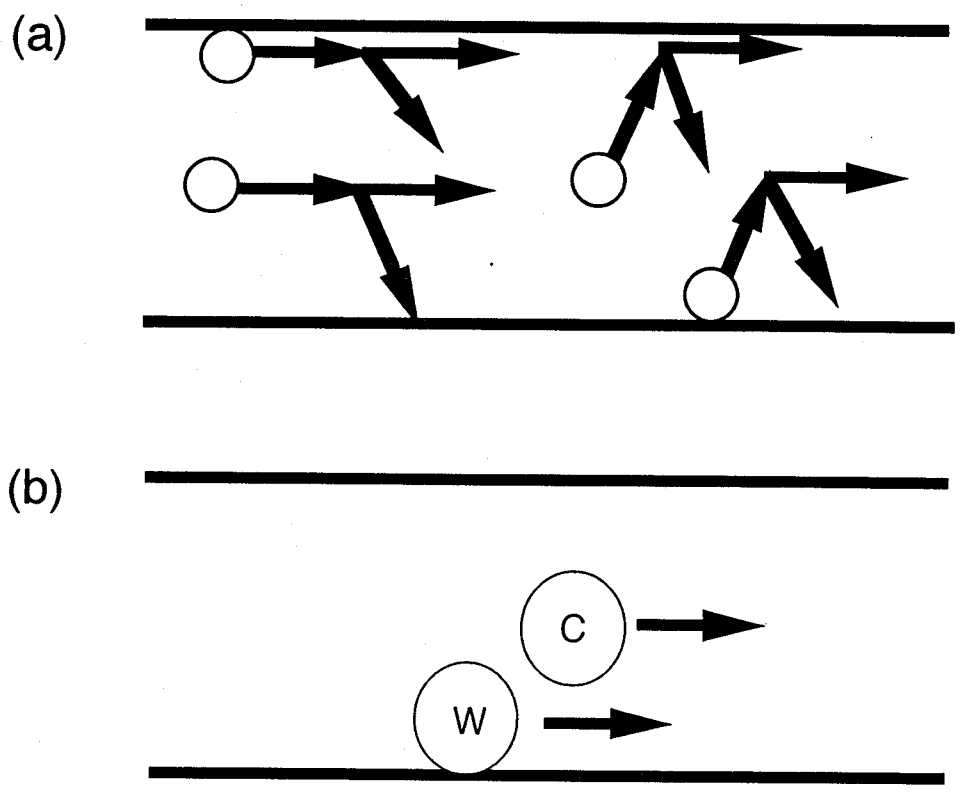

Figure 5.6 Parallel diffusion model.

diffusion. The diffusive flux is generally written as

$$\begin{aligned} J &= -D_F \frac{dC}{dz} \\ &= -D \frac{d \ln p}{d \ln C} \frac{dC}{dz} \\ &= -D \frac{d \ln p}{d \ln C} \frac{dC}{dp} \frac{dp}{dz} \end{aligned} \tag{5.3}$$

where, D_F represents the Fickian diffusivity, D, the corrected diffusivity which is independent of pressure and concentration, P, the pressure in a membrane and C, the concentration of molecule in a membrane, respectively. In this case, the adsorption equilibrium at the interface between gas phase and membrane is accomplished. If gas adsorption on a zeolitic membrane at temperatures higher than room temperature is assumed to follow the Henry's law, the derivatives are

$$\frac{d \ln p}{d \ln C} = 1 \tag{5.4}$$

$$\frac{dC}{dp} = \frac{K_H}{RT} = \frac{K_{H0}}{RT} \exp\left(\frac{q_{st}}{RT}\right) \tag{5.5}$$

where K_H and q_{st} represent the Henry's constant and isosteric heat of adsorption, respectively. Diffusivity in activated process can be written as

$$D = D_0 \exp\left(\frac{-E}{RT}\right) \tag{5.6}$$

where D and E represent diffusivity and activation energy of diffusion, respectively. By introducing Eqs. 5.5 and 5.6 into Eq. 5.3, we obtain

$$J = -\frac{D_0 K_{H0}}{RT} \exp\left(\frac{q_{st} - E}{RT}\right)\frac{dp}{dz} . \tag{5.7}$$

At the steady state,

$$\frac{dJ}{dz} = 0 \quad and \quad \frac{dp}{dz} = \frac{\Delta p}{d} \tag{5.8}$$

where Δp and d represent the pressure difference and the membrane thickness, respectively. The permeance through a zeolitic membrane is, then, expressed as

$$P = -\frac{\varepsilon}{\tau d}\frac{D_0 K_{H0}}{RT} \exp\left(\frac{q_{st} - E}{RT}\right) . \tag{5.9}$$

Where ε and τ are the porosity and tortuosity of the membrane, respectively.

Here, a parallel diffusion mechanism is applied to Eq. 5.9. The molecules adsorbed in the micropore diffuse in parallel through the central region of a pore and along the wall region of a pore. The permeance is expressed as the sum of both contributions,

$$P = -\frac{\varepsilon}{\tau d}\sum_{i=c,w} f_i \frac{D_{0,i} K_{H0,i}}{RT} \exp\left(\frac{q_{st,i} - E_i}{RT}\right) \tag{5.10}$$

where f_i is constant. Suffixes, c and w, correspond to the diffusion through the central region of a pore and along the wall region of the pore, respectively.

It seems likely that both types of diffusion contributed to the

permeation of inorganic gases under the present experimental conditions, except for the permeation of H_2, He and CH_4 through the MOR membrane. The parameter fitting was carried out using Eq. 5.10 on the assumption that molecules dominantly diffuse through the central region at higher temperatures and along the wall region at lower temperatures. Solid lines in **Figure 5.4** represent the values calculated by Eq. 5.10. The proposed parallel diffusion model expresses the experimental data well.

Based on the calculated results, we separated the permeance, P, into two types of mass transportation through the central region of a pore, P_c, and along the wall region of a pore, P_w, where $P = P_c + P_w$. **Figure 5.7** shows the temperature dependence of P_c, P_w and P calculated for He and CO_2 through the FER membrane, suggesting that the diffusion along the wall region of the FER pore cannot be ignored even for the permeation of He. The adsorbable gas, CO_2, diffuses dominantly along the pore wall at room temperature for the FER membrane.

Figure 5.8 shows the ratios of P_w to P for each gas. The diffusants along the wall region were more dominant through the FER membrane compared with those through the MOR membrane. This seems reasonable because the interaction between molecules and a pore wall should become more significant in a narrower pore. In the MOR membrane, H_2, He and CH_4 exclusively diffuse through the central region of the pore. In other words, the interaction between molecules and the pore wall of MOR was not strong enough to make the diffusion along the pore wall remarkable. For both membranes, the values of P_w/P for CO_2 were greater than any other gas and those for He were the smallest. These results imply that the parallel diffusion model accounts for the effect of the interaction between molecules and a pore wall.

Table 5.4 summarizes the fitting parameters, $(q_{st,i} - E_i)$. All the

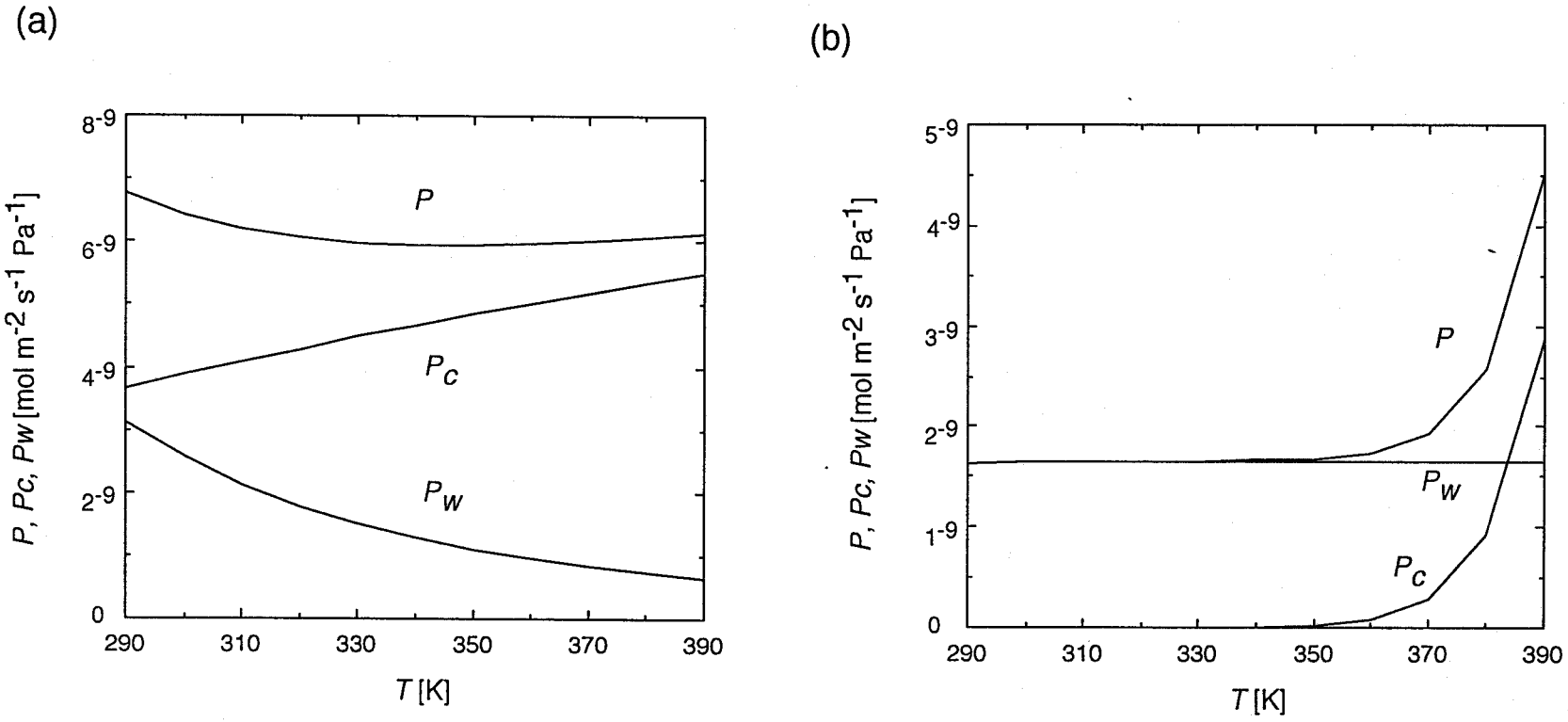

Figure 5.7 P, P_c and P_w for (a) He and (b) CO_2 through FER membrane.

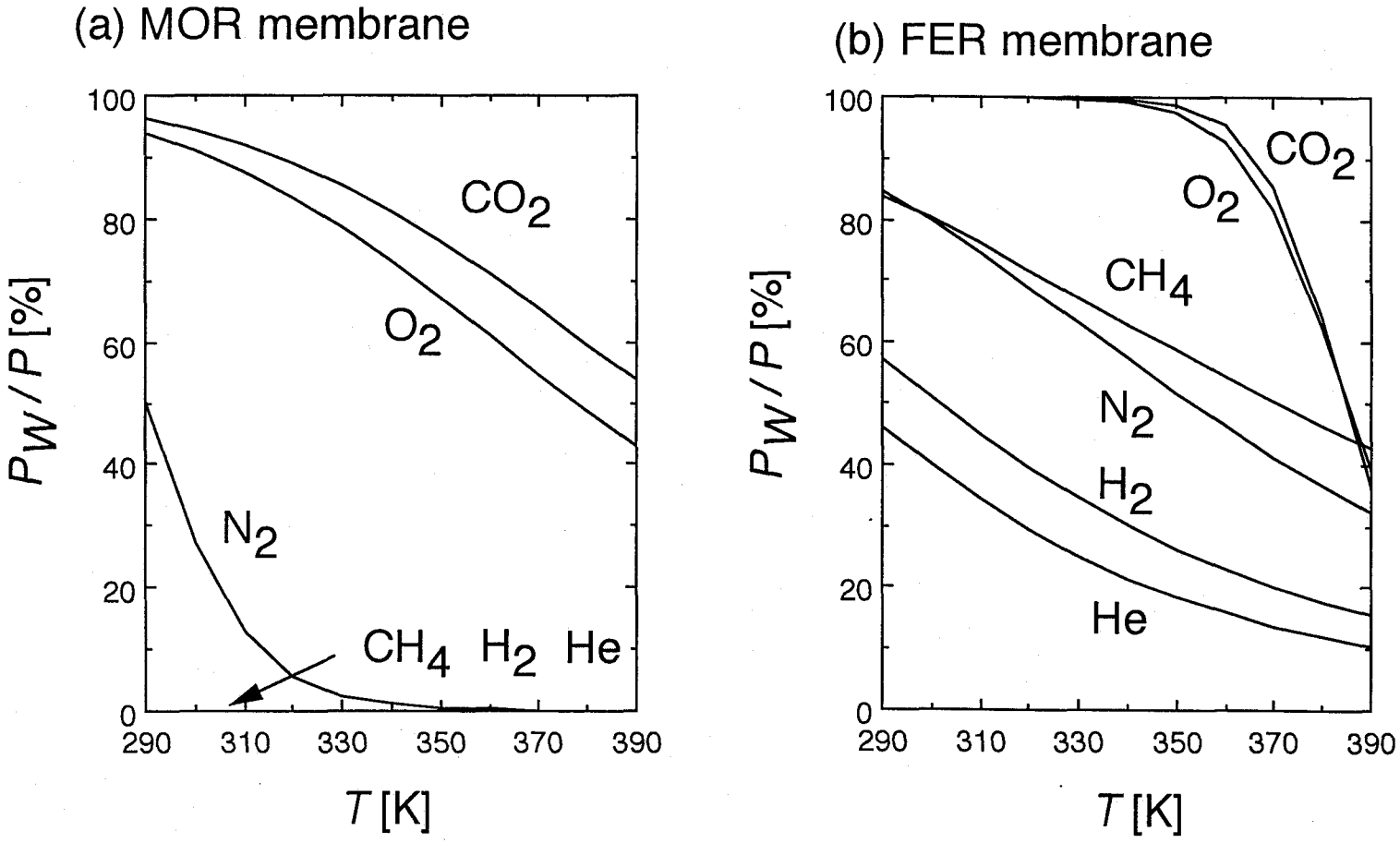

Figure 5.8 Temperatute dependence of P_w/P.

values of ($q_{st,w}$ - E_w) were much greater than those of ($q_{st,c}$ - E_c), i.e., the values of ($q_{st,w}$ - $q_{st,c}$) were much greater than those of (E_w - E_c). This result suggests that the activation energies of diffusion along the pore wall, E_w, are not much greater than those through the central region of pore, E_c, although there are large differences in the heats of adsorption between molecules on the pore wall, $q_{st,w}$, and in the central region, $q_{st,c}$. The value of ($q_{st,c}$ - E_c) for CO_2 was much less than that of any other gas for both MOR and FER membranes, possibly suggesting that the activation energy, E_c, of CO_2 was much greater than those for other gases.

Table 5.4 (q_{st} - E) for MOR and FER membranes

	MOR [kJ mol^{-1}]		FER [kJ mol^{-1}]	
	q_{stc} - E_c	q_{stw} - E_w	q_{stc} - E_c	q_{stw} - E_w
H_2	- 5.1		- 9.8	8.9
He	- 5.5		- 6.6	12.0
CH_4	- 5.0		- 13.9	4.2
N_2	- 6.6	34	- 18.9	3.9
O_2	- 23.4	4.9	- 116.0	0.7
CO_2	- 26.9	2.1	- 143.0	- 2.8

5.4. Conclusions

The permeances of H_2, He, CH_4, N_2, O_2 and CO_2 through defect-free MOR and FER membranes were determined at 290 - 400 K. The temperature dependencies of the permeances were analyzed using a parallel diffusion model in which the permeance was separated into two contributions, that is, diffusions through the central region of the pore and along the wall region of the pore. The contribution of the diffusion at the wall region to the total permeation decreased with increasing temperature. The effect of diffusion along the pore wall on the total permeation was significant for adsorbable gas like CO_2. In contrast, the diffusion through the central region of the pore was dominant for He. The molecules which diffuse along the pore wall were more dominant through the FER membrane compared with those through the MOR membrane, indicating the effect of difference in the pore size between MOR and FER. The proposed parallel diffusion model is useful for analyzing the interaction between gas molecules and a pore wall.

Chapter 6 Pervaporation Performance of Zeolitic Membranes

6.1. Introduction

The term "pervaporation" is a coinage originated from "permeation" and "evaporation". Pervaporation is useful a technique for separating azeotropic, close-boiling or aqueous organic mixtures.

Separation of water/alcohol mixtures was carried out by permeation through a LTA membrane on a porous glass support (Ishikawa, 1989). The LTA membrane was water preferential and had a separation factor of 2500 and 1600 for water/BuOH and water/EtOH mixtures, respectively. Highly selective separation for water/organic mixture were reported by Kita et al. (Kita et al., 1995; Kita, 1995) who synthesized LTA membranes on an alumina support.. The separation factor (water/ethanol) and the total flux were greater than 10000 and 2.15 kg m^{-2} h^{-1}, respectively, showing that the performance of LTA membrane was the most favorable for pervaporation membranes and good enough to put this membrane into practical use. They claimed that a combination of capillary condensation of water in intercrystalline pores between crystals and molecular sieving of zeolite micropores may be operative.

Only silicone rubber membrane has been used as hydrophobic membrane which separates ethanol from the aqueous solution. Recently, much attention has been given to high silica zeolites as attractive materials for organic-selective separation due to their strong hydrophobic nature.

MFI (Al-free) membrane were prepared on a porous support of stainless steel and α-alumina by Sano et al. (1992e, 1994a, 1994b). The MFI membrane exhibited a high selectivity for ethanol with a separation factor α ($EtOH/H_2O$) of more than 60 for a 5 vol% aqueous solution. The diameter of pinholes among MFI grains was estimated about 1 nm because

perfluorotri-n-butylamine with a kinetic diameter of 1.02 nm hardly passed through the membrane compared with p-diisopropylbenzene (0.71 nm) and 1,3,5-triisopropylbenzene (0.85 nm). Adsorption experiments for alcohol and water suggested that the high alcohol selectivity was attributed to the sorption of alcohol into the MFI membrane. In their conclusion, the separation of ethanol/water mixture took place mainly through the 1 nm pinholes with the high hydrophobic property.

In their experiments a lower separation factor for ethanol/water mixture was obtained when the alumina supported MFI membrane was used than when the stainless steel supported MFI membrane was used. They suggested that aluminum was incorporated into the framework of MFI in the vicinity of the alumina support. Liu et al. (1996) also reported that the separation factor for methanol/water pervaporation was higher for stainless steel support than that for an alumina support. In their study, methanol, ethanol and acetone were separated from their aqueous solutions by pervaporation through the MFI (Al-free) membranes. For methanol/water separation, a relatively constant separation factor between 11 and 14 was obtained over a wide feed range of methanol feed concentration. Separation factors as high as 255 were obtained at an acetone concentration of 0.8 wt%. Generally, the overall selectivity of pervaporation process is determined by (1) sorption property of molecule from a liquid phase into a membrane and (2) mobility of molecule in the membrane. Mobility of acetone might be smaller than water in the MFI membrane because acetone has a bigger molecular size and stronger affinity to MFI than water. Therefore, they concluded that the overall separation is determined by the sorption step, similarly to the conclusion by Sano et al. (1994). Liu et al. claimed that the membrane had pinholes since molecules as big as i-octane (0.62 nm) permeated through the MFI membrane.

Hence, intercrystalline pores affected the separation performance of the membrane. In their opinion, the separation performance can be further enhanced by minimizing these defects.

Methylethylketone was preferentially removed from aqueous solution by pervaporation through an MFI (Al-free) membrane (Smetana et al., 1996). Separation factors ranged from 70 to 140 for feed concentrations of 1-15 wt% at 307 K. The MFI membrane did not have good N_2/SF_6 pure gas permeance ratio (equal to 14). An alumina-supported MFI membrane was shown to have lower separation factors than that for the stainless steel supported MFI membrane for the methylethylketone/water, although the alumina-supported MFI membrane had good N_2/SF_6 pure gas permeance ratio (equal to 200).

From the results of Sano et al., Liu et al. and Smetana et al., the hydrophobic nature of the MFI (Al-free) appears to be most important factor for separating organic/water mixtures, and a high separation factor can be obtained using an Al-free MFI membrane even though it contains some microcracks or pinholes.

Recent studies on separation tests by pervaporation have indicated that zeolitic membranes have a high separation potential for a variety of organic/water mixtures including water/ethanol, water/acetone and water/methylethylketone. These separation performance is governed by hydrophilic/hydrophobic nature of zeolites. On the other hand, the separation of aromatic hydrocarbons can be achieved by the shape selectivity of zeolites as well as the interaction between molecules and pore walls of zeolite. However, only a few attempts have so far been made for the separation of aromatic hydrocarbons. In this chapter cyclohexane and three aromatic hydrocarbons such as benzene, p-xylene and o-xylene were examined for the pervaporation tests using a ferrierite (FER) and a

mordenite (MOR) membranes prepared by a vapor-phase transport (VPT) method.

6.2. Experimental

The FER and MOR membranes were prepared by the VPT method in the same procedures as described in section 3.2.

Pervaporation measurements using cyclohexane, benzene, p-xylene and o-xylene were performed at room temperature. The zeolitic membrane was set in the solution and the permeate side was kept under vacuum. The permeant was collected using a liquid N_2 trap. The compositions of feed and permeant were determined by gas chromatograph. The apparatus for the pervaporation tests was shown in **Figure 3.5**.

Flux and separation factor α (A/B) were calculated from the following equations

$$Flux = \frac{n}{t \cdot A} \tag{6.1}$$

$$\alpha\,(a/b) = \frac{(x_a / x_b)_{permeate}}{(x_a / x_b)_{feed}} \tag{6.2}$$

where *n, t, A and x* are permeation amount [mol], permeation time [s], the membrane area [m^2] and the mole fractions [-], respectively.

6.3. Results and discussion

6.3.1. Single-component

Figure 6.1 shows the pervaporation results using the FER membrane for cyclohexane, benzene, p-xylene and o-xylene at 303 K. The pervaporation was carried out consecutively in this order. The ratios of each flux to that of o-xylene are shown together in **Figure 6.1**. The

fluxes of cyclohexane and benzene were about a hundred times greater than those of p-xylene and o-xylene. The flux of p-xylene was about five times greater than that of o-xylene.

The permeation test for TIPB was carried out after that for o-xylene. No permeation of TIPB was detected. After the permeation test for TIPB, the pervaporation using benzene was performed again, which resulted in a comparable flux of benzene to that before the TIPB permeation test, as shown in **Figure 6.1**.

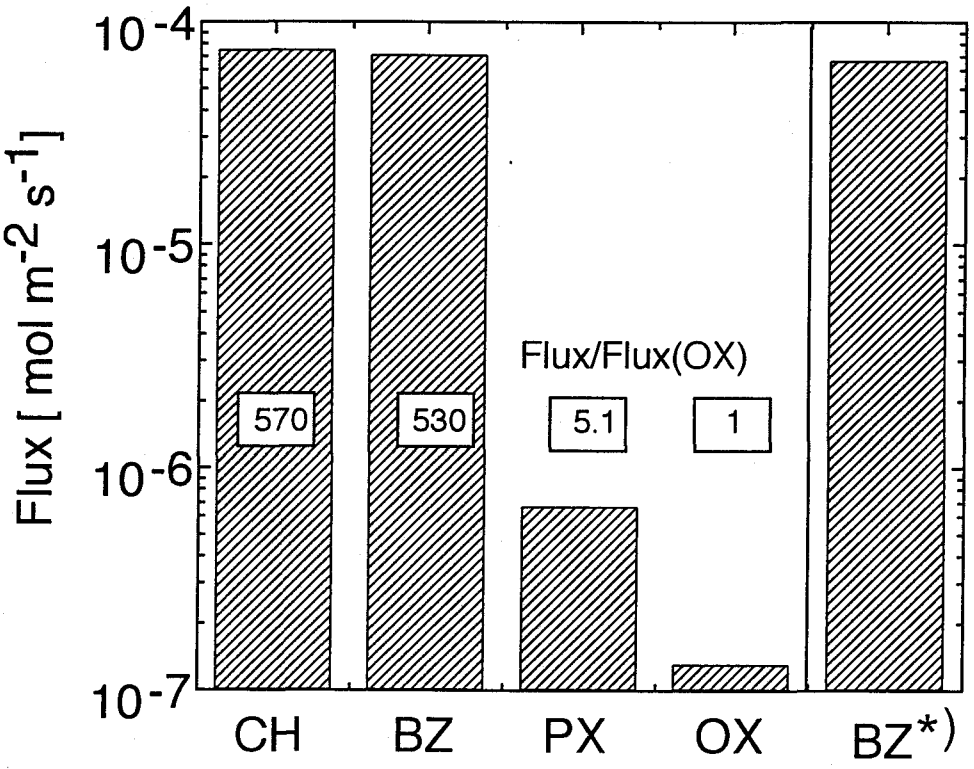

Figure 6.1 Pervaporation results for single liquid components using FER membrane. (T = 303 K)
CH: cyclohexane, BZ: benzene, PX: p-xylene, OX: o-xylene.
*) After permeation test for 1,3,5-triisopropylebenzene.

Thus, no TIPB existed in the micropore of FER. In addition, the TIPB adsorbed around the entrance of micropore could easily be substituted by benzene. Therefore, it is concluded that there existed no pinhole and no crack which would allow the entrance of TIPB into the FER membrane, strongly supporting the conclusion in chapter 3 that the FER membrane was practically defect-free.

6.3.2. Binary component

1. MOR membrane

The pervaporation of a benzene/p-xylene mixture through the MOR membrane was experimentally studied at 295 K. The molar ratio of benzene to p-xylene was 0.86. **Figure 6.2** shows the time course of the fluxes of benzene and p-xylene. The separation factor, α (benzene/p-xylene), was compared with a theoretical one determined from the vapor-liquid equilibrium. The pervaporation for p-xylene had been carried out before the pervaporation for the benzene/p-xylene mixture, though the result is not shown here. Thus, the flux of p-xylene was greater than that of benzene in the initial period. With elapse of time, the flux of benzene increased and that of p-xylene decreased. Both fluxes leveled off after 10 h. In the steady state, the separation factor exceeded about 160, which was much greater than the value of 11.3 theoretically predicted by the vapor-liquid equilibrium.

After the permeation test for TIPB, the pervaporation for a benzene/p-xylene mixture was performed again. As shown in **Figure 6.2**, the fluxes of benzene and p-xylene were 1.3×10^{-4} and 2.6×10^{-6} mol m^{-2} s^{-1}, respectively, which were comparable to those in the previous pervaporation tests described above. Similarly to the discussions for the FER membrane,

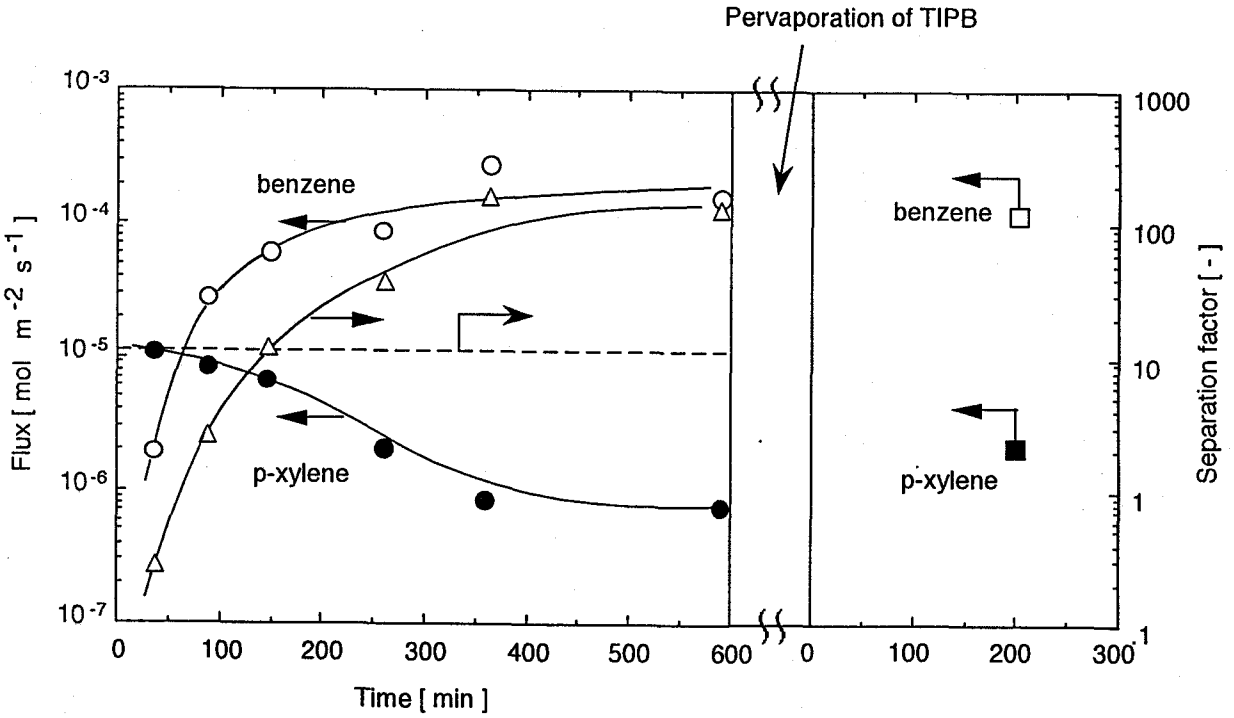

Figure 6.2 Pervaporation results for a benzene/p-xylene mixture through MOR membrane at 295 K. ○, □: Flux of benzene, ●, ■: flux of p-xylene and △: separation factor. Dashed line: theoretical separation factor (11.3) determined at the vapor-liquid equilibrium.

these results indicated that no TIPB existed in the micropore of MOR and there were no pinholes into which TIPB molecules could enter.

2. FER membrane

Figure 6.3 shows the pervaporation results using the FER membrane for binary mixtures, cyclohexane/benzene, benzene/p-xylene and p-xylene/o-xylene at 303 K. Theoretical separation factors from vapor-liquid equilibrium were calculated and are shown in **Figure 6.3** together. The separation factors for these three mixtures were greater than those at vapor-liquid equilibrium. It is noteworthy that a separation factor α (p-xylene/o-xylene) was about 3, taking into account that the MFI membrane which possesses pinholes with a diameter of about 1 nm showed no selectivity for a p-xylene/m-xylene mixture (Sano et al. 1994a).

The fluxes of both benzene and p-xylene through the FER membrane were about a quarter of those through the MOR membrane. The difference in fluxes between two types of zeolitic membrane can be attributed to the difference in pore dimensions of MOR (0.70 x 0.65 nm) and FER (0.54 x 0.42 nm). The separation factors for the benzene/p-xylene mixture exceeded 100 which was much greater than 10.3 predicted from the vapor-liquid equilibrium.

Vapor permeation of p-xylene, m-xylene, ethylbenzene and toluene through an MFI membrane was carried out by Baertsch et al. (1996) who reported that no separation was achieved for binary mixtures of p-xylene/o-xylene, p-xylene/ethylbenzene, p-xylene/toluene and m-xylene/ethylbenzene at 380 - 480 K. They claimed that the molecule with the slowest permeation rate limits diffusion and slows the other species down to its own rate in single-file transport. Funke et al. (1996) used the same MFI membrane as used by Baertsch et al. for the separation of octane

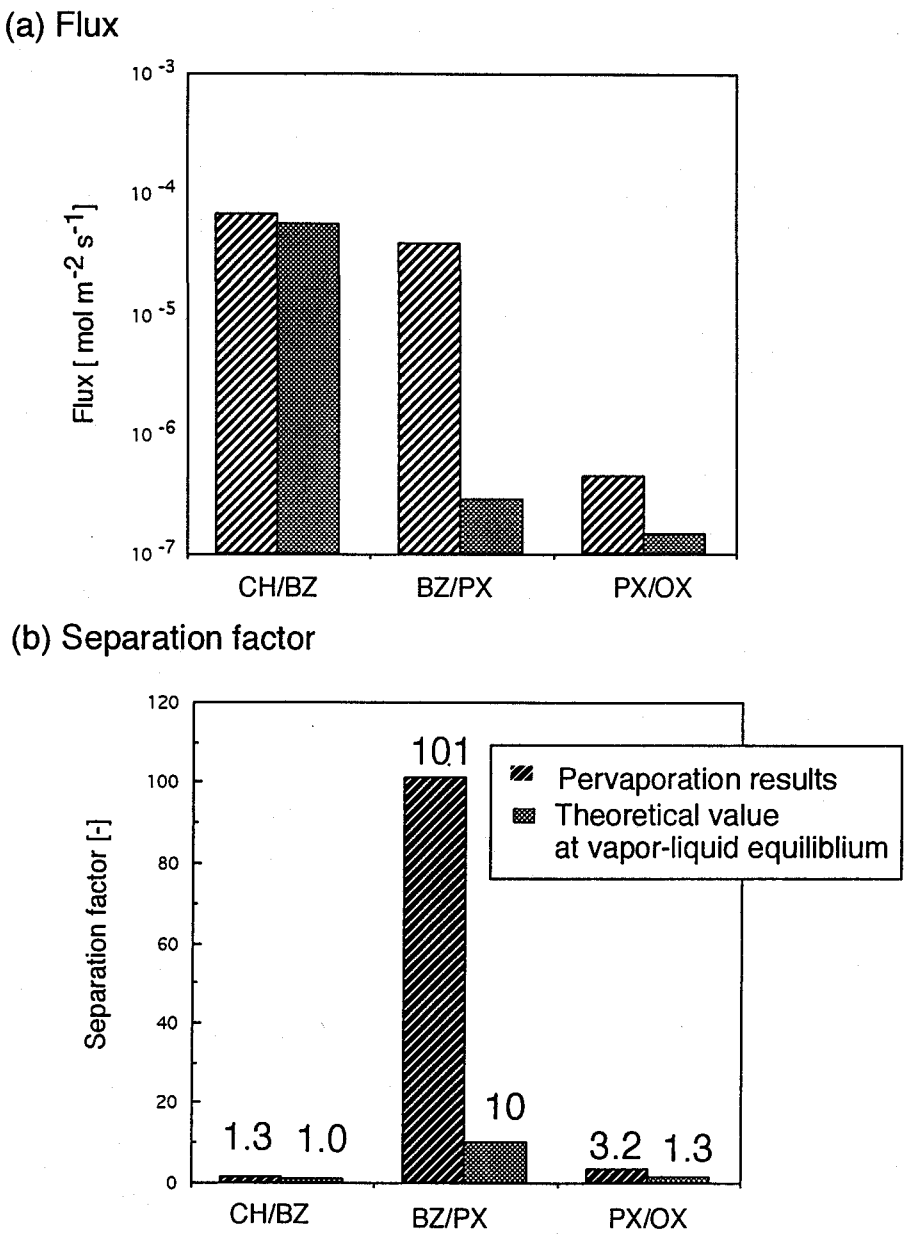

Figure 6.3 Pervaporation results for mixtures using FER membrane. (T = 303 K)

CH: cyclohexane, BZ: benzene, PX: p-xylene, OX: o-xylene.
Feed mole ratios of CH/BZ, BZ/PX and PX/OX were 0.95, 1.34 and 0.96, respectively.

isomers and found that n-octane preferentially permeated through the MFI membrane. They concluded that n-octane molecules prevented i-octane molecules from entering the zeolite pores.

When the single-file transport occurs in the membrane, the overall selectivity is always governed by the selectivity on the feed side of the membrane as shown in **Figure 6.4**. Thus, taking it into account that the FER-alumina composite layer is compact, high selectivities for the benzene/p-xylene mixtures suggest that the shape selectivity for the benzene/p-xylene mixture appears at the pore mouths of FER on the feed side of the FER-alumina composite layer. The intracrystalline diffusivities of benzene in MFI crystal were reported to be comparable to those of p-xylene (Shah and Liu, 1994a, b). In addition, there has been no report on high-selective separation of benzene from p-xylene by adsorption equilibrium operation. Therefore, it seems that the difference in sorption

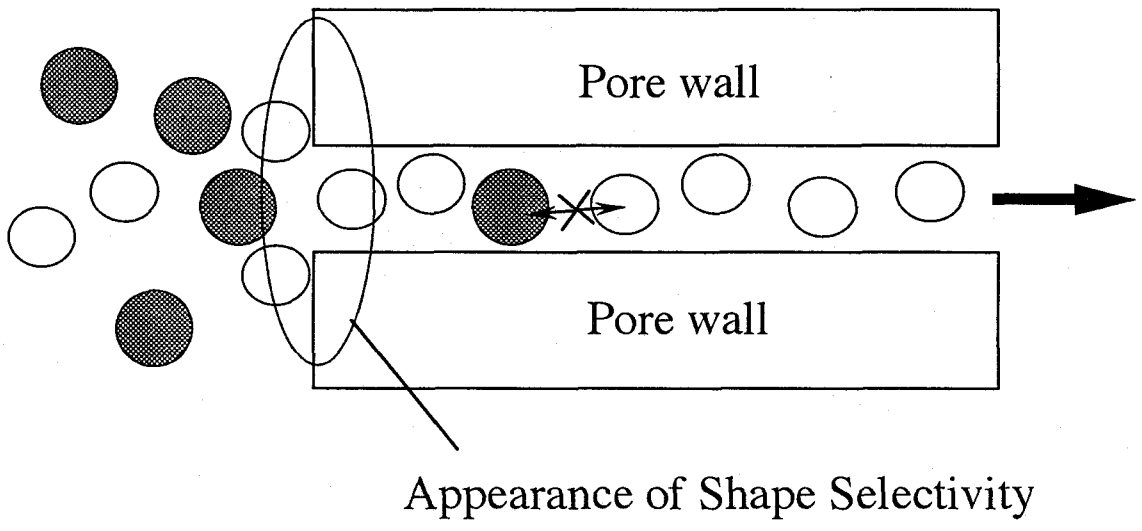

Figure 6.4 Appearance of shape selectivity at the pore mouth.

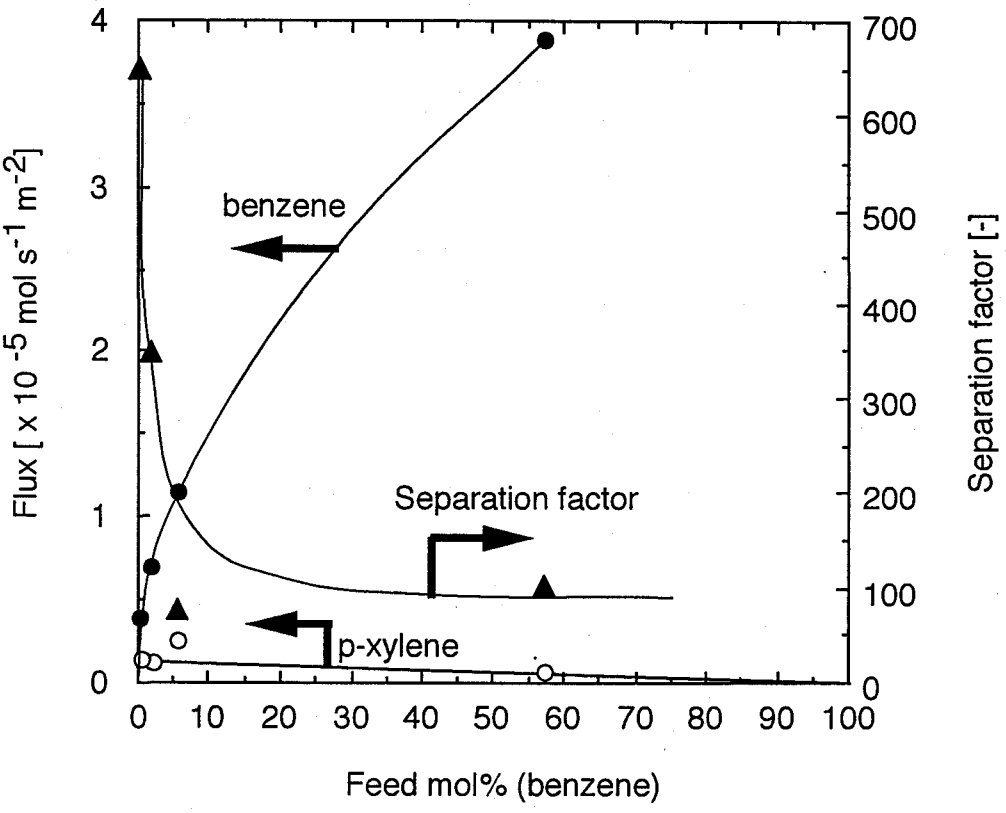

Figure 6.5 Effect of benzene feed concentration on fluxes of benzene and p-xylene and separation factor in pervaporation of benzene/p-xylene mixtures using FER membranes. Temperature: 303 K, ●: flux of benzene, ○: flux of p-xylene, ▲: separation factor.

rate of benzene and p-xylene molecules into the zeolite pores on the feed side governed the selectivity in the present pervaporation.

The pervaporation tests for benzene/p-xylene mixtures with various feed concentration were performed at 303 K. **Figure 6.5** shows the change in fluxes of benzene and p-xylene and the separation factor as a function of feed concentration of benzene. When the molar fraction of benzene in the feed solution was 57 mol%, the separation factors for the benzene/p-xylene mixture exceeded 100 which was much greater than 10.3 predicted from the vapor-liquid equilibrium. The separation factor for benzene/p-xylene mixtures largely increased with decreasing benzene concentration in the feed. The separation factor α (benzene/p-xylene) was as high as 600 when the feed concentration of benzene was 0.5 mol%. The flux of p-xylene varied in proportion to the p-xylene concentration in the feed. On the other hand, a large increase in the flux of benzene was observed with increasing concentration from 0 to 5 mol%. In other words, the benzene flux did not monotonously decrease with decreasing feed concentration, suggesting that even when the concentration of benzene in feed solution was extremely small, the sorption rate of benzene into the FER pores was still high. Therefore, a high separation factor was obtained at the low feed concentration of benzene.

6.5. Conclusions

The pervaporation test of a benzene/p-xylene mixture of which the molar ratio was 0.860, was carried out using a MOR membrane. The separation factor of a benzene/p-xylene mixture exceeded 160.

Cyclohexane, benzene, p-xylene and o-xylene were examined for pervaporation test at room temperature using a FER membrane. The separation factors of a p-xylene/o-xylene and a benzene/p-xylene mixtures

were found to be about 3 and about 100, respectively,. High selectivity for the benzene/p-xylene mixture suggests that the shape selectivity for the benzene/p-xylene mixture appeared at the pore mouths of FER and MOR on the feed side, because benzene and p-xylene molecules do not easily pass through each other in the micropore of FER and MOR (Single-file transport).

The pervaporation for the benzene/p-xylene mixture was performed at 303 K by changing feed concentration. Even when the concentration of benzene in feed solution was extremely small, the flux of benzene through the FER membrane was still large. Therefore, separation factor a benzene/p-xylene mixture was as high as 600 when the feed concentration of benzene was 0.5 mol%. The zeolitic membranes showed a promising potential to separate organic compounds such as aromatic hydrocarbons.

Chapter 7 Summary

This thesis deals with synthesis of zeolitic membranes and their separation properties. A novel synthetic method of zeolites and zeolitic membranes " vapor-phase transport (VPT) method" was developed.

In chapter 2, the potential of synthesizing zeolites by the VPT method was confirmed. Various types of zeolites, ferrierite (FER), ZSM-5 (MFI) and analcime (ANA) and so on, were produced by the VPT method. In crystallization of FER by the VPT method, EDA acted as a structure-directing agent and both Et_3N and water encouraged crystallization. The crystallization process of FER and MFI were studied and it was found that all Al atoms were incorporated in zeolitic framework in the early stage of crystallization and crystallization of a Si-rich phase followed. Transformation of FER to MFI occurred with prolonged crystallization. This synthetic method offers promising prospects for (1) synthesis of zeolites possessing the same SiO_2/Al_2O_3 ratio with that of parent gel, (2) continuous production of zeolites, and (3) production of zeolites shaped in advance, as mentioned in the introduction.

In chapter 3, the VPT method was applied to prepare zeolitic membranes. The synthetic conditions to prepare a compact layer on a porous alumina support were first explored prior to crystallization studies. A high pH around 12 of the gel was required for the preparation of the continuous dry gel in a compact form. Membranes with low silica zeolites, analcime (ANA) and mordenite (MOR), were formed because alumina was partly dissolved and incorporated into the framework of zeolite. Coating of the alumina support with colloidal silica depressed the dissolution of alumina. The compactness of the MOR and FER membranes was confirmed by the pervaporation test of TIPB. Since no permeation of

TIPB was detected, it was concluded that there existed no pinholes and cracks in the zeolitic membranes. The gel in the alumina pore was crystallized to zeolite in a compact form. A forced penetration of a gel into an alumina support was found to be necessary to obtain a defect-free FER membrane.

In chapter 4, the morphology and formation process of the zeolitic membranes were studied. A large zeolite crystals were composed of aggregate of zeolite nano-crystals. Gel was successively supplied from the gel layer on the support. Finally a compact composite layer of zeolite and alumina formed in the support.

In chapter 5, the permeances of H_2, He, CH_4, N_2, O_2 and CO_2 through defect-free MOR and FER membranes were determined at 290 - 400 K. The temperature dependencies of the permeances were analyzed using a parallel diffusion model in which the permeance was separated into two contributions, that is, diffusions through the central region of the pore and along the wall region of the pore. The contribution of the diffusion at the wall region to the total permeation decreased with increasing temperature. The effect of diffusion along the pore wall on the total permeation was significant for adsorbable gas like CO_2. In contrast, the diffusion through the central region of the pore was dominant for He. The molecules which diffuse along the pore wall were more dominant through the FER membrane compared with those through the MOR membrane, indicating that the effect of difference in the pore size between MOR and FER appeared. The proposed parallel diffusion model is useful for analyzing the interaction between gas molecules and a pore wall.

In chapter 6, pervaporation of cyclohexane and three aromatic hydrocarbons such as benzene, p-xylene and o-xylene were examined using the FER and MOR membranes. The pervaporation test of a benzene/p-

xylene mixture of which the molar ratio was 0.860, was carried out using a MOR membrane. The separation factor of a benzene/p-xylene mixture exceeded 160.

Cyclohexane, benzene, p-xylene and o-xylene were examined for pervaporation tests at room temperature using a FER membrane. The separation factors of a p-xylene/o-xylene and a benzene/p-xylene mixtures were found to be about 3 and about 100, respectively. A high selectivity for the benzene/p-xylene mixture suggests that the shape selectivity for the benzene/p-xylene mixture appeared at the pore mouths of FER and MOR on the feed side, because benzene and p-xylene molecules do not easily pass through each other in the micropore of FER and MOR (Single-file transport).

The pervaporation for the benzene/p-xylene mixture was performed at 303 K with various feed concentrations. Even when the concentration of benzene in feed solution was extremely small, the flux of benzene through the FER membrane was still large. Therefore, the separation factor for a benzene/p-xylene mixture was as high as 600 when the feed concentration of benzene was 0.5 mol%. The zeolitic membranes showed a promising potential to separate organic compounds such as aromatic hydrocarbons.

Nomenclature

A	membrane area, m^2
C	concentration of molecule in membrane, mol m^{-3}
D_F	Fickian diffusivity, m^2 s^{-1}
D	intrinsic diffusivity, m^2 s^{-1}
d	membrane thickness, m
E	activation energy, J mol^{-1}
f	constant, -
J	flux, mol m^{-2} s^{-1}
K_H	Henry's constant, -
p	pressure, Pa
Δp	pressure difference, Pa
P	permeance, mol m^{-2} s^{-1} Pa^{-1}
P'	permeability, mol m m^{-2} s^{-1} Pa^{-1}
q_{st}	isosteric heat of adsorption, J mol^{-1}
R	gas constant, 8.314 J mol^{-1} K^{-1}
T	temperature, K
x	mole fraction, mol%
z	direction coordinate, m

Greek letters

α	separation factor, -
ε	membrane porosity, -
τ	tortuosity of membrane, -

Subscripts

c	center of pore
i	c or w
w	wall of pore
0	constant

Structure code

AFI	$AlPO_4$-5, SAPO-5, VAPO-5	0.73 nm
ANA	analcime	0.26 nm
BEA	beta	0.65x0.56, 0.75x0.57 nm
DDR	deca-dodecasile	0.44x0.36 nm
FAU	faujasite, X-type, Y-type	0.74 nm
FER	ferrierite, ZSM-35	0.42x0.54, 0.35x0.48 nm
GME	gmelinite	0.36x0.39, 0.7 nm
LTA	A-type	0.41 nm
LTL	L-type	0.71 nm
MEL	ZSM-11	0.53x0.54 nm
MFI	ZSM-5, silicalite	0.53x0.56, 0.51x0.55 nm
MOR	mordenite	0.65x0.70, 0.26x0.57 nm
MTW	ZSM-12	0.57x0.61 nm
SOD	sodalite	
TON	KZ-2	0.44x0.55 nm
VFI	VPI-5, $AlPO_4$-54	1.2-1.3 nm

Literature cited

Alexander, G., Chemistry in action series 1, Silica and me, Doubleday & Company, Inc. (1967)

Althoff, R., K. Unger and F. Schuth, "Is the formation of a zeolite from a dry powder via a gas phase transport process possible?", *Microporous Materials*, **2**, 557-562 (1994)

Argauer, R. J., Md. Kensington, R. L. George and N. J. Audubon, assignors to Mobil oil Co., US Patent 3702886 (1972)

Baertsch, C. D., H. H. Junke, J. L. Falconer and R. D. Noble, "Permeation of aromatic hydrocarbon vapors through silicalite-zeolite membranes", *J. Phys. Chem.*, **100**, 7676-7679 (1996)

Bai, C., M.-D. Jia, J. L. Falconer, R. D. Noble, "Preparation and separation properties of silicalite composite membranes", *J. Memb. Sci.*, **105**, 79-87 (1995)

Bakker, W. J. W., G. Zheng, F. Kapteijn, M. Makkee, J. A. Moulijn, E. R. Geus, H. van Bekkum, "Single and multi-component transport through metal-supported MFI zeolite membranes" In: Precision Process Technology, (M. P. C. Weijenen and A. A. H. Drinkenburg, Eds.), Kluwer, Dordrecht, pp425-436 (1993)

Bakker, W. J. W., F. Kapteijn, J. Poppe and J. A. Moulijn, "Permeation characteristics of a metal-supported silicalite-1 zeolite membrane", *J. Memb. Sci.*, **117**, 57-78 (1996)

Barrer, R. M. and P. J. Denny, "Hydrothermal chemistry of the silicates. Part 4 Nitrogenous aluminosilicates", J. Chem. Soc., 971-982 (1961)

Barrer, R. M., "Porous crystal membrane", *J. Chem. Soc. Faraday Trans.*, **86**, 1123 (1990).

Barrer, R. M., "Zeolite as membrane: The role of the gas-crystal interface", *Stud. Surf. Sci. Catal.*, **65**, 257 (1991)

Bellobono, I. R., F. Muffato, C. Ermondi, E. Sellli, L. Righetto and M. Zeni, "Thermodynamic study of sorption of n-alkanes onto 5A zeolites immobilized in photosynthetic membranes", *J. Memb. Sci.*, **55**, 263-272 (1991)

Bibby, D. M. and M.P. Dale, "Synthesis of silica-sodalite from non-aqueous systems", *Nature*, **317**, 157-158 (1985)

Boxhoorn, G., O. Sudmeijer, and P. H. G. van Kasteren, "Identification of a double five-ring silicate, a possible precursor in the synthesis of ZSM-5", *J. Chem. Soc., Chem. Commun.*, 1416-1418 (1983)

Chao, K. J., and C. N. Wu, "Vertical-aligned MeAPO4-5 crystals grown on anodic alumina membrane", *Stud. Surf. Sci. Catal.*, in press. OC23 (1996)

Chiou, Y. H., T. G. Tsai, S. L. Sung, H. C. Shih, C. N. Wu and K. J. Chao, "Synthesis and characterization of zeolite(MFI) membrane on anodic alumina", *J. Chem. Soc., Faraday Trans.*, **92**, 1061-1066 (1996)

Costa, E., M. A. Uguina, A. De Lucas, and J. Blanes, "Synthesis of ZSM-5 zeolites in the C_2H_5OH-Na_2O-Al_2O_3-H_2O system", *J. Catal.*, **107**, 317-324 (1987)

Crea, F., R. Aiello, A. Nastro and J. B. Nagy, "Synthesis of ZSM-5 zeolite from very dense synthesis: Formation of pelleted ZSM-5 zeolite from (Na, Li, TPA, Si, Al) hydrogels, *Zeolites*, **11**, 521-527 (1991)

Demertzis, M. and N. P. Evmiridis, "Potentials of ion-exchanged synthetic zeolite-polymer membranes", *J. Chem. Soc., Faraday Trans.* 1, **82**, 3647-3655 (1986)

Dong, J., T. Dou, X. Zhao and L. Gao, "Synthesis of membranes of zeolites and ZSM-5 and ZSM-35 by the vapor phase method", *J. Chem. Soc., Chem. Commun.*, 1056-1058 (1992)

Exter, M. J. den, J. C. Jansen, J van de Graaf, F. Kapteijn and H. van Bekkum, "Zeolite-based membranes, preparation, performance and Prospects", *Stud. Surf. Sci. Catal.*, **102**, 413-454 (1996)

Funke, H., A. M. Argo, C. D. Baertsch, J. L. Falconer and R. D. Noble, "Separation of close-boiling hydrocarbons with silicalite zeolite membranes", *J. Chem. Soc., Faraday Trans.*, **92**, 2499-2502 (1996)

Geus, E. D., H. Bekkum, W. J. W. Bakker and J. A. Moulijin, "High-temperature stainless steel supported zeolite(MFI) membranes:

preparation, module concentration, and permeation experiments", *Microporous Materials*, **1**, 131-147 (1993)

Gies, H., and R. P. Gunawardane, "One-step synthesis, properties and crystal structure of aluminum-free ferrierite", *Zeolites*, **7**, 442 (1987)

Hagiwara, H., Y. Kiyozumi, M. Kurita, T. Sato, H. Simada, K. Suzuki, S. Shin, A. Nishijima, and N. Todo, "A new method for the preparation of zeolite ZSM-5 by using sodium n-dodecylbenzene sulfonate", *Chem. Lett.*, 1653-1566 (1981)

Hennepe, H. J. C. te, W. B. F. Boswerger, M. H. V. Mulder, C. A. Smolders, "Zeolite-filled silicone rubber membranes. Membrane preparation and pervaporation results, *J. Memb. Sci.*, **35**, 39-55 (1987)

Hennepe, H. J. C. te, C. A. Smolders, D.Bargeman, M. H. V. Mulder, "Exclusion and tortuosity effects for alcohol/water separation by zeolite-filled silicone rubber membranes", *Sep. Sci. Technol.*, **26**, 585-596 (1991)

Hennepe, H. J. C. te, W. B. F. Boswerger, D.Bargeman, M. H. V. Mulder, C. A. Smolders, "Zeolite-filled silicone rubber membranes. Experimental determination profiles", *J. Memb. Sci.*, **89**, 185-196 (1994)

Huo, Q., S. Feng and R. Xu, "First synthesis of pentasil-type silica zeolites from non-aqueous systems", *J. Chem. Soc., Chem. Commun.*, 1486-1487 (1998)

Inui, T., *Syokubai*, 25, 261-270 (1984)

Ishikawa, A., T. H. Chiang and F. Toda, "Separation of water-alcohol mixtures by permeation through a zeolite membrane on porous glass, *J. Chem. Soc., Chem. Commun.*, 764-765 (1989)

Jansen, J. C., D. Kashchiev and A. Erdem-Senatalar, "Preparation of coatings of molecular sieve crystals for catalysis and separation", *Stud. Surf. Sci. Catal.*, **85**, 215-250 (1994)

Jia, M., K.-V. Peinemann and R.-D. Behling, "Molecular sieving effect of the zeolite-filled silicone rubber membranes in gas permeation", *J. Memb. Sci.*, **57**, 289-296 (1991)

Jia, M., K.-V. Peinemann and R.-D. Behling, "Preparation and characterization of thin-film zeolite-PDMS composite membranes", *J. Memb. Sci.*, **73**, 119-128 (1992)

Jia, M.-D., K.-V. Peinemann and R.-D. Behling, "Ceramic zeolite composite membranes. Preparation, characterization and gas permeation", *J. Memb. Sci.*, **82**, 15-26 (1993)

Jia, M. D., B. Chen, R. D. Noble and J. L. Falconer, "Ceramic-zeolite composite membranes and their application for separation of vapor/gas mixtures", *J. Memb. Sci.*, **90**, 1-10 (1994)

Kapteijn, F., W. J. W. Bakker, G. Zheng, J. A. Moulijn, "Temperature- and occupancy-dependent diffusion of n-butane through a silicalite-1 membrane", *Microporous Materials*, **3**, 227-234 (1994)

Kapteijn, F., W. J. W. Bakker, J. van de Graaf, G. Zheng, J. Poppe, J. A. Moulijn, "Permeation and separation behavior of a silicalite-1 membrane", *Catalysis Today*, **25**, 213-218 (1995a)

Kapteijn, F., W. J. W. Bakker, G. Zheng, J. Poppe, J. A. Moulijn, "Preparation and separation of light hydrocarbons through a silicalite-1 membrane. Application of the generalized Maxwell-Stefan equations", *Chem. Eng. J.*, **57**, 145-153 (1995b)

Kapoor, A., and R. T. Yang, "Surface diffusion on energetically heterogeneous surfaces", *AIChE J.*, **35**, 1735 (1989).

Kim, M. H., H. X. Li and M. E. Davis, "Synthesis of zeolite by water-organic vapor-phase transport", *Microporous Materials*, 1, 191-200 (1993)

Kita, K. Horii, Y. Ohtoshi, K. Tanaka and K. Okamoto, "Synthesis of a zeolite NaA membrane for pervaporation of water/organic liquid mixtures", *J. Mater. Sci. Lett.*, **14**, 206-208 (1995)

Kita, H., "Pervaporation through zeolite membranes", *Maku (Membrane)* , **20**, 169-182 (1995)

Kiyozumi, Y., F. Mizukami, K. Maeda, T. Kozasa, M. Toda and S. Niwa, "Synthesis of oriented zeolite film on mercury surface", *Stud. Surf. Sci. Catal.*, in pres. PP17 (1996)

Kolsch, P., D. Venzke, M. Noack, P. Toussaint and J. Caro, "Zeolite-in metal membranes: Preparation and testing", *J. Chem. Soc., Chem. Commun.*, 2491-2492 (1994)

Krishna, R., "Problems and pitfalls in the use of the Fick formulation for intraparticle diffusion", Chem. Eng. Sci., 48, 845 (1993)

Krishna, R., and L. J. P. van den Broeke, "The Maxwell-Stefan description of mass transport across zeolite membrane", *Chem. Eng. J.*, **57**, 155 (1995)

Kusakabe, K., S. Yoneshige, A. Murata, S. Morooka, "Morphology and gas permeance of ZSM-5-type zeolite membrane formed on porous a-alumina support tube", *J. Memb. Sci.*, **116**, 39-46 (1996)

Kusakabe, K., A. Murata, T. Kuroda and S. Morooka, "Preparation of MFI zeolite membranes and their use in separating n-butane and i-butane", *J. Chem. Eng. Japan*, in press.

Lechert, H., P. Staelin and C. Kuntz, "Quantitative relations of the batch composition and the Si/Al ratio in the product of zeolites", *Zeolites*, **16**, 149-156 (1996)

Li, J., J. Dong, G. Liu, S. Gong and F. Wu, "Zeolite ZSM-35 Synthesized by the 'Kneading' method in a Nonaqueous System", *J. Chem. Soc., Chem. Commun.*, 659-660 (1993)

Liu, Q., R. D. Noble, J. L. Falconer and H. H. Funke, "Organics/water separation by pervaporation with a zeolite membrane", *J. Memb. Sci.*, **117**, 163-174 (1996)

Lok, B. M., T. R. Cannan, and C. A. Messina, "The role of organic molecules in molecular sieve synthesis", *Zeolites*, **3**, 282-291 (1983)

Meriaudeau, P., A. Thangaraj and C. Naccache, "Preparation and characterization of silicalite molecular sieve membranes over supported porous sintered glass", *Microporous Materials*, **4**, 213-219 (1995)

Mole, T. and J. A. Whiteside, "Conversion of methanol to ethylene over ZSM-5 zeolite in the presence of deuterated water", *J. Catal.*, **75**, 284-290 (1982)

Myatt, G. J., P. M. Budd, C. Price, S. W. Carr, "Synthesis of a zeolite NaA membrane", *J. Mater. Chem.*, **2**, 1103-1104 (1992)

Narita, E., K. Sato, and T.Okabe, "A convenient method for crystallization of zeolite ZSM-5 by using seed crystals in acetone/water mixture system", *Chem. Lett.*, 1055-1058 (1984)

Nastro, A., C. Colella, and R. Aiello, "Synthesis of ZSM-5 type zeolites in the system (Na, K)O_2-Al_2O_3-SiO_2-H_2O", in B. Drzaj, S. Hocevar, and S. Penjovnic (Eds), "Zeolites. Synthesis, Structure, Technology and Application", pp.39-46 (1985)

Niwa, M., S. Kato, T. Hattori and Y. Murakami, "Fine control of the pore-opening size of zeolite ZSM-5 by chemical vapor deposition of silicon methoxide", *J. Chem. Soc., Faraday Trans.*,**80**, 3135-3145 (1984)

Noble, R. D. and J. L. Falconer, "Silicalite-1 zeolite composite membranes", *Catalysis Today*, **25**, 209-212 (1995)

Prank, C. J., E. J. Rosinski, M. K. Rubin and B. C. Pa, US Patent 4046859, assigned to Mobil Oil Co. (1977)

Rao, P. R. H. P., K. Ueyama and M. Matsukata, "Dry gel conversion technique for synthesis of zeolite BEA", *Chem. Commun.*, 1441-1442 (1996)

Sano. T, Y. Kiyozumi, M. Kawamura, F. Mizukami, H. Takaya, T. Mouri, W. Inaoka, Y. Toida, M. Watanabe and K. Toyoda, "Preparation and characterization of ZSM-5 zeolite film", *Zeolites*, **11**, 842-845 (1991)

Sano, T., Y. Kiyozumi, F. Mizukami, H. Takaya, T. Mouri and M. Watanabe, "Steaming of ZSM-5 zeolite film", *Zeolites*, **12**, 131-134 (1992a)

Sano, T., F. Mizukami, H. Takaya, T. Mouri, and M. Watanabe, "Growth process of ZSM-5 zeolite film", *Bull. Chem. Soc. Jpn.*, **65**, 146-154 (1992b)

Sano, T., Y. Kiyozumi, K. Maeda, M. Toba, S. Niwa and F. Mizukami, "New preparation method for highly siliceous zeolite films", *J. Mater. Chem.*, **2**, 141-142 (1992c)

Sano, T., H. Yanagisita, Y. Kiyozumi, D. Kitamoto and F. Mizukami, "Separation of ethanol/water mixture by silicalite membrane", *Chem Lett.*, 2413-2414 (1992e)

Sano, T., M. Hasegawa, Y. Kawakami, Y. Kiyozumi, H. Yanagishita, D. Kitamoto and F. Mizukami, "Potentials of Silicalite membranes for the separation of alcohol/water mixture", *Stud. Surf. Sci. Catal.*, **84**, 1175-1182 (1994a)

Sano, T., H. Yanagisita, Y. Kiyozumi, F. Mizukami, and K. Haraya, "Separation of ethanol/water mixture by silicalite membrane on pervaporation", *J. Memb. Sci.*, **95**, 221 (1994b).

Sano, T., K. Yamada, S. Ejiri, M. Hasegawa and Y. Kawakami, "Silation of silicalite membrane and its pervaporation performance", *Stud. Surf. Sci. Catal.*, in pres. OC22 (1996a)

Seidel, A., and P. S. Carl, "The concentration dependence of surface diffusion for adsorption on energetically heterogeneous adsorbents", *Chem. Eng. Sci.*, **44**, 189 (1989)

Shah, D. B., S. Chokchal-acha and D. T. Hayhurst, "Measurement of transport rates of C_4 hydrocarbons across a single-crystal silicalite membrane", *J. Chem. Soc., Faraday Trans.*, **89**, 3161-3167 (1993)

Shah, D. B. and H. Y. Liou, "Time-lag measurements for diffusion of aromatics through a silicalite membrane", *Zeolites*, **14**, 541-548 (1994a)

Shah, D. B. and H. Y. Liou, "Diffusion of aromatics through a silicalite membrane", *Stud. Surf. Sci. Catal.*, **84**, 1347-1354 (1994b)

Shelekhin, A. B., A. G. Dixon, and Y. H. Ma, "Theory of gas diffusion and permeation in inorganic molecular-sieve membranes", *AIChE J.*, **41**, 58 (1995)

Sie, S. T., "Past, present and future role of microporous catalysts in the petroleum industry", *Stud. Surf. Sci. Catal.*, **84**, 587-631 (1994)

Smetana, J. F., J. L. Falconer, R. D. Noble, "Separation of methyl ethyl ketone from water by pervaporation using a silicalite membrane", *J. Memb. Sci.*, **114**, 127-130 (1996)

Szostak, R., Handbook of molecular sieves, Van Nostrand Reinhold, New York (1992)

Tsikoyiannis, J.G. and W.O. Haag, "Synthesis and characterization of a pure zeolitic membrane", *Zeolites*, **12**, 126-130 (1992)

Vroon, Z. A. E. P., K. Keizer, M. J. Gilde, H. Verweij and A. J. Burggraaf, "Transport properties of alkanes through ceramic thin zeolite MFI membranes", *J. Memb. Sci.*, **113**, 293-300 (1996)

Xu, W., J. Li, W. Li, H. Zhang and B. Liang, "Nonaqueous synthesis of ZSM-35 and ZSM-5", *Zeolites*, **9**, 468-473 (1989)

Xu, W., J. Dong, J.(Jinping) Li, J.(Jianquan) Li and F. Wu, "A novel method for the preparation of zeolite ZSM-5", *J. Chem. Soc., Chem. Commun.*, 755-756 (1990)

Yan, Y., M. Tsapatsis, G. R. Gavalas and M. E. Davis, "Zeolite ZSM-5 membranes grown on porous α-Al_2O_3", *J. Chem. Soc., Chem. Commun.*, 227-228 (1995a)

Yan, Y., M. E. Davis and G. R. Gavalas, "Preparation of zeolite ZSM-5 membranes by in-situ crystallization on porous α-Al_2O_3", *Ind. Eng. Chem. Res.*, **34**, 1652-1661 (1995b)

List of Publications

Papers:

1. Synthesis of zeolites under vapor atmosphere: Effect of synthetic conditions on a zeolite structure
   Matsukata, M., N. Nishiyama and K. Ueyama
   Microporous Materials, **1**, 219-222 (1993)

2. A zeolitic membrane synthesized on a porous alumina support
   Matsukata, M., N. Nishiyama and K. Ueyama
   J. Chem. Soc. Chem. Commun., 339-340 (1994)

3. Preparation of tight and thin zeolitic membrane
   Matsukata, M., N. Nishiyama and K. Ueyama
   Stud. Surf. Sci. Catal., **84**, 1183-1190 (1994)

4. A defect-free mordenite membrane synthesized by vapor phase transport method
   Nishiyama, N., K. Ueyama, and M. Matsukata
   J. Chem. Soc. Chem. Commun., 1967-1968 (1995)

5. Crystallization of FER and MFI zeolites by a vapor-phase transport method
   Matsukata, M., N. Nishiyama and K. Ueyama
   Microporous Materials, **7**, 109-117 (1996)

6. Synthesis of defect-free zeolite-alumina composite membranes by a vapor-phase transport method
   Nishiyama, N., K. Ueyama, and M. Matsukata
   Microporous Materials, in press.

7. Synthesis of FER membrane on an alumina support and its separation properties
   Nishiyama, N., K. Ueyama, and M. Matsukata
   Stud. Surf. Sci. Catal., in press.

8. Gas permeation through zeolitic-alumina composite membranes
   Nishiyama, N., K. Ueyama, and M. Matsukata
   Submitted to *AIChE J.*

9. Formation process of FER membranes by vapor-phase transport method and separation of benzene/p-xylene mixtures

Nishiyama, N., T. Matsufuji, K. Ueyama and M. Matsukata
Submitted to *J. Memb. Sci.*

Proceedings:

1. A new synthetic method of ferrierite and ZSM-5
   Matsukata, M., N. Nishiyama and K. Ueyama
   Proceeding of International Symposium on Zeolites and Microporous Crystals, 249-250 (1993)

2. Synthesis of an alumina-mordenite composite membrane and its separation properties
   Nishiyama, N., K. Ueyama, and M. Matsukata
   Proceeding of 7th Japan-China-USA Symposium on Catalysis 7-8 (1995)

3. A defect-free FER membrane
   Matsukata, M., N. Nishiyama and K. Ueyama
   Proceeding of International Forum on Environmental Catalysis '95, 73 (1995)

4. Synthesis of zeolites and $AlPO_4$ by a vapor phase transport method
   Nishiyama, N., T. Sekine, K. Ueyama, and M. Matsukata
   Proc. 1995 Intern. Chem. Congress of Pacific Basin Soc., INOR 951 (1995)

5. Gas permeation of zeolitic-alumina composite membranes
   Nishiyama, N., K. Ueyama, and M. Matsukata
   Proc. 5th World Congr. Chem. Eng., vol. 4, 834-839 (1996)

6. Appearance of molecular sieving properties by zeolitic membrane
   Matsukata, M., N. Nishiyama and K. Ueyama
Proc. 1996 Intern. Congress on Membranes and Membrane Processes, 464-465 (1996)

Acknowledgment

The author wishes to express his most sincere gratitude and thank to Professor Dr. Korekazu Ueyama and Associated Professor Dr. Masahiko Matsukata (Dept. of Chemical Science and Engineering, Osaka University) for their constant guidance and helpful advice throughout this study.

The author gratefully acknowledges the helpful comments and suggestions of Professors Dr. Shoji Kimura, Dr. Setsuji Tone, and Dr. Tomoshige Nitta (Dept. of Chemical Engineering, Osaka University).

The author would like to thank Mr. Hiroshi Okuda (Dept. of Chemical Engineering, Osaka University) for the solid NMR measurements of zeolites. The author also thanks Mr. Masao Kawashima (Dept. of Chemical Engineering, Osaka University) for the field emission SEM measurements. The author is thankful to Mr. Koh Kidena (Nomura Lab., Dept. of Applied Chemistry, Faculty of Engineering, Osaka University) for the SEM measurements.

The author is indebted to Nihon Gaishi Co. and Noritake Co. for providing porous alumina supports of zeolitic membranes.

The author gratefully acknowledges the financial support of this work from the Research Fellowships of the Japan Society for the Promotion of Science for Young Scientists.

Thanks are given to the author's coworkers, Dr. Hari Prasad Rao, Miss Jiandong Wang, Mr. Takashi Sekine, Mr. Takaaki Matsufuji, Mr. Atsuo Suzuki and all the other members of Ueyama Laboratory for their collaboration.

Finally, the author wishes to thank his mother, Fumiko Nishiyama and his grandfather and grandmother, Susumu and Kayako Nishiyama, for their continuous and hearty encouragement.